Periodic Control of Automotive Vehicles to Improve Fuel Economy

by

Su-Yang Shieh

A dissertation submitted in partial fulfillment
of the requirements for the degree of
Doctor of Philosophy
(Mechanical Engineering)
in The University of Michigan
2021

Doctoral Committee:

Dr. Tulga Ersal, Co-Chair
Professor Huei Peng, Co-Chair
Professor Gabor Orosz
Professor Jing Sun

Su-Yang Shieh

syshieh@umich.edu

ORCID iD: 0000-0002-9333-2412

© Su-Yang Shieh 2021

To my wife, June.

See you in the next incarnation.

ACKNOWLEDGEMENTS

I would like to express my deepest gratitude to my Advisor Professor Huei Peng. Without his precious advice on my research, I could not have completed this dissertation. I also genuinely appreciate his encouragement and patience along the way. I would also like to express my gratitude to my Co-Advior, Dr. Tulga Ersal wholeheartedly. In additional to the precious guidance and advice on my research, his mentorship has supported me in this journey. I would also like to thank my committee members, Professor Jing Sun and Professor Gabor Orosz for the precious comments and suggestions, as well as their precious time for helping me complete the dissertation.

I am also grateful to my labmates, Byung-Joo, Xiaowu, Tianyou, Ding, Ziheng, Steve, Yuxiao, Geunsob, Songan, Nauman, Boqi, Minghan, Xinpeng, Yuanxin, Shaobing, Pingping, Lu, and Juhui. I am grateful for their help and assistance with the research. They broaden my eyes and enrich my life. Especially, I would like to thank Xinpeng for being willing to risk his life doing experiments with me. I also wish to thank Professor Changsun Ahn for the instructions on my microgrid research.

I also wish to shout out to the true brothers of CK55th 324, Lauda, Weeds, Pachuching, Biology, Nianinun, Niuyu, Danaibo, Father, Miniouchi, Icemaker, Alabo, Yieshuan, and Lautsai, and my comrades Jessica, Alejandro, Izzy, and Judy. My greatest appreciation also needs to go to my parents, my aunt, and my sister.

Finally, I wish to thank Dr. Wendy and Dr. Gertruda for the covering fire from Europe. Last but definitely not least, biggest thanks to my best roommate, Michy.

TABLE OF CONTENTS

DEDICATION ii

ACKNOWLEDGEMENTS iii

LIST OF FIGURES vii

LIST OF TABLES x

LIST OF ABBREVIATIONS xi

ABSTRACT xiii

CHAPTER

I. Introduction 1

1.1 Motivation 1
1.2 Literature Review 7
1.2.1 Pulse-and-Glide Operations 7
1.2.2 Cooperative Adaptive Cruise Control 10
1.3 Objectives, Scope of the Study, and Approaches 14
1.4 Contributions 15
1.5 Outline of the Dissertation 16

II. Pulse-and-Glide Operations in Car-Following 17

2.1 Introduction 17
2.2 Vehicle Model 18
2.2.1 Vehicle Dynamics 18
2.2.2 SOC Dynamics 20
2.3 Methodology 22
2.3.1 Problem Formulation 22
2.3.2 Solution Strategy 27
2.3.3 The Ride Comfort Requirement 33
2.4 Simulation Results and Discussions 34

2.4.1 Constant-Speed Preceding Vehicle 35
2.4.2 Varying-Speed Preceding Vehicle 37
2.4.3 Preceding Vehicle with Speed from the Safety Pilot Dataset 40
2.5 Conclusions and Future Work 46

III. Pulse-and-Glide Synchronization for Heterogeneous Platoons 49

3.1 Introduction 49
3.2 Problem Setup 51
3.2.1 The Vehicle Platoon 51
3.2.2 Vehicle Dynamics 51
3.3 A Preliminary Study on the Potential of PnG Synchronization 52
3.4 Methodology 55
3.4.1 The Pulse-and-Glide Strategy 55
3.4.2 Solution Strategy 56
3.4.3 Safety Monitoring 57
3.4.4 Synchronization of Pulse-and-Glide Operation . . . 57
3.4.5 Range Keeping 63
3.5 Simulation Results and Discussions 65
3.6 Conclusions and Future Work 70

IV. Analysis on Pulse-and-Glide Platoons 72

4.1 Introduction 72
4.2 Sensitivity Analysis of a Single PnG Vehicle 74
4.2.1 The Assumption of Constant Acceleration and Deceleration 74
4.2.2 The Sensitivity Analysis of Speed-PnG 76
4.3 Analysis on the Proposed Approach for PnG Platooning . . . 84
4.3.1 The Role of the PnG Period 84
4.3.2 The Influence of Virtual Oscillators on Platooning . 87
4.3.3 The Individual Tracking Controllers 87
4.3.4 The Influence of Communication Topology 90
4.3.5 The Guidelines for Control Design 92
4.4 Simulation Studies 94
4.4.1 Actuator Dynamics and PnG Platooning 94
4.4.2 All-to-All and Bidirectional Communication Topology 95
4.4.3 The Influence of Kuramoto Gain 98
4.5 Further Discussions on the Analysis Results 100
4.6 Conclusions and Future Work 101

V. Experimental Study 103

5.1 Introduction 103

5.2 The Test Vehicle 104
5.3 Methodology 105
5.3.1 Experiment Setup 105
5.3.2 Control Implementation 108
5.3.3 Data Processing 112
5.4 Results and Discussions 115
5.4.1 The RTK Performance 115
5.4.2 The Performance of Throttle Control 116
5.4.3 The Fuel Saving Results of PnG Operation 117
5.5 Conclusions and Future work 119

VI. Conclusions and Future Work 127

6.1 Conclusions 127
6.2 Future Work 128

BIBLIOGRAPHY 131

LIST OF FIGURES

Figure

1.1	The U.S. gasoline and crude oil prices in recent years.	2
1.2	The U.S. transportation sector energy consumption in recent years and prediction.	2
1.3	The mechanism of PnG for fuel saving.	4
2.1	The engine map of the simulation studies of PnG in car-following.	19
2.2	The motor efficiency map of the simulation studies of PnG in car-following.	19
2.3	The voltage and battery resistance of the simulation studies.	21
2.4	The fuel-rate curve for step-gear transmission at given speeds with gear 6.	23
2.5	The fitting of the SOC dynamics during charging.	28
2.6	The MPG improvement of constant-speed driving at different speeds in engine mode.	36
2.7	The MPG improvements of constant-speed driving at different speeds with pure SOC-PnG.	36
2.8	The MPG improvements and root-mean-square accelerations of Speed-PnG with 10% speed oscillation at different speeds.	37
2.9	The MPG improvements and root-mean-square accelerations of SOC-PnG with 10% speed oscillation at different speeds.	38
2.10	The simulation results of constant-speed PV at 40 mph with gear 6.	39
2.11	The speed trajectory used in the case of varying-speed PV.	40
2.12	The simulation results of varying-speed PV at 40 mph with gear 6 and starting in pulsing.	41
2.13	The simulation results of varying-speed PV at 40 mph with gear 6 and starting in gliding.	42
2.14	The statistics of Safety Pilot data on local roads used in the simulations.	43
2.15	The simulation results using the Safety Pilot data on local roads.	44
2.16	The statistics of Safety Pilot data on highways used in the simulations.	44
2.17	The simulation results using the Safety Pilot data on highways.	45
2.18	The results of MPG improvements and the PV accelerations using the Safety Pilot data.	46

2.19 The simulation results using the Safety Pilot data on local roads with different acceleration limits. 47
2.20 The simulation results using the Safety Pilot data on highways with different acceleration limits. 47
3.1 The engine map of the simulation studies of PnG synchronization. . 53
3.2 The schematic diagram of the virtual spring-damper approach for homogeneous platoons. 53
3.3 The MPG improvements of the study of PnG synchronization for homogeneous platoons. 55
3.4 The control concept of the proposed PnG synchronization method. . 56
3.5 The example of target phase portrait. 60
3.6 The example of parameterizing the target phase portrait with phase angle. 61
3.7 The trajectories of the case with synchronization. 66
3.8 The synchronization of the phase angles of the virtual oscillators. . . 67
3.9 The steady state phase portraits of the vehicles with synchronization. 68
3.10 The example of deviations from desired trajectories of the case with PnG synchronization. 68
3.11 The trajectories of the case without synchronization. 69
3.12 The summary of the MPG improvements of PnG synchronization. . 70
4.1 Validation of the assumption of constant acceleration/deceleration in pulsing with 10% speed oscillation. 75
4.2 Validation of the assumption of constant acceleration/deceleration in gliding with 10% speed oscillation. 75
4.3 Validation of the assumption of constant acceleration/deceleration in pulsing with 30% speed oscillation. 76
4.4 Validation of the assumption of constant acceleration/deceleration in gliding with 30% speed oscillation. 76
4.5 Variations of MPG with respect to the variations of vehicle mass, speed oscillation, and road grade: 40 mph. 82
4.6 Variations of MPG with respect to the variations of vehicle mass, speed oscillation, and road grade: 60 mph. 83
4.7 Road grade statistics. 83
4.8 The road grade profile and statistics of Sutton Road in Ann Arbor. 84
4.9 The road grade profile and statistics of Sutton Road in Ann Arbor in one round trip. 85
4.10 The adjusted road grade profile and statistics in one round trip. . . 85
4.11 The MPG results for different road grade profiles. 86
4.12 The control loop of target state tracking in PnG synchronization. . 90
4.13 The target phase portraits of the case with $\tau_{\mathrm{PV}} = 0.5$ s. 95
4.14 The target phase portraits of the case with $\tau_{\mathrm{PV}} = 1$ s. 96
4.15 The trajectories of the case with all-to-all communication. 97
4.16 The trajectories of the case with bidirectional communication. . . . 97
4.17 The results of MPG improvements of the study of communication topology. 98

4.18 The trajectories of the case with 10 times the Kuramoto gain from theory. 99
4.19 The results of MPG improvements of the study of Kuramoto gain. . 99
5.1 The test route for low speed cases for the PnG experiment. 106
5.2 The test route for high speed cases for the PnG experiment. 107
5.3 The example of the phase portrait for deciding the PnG switching timing. 110
5.4 The schematic diagram of the linear regression approach for correcting MPG due to SOC variations. 112
5.5 The schematic diagram of the moving window approach for correcting MPG. 114
5.6 The schematic diagram of the linear regression approach for correcting MPG for both SOC and elevation variations. 114
5.7 The latitude, longitude, and elevation from RTK in low speed cases. 115
5.8 Part of the speed trajectory of the PnG case at 30 mph with 0.8 m/s^2 target pulsing acceleration. 116
5.9 The experiment results of cases with 30 mph. 120
5.10 The experiment results of cases with 40 mph. 121
5.11 The experiment results of cases with 50 mph. 121
5.12 The experiment results of cases with 60 mph. 122
5.13 The experiment results of cases with 70 mph. 122
5.14 The experiment trajectories of the CS case at 40 mph. 123
5.15 The experiment trajectories of the PnG case at 40 mph. 124
5.16 The experiment trajectories of the CS case at 60 mph. 125
5.17 The experiment trajectories of the PnG case at 40 mph. 126

LIST OF TABLES

Table

2.1 The vehicle parameters of the simulation studies of PnG in car-following. 21
3.1 The vehicle parameters of the simulation of PnG synchronization. . 52
4.1 Sensitivity coefficients of average power required for Speed-PnG. . . 79
5.1 The vehicle parameters of 2015 Lincoln MKZ hybrid used in the PnG experiment. 104
5.2 Improvements of corrected MPG in the PnG experiment. 117

LIST OF ABBREVIATIONS

PnG pulse-and-glide

PS pseudo-spectral method

LGR Legende-Gauss-Radau

PV preceding vehicle

FV following vehicle

MPC model predictive control

CAFE corporate average fuel economy

MPG miles per gallon

CAV connected and automated vehicle

V2V vehicle-to-vehicle

V2I vehicle-to-infrastructure

CACC cooperative adaptive cruise control

ACC adaptive cruise control

DSRC dedicated short-range communications

ICE internal combustion engine

ecoAND eco-approach and departure

RTK real-time kinetics

OBD on-board diagnostics

CANbus controller area network

PID proportional-integral-derivative

SOC state of charge

CCC connected cruise control

A2A all-to-all communication

BD bidirectional communication

PF predecessor-follower communication

2PF two-predecessor-follower communication

PLF predecessor-leader-follower communication

ABSTRACT

This research studies the intersection of two technologies to improve fuel economy, i.e., pulse-and-glide (PnG) and cooperative adaptive cruise control (CACC). By exploiting the characteristics of internal combustion engines (ICEs), PnG periodically turns on and off the engine to save fuel. On the other hand, CACC facilitates the vehicle platooning via vehicle-to-vehicle (V2V) communication. CACC is promising to both increase the traffic throughput and reduce the fuel consumption. This research explores the possibilities for more fuel saving potential by introducing PnG into CACC. It also addresses the speed oscillation problem resulting from PnG operations, which is a challenge to vehicle platooning in terms of both string stability and ride comfort.

To address these challenges, first the PnG operation of a hybrid electric vehicle (HEV) in the car-following scenario is studied with ride comfort considerations. The proposed control consists of two minimum-time control problems, one for the pulsing phase and another for the gliding phase. These two problems are solved using model-predictive control (MPC). After a series of simplification, convexification, and sparsity optimization, the two minimum-time control problems are reformulated as quadratic programming (QP) problems using the pseudo-spectral (PS) method to be solved on-line efficiently. This proposed control establishes a framework that can effectively leverage PnG for fuel savings, while satisfying the ride comfort and safety constraints.

For the problem of platooning heterogeneous PnG vehicles, the concept of PnG synchronization is proposed as a solution. A control approach is developed based on the Kuramoto oscillator model to realize this concept. More specifically, individual ve-

hicles in the platoon maintain their own virtual oscillators. With the synchronization mechanism provided by the Kuramoto model, the virtual oscillators are synchronized via only local communications. By tracking the target trajectories given by the virtual oscillators, PnG synchronization is achieved. A range-keeping approach via V2V communication is also developed. This proposed method of PnG synchronization is able to maintain the fuel saving potentials of individual PnG vehicles while keeping the platoon compact, which is ideal for achieving high throughput.

The naturalistic driving data from the Safety Pilot project are utilized to analyze the levels of acceleration that people experience in everyday driving. Also, a PnG experiment is conducted using an automated Lincoln MKZ. The results from this experiment validate the fuel saving ability of the proposed PnG technique, especially at lower speeds, and offer a better knowledge about the influence of PnG operations on ride comfort.

CHAPTER I

Introduction

1.1 Motivation

According to the U.S. Energy Information Administration, 38,434 trillion BTU of energy was consumed for transportation in the U.S. in 2019, occupying 28.3% of the total energy usage [1]. In 2020, the pandemic caused by the novel coronavirus disease (COVID-19) forced governments of countries around the world to take different mitigation efforts to slow down its spreading, which significantly impacted the everyday mobility of people. Compared to 2019, the energy consumption for transportation in the first 7 months of 2020 decreased by around 15% [1]. Even so, the gasoline price has recovered from the drop in early 2020 and is predicted to continue increasing in the near future, as shown in Figure 1.1 [2]. Given that fossil fuel is non-renewable, improving the efficiency of transportation is still an important topic.

In transportation, a large portion of the energy is consumed by light-duty vehicles and a significant amount is in the form of motor gasoline [3]. This trend is predicted to remain the same in the future, as shown in Figure 1.2. The OEMs are thus required to improve the fuel economy of their production vehicles according to the regulation of corporate average fuel economy (CAFE) [4]. The CAFE standard sets the requirement of fuel economy based on the size of the vehicles. For passenger cars and light trucks, by 2025 they respectively need to achieve 45.61 to 61.07 miles per

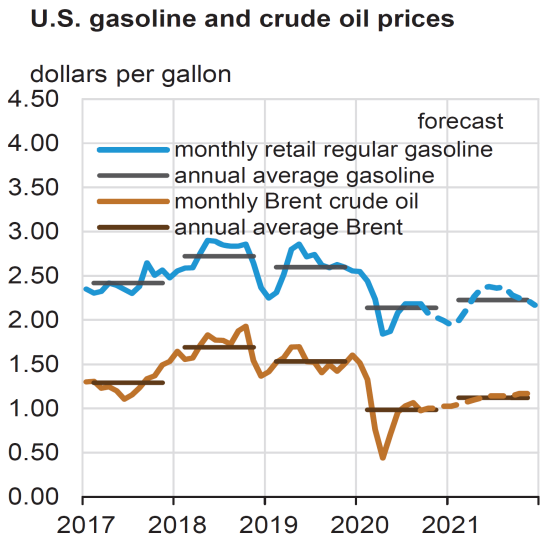

Figure 1.1: The U.S. gasoline and crude oil prices in recent years [2].

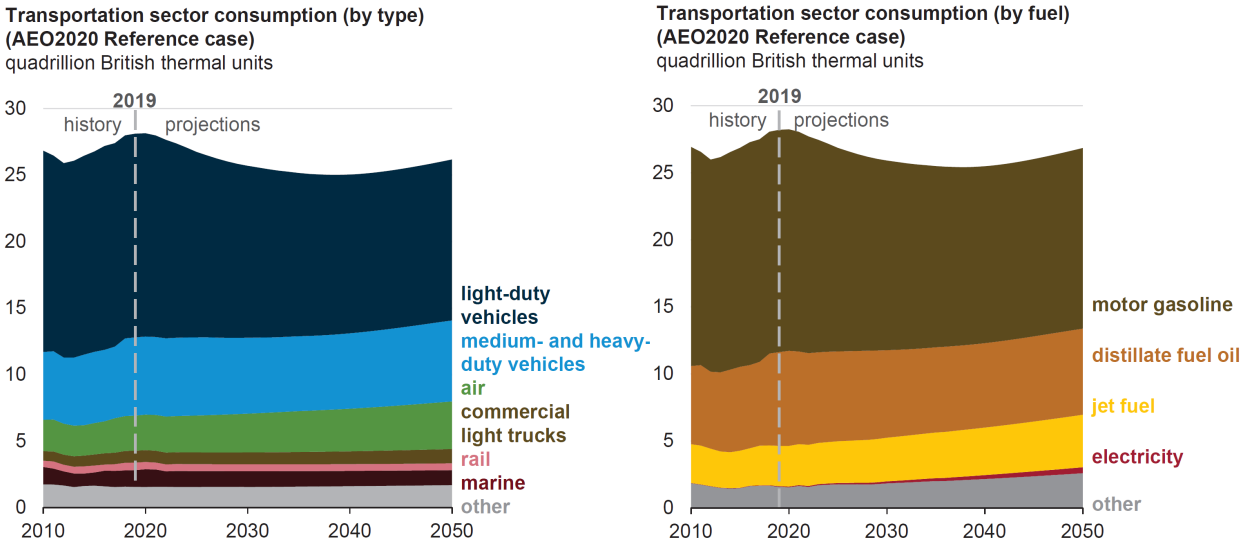

Figure 1.2: The U.S. transportation sector energy consumption in recent years and prediction [3].

gallon (MPG) and 30.19 to 50.39 MPG, with the principle that the larger the vehicle size is, the lower the MPG value is.

Several well-established technologies have been developed and implemented to reduce the fuel consumption during the past decades, such as engine downsizing and boosting [5], vehicle light-weighting [6], aerodynamic improvements [7], rolling resistance reduction [8], engine efficiency improvements [9], waste heat recovery [10], auxiliary and parasitic load reduction [11, 12], electrification and hybridization [13, 14]. These measures basically achieve improvement of fuel economy by modifications or new design of vehicle components. With hybridization, one more power source is added to the powertrain, which creates more possibilities for better powertrain efficiency. Many research efforts have been devoted to the power management control of hybrid vehicles. In power management control, the outputs of engine and motor(s) are optimally determined to meet the driver's demand. A detailed review for power management strategies for hybrid vehicles is given in [15]. However, the driver's demand itself may not be optimal in terms of fuel saving. This leads to the topic of eco-driving, which explores how the vehicle can be driven in a way that consumes less fuel, rather than simply managing the power outputs from different sources for a given speed profile. In fact, eco-driving is not limited to hybrid vehicles, but also a topic for conventional internal combustion engine (ICE) vehicles. In [16], it is reported that, as much as 10% fuel consumption can be influenced by how the vehicle is driven by the driver.

As early as 1976, an eco-driving technique realized by the periodic control of ground vehicles has been introduced [17]. This periodic control has later on been called pulse-and-glide (PnG) [18] and is a technique that is often utilized in the super-mileage competitions [19]. The mechanism of PnG operations for saving fuel can be explained with the help of Figure 1.3. The concave-convex shape of the fuel-rate curve of best fuel rate against engine power output leads to the improvement

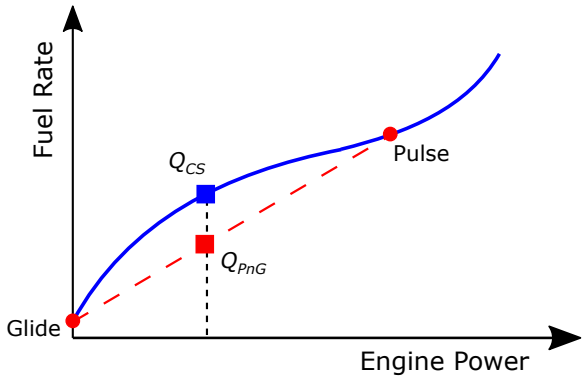

Figure 1.3: The mechanism of PnG for fuel saving. The fuel rate of constant-speed driving is denoted by Q_{CS} and that of PnG operation is by Q_{PnG}. In the concave region, Q_{PnG} is below Q_{CS}, leading to reduced fuel consumption.

of fuel economy using PnG. As shown in Figure 1.3, the average fuel consumption resulting from switching between the pulsing and gliding points is lower than the constant-speed operation at the same drive power. In particular, the pulsing and gliding points respectively correspond to operating the engine at the most efficient point and turning off the engine. This alternate switching of PnG operation leads to the oscillation of vehicle speed.

The PnG mechanism is actually in line with the concept of velocity relaxation introduced in [20], in which the target speed profile is relaxed to create the room to optimize the fuel economy and in fact the PnG-like behavior is observed accordingly. In [21], the results of a controller established via stochastic dynamic programming also show PnG-like behavior. In addition to numerical simulations, real driving experiments in [22] using an ICE vehicle achieves 43.4% improvement of fuel consumption around 40 kph with PnG.

On the other hand, for a hybrid vehicle with a battery, the battery can serve as yet another energy buffer in addition to the vehicle body, which is the only choice for ICE vehicles. In other words, during the pulsing phase the energy from engine can either be temporarily stored in the battery or vehicle body. The stored energy is then released to drive the vehicle during the gliding phase. The PnG operation

using vehicle bodies as the energy buffer is termed Speed-PnG, while the one using batteries is called SOC-PnG [23]. Even though SOC-PnG can avoid the ride comfort concerns of Speed-PnG caused by the speed oscillations, its fuel saving potential is lower than that of the Speed-PnG [23, 24]. It also reveals the nature of trade-off between fuel saving and ride comfort in the PnG operations. In this dissertation, when using the term "PnG", we mean the type of PnG operations that will result in speed oscillations rather than pure SOC-PnG using batteries as the only energy buffer, unless stated otherwise.

In recent years, connected and automated vehicle (CAV) technologies have been developed and are believed to have the potential to improve not only the safety, but also the fuel economy of ground transportation [25, 26]. CAV technologies involve the automation of vehicle controls and the connection between individual vehicles and/or infrastructures. With the sharing of information between surrounding vehicles and nearby infrastructures via connectivity, the vehicles can be better informed about their traffic environment. Actually, by communication between only a few vehicles in a vehicle string, the traffic efficiency and stability can already be improved, as pointed out in [27] with the concept of connected cruise control (CCC). If a series of vehicles are all equipped with CAV capabilities, more sophisticated control strategies can be implemented to further achieve better performance, which might not be possible by only human drivers. The communication between vehicles is called vehicle-to-vehicle (V2V) communication, while that between vehicles and infrastructure is called vehicle-to-infrastructure (V2I) communication. They are together called V2X communication [28]. Researchers have focused on several applications for different driving scenarios using the CAV technologies. Examples include merging at highway on-ramps [29], roundabout entering [30], speed harmonization in highway traffic [31], eco-approach and departure (ecoAND) at road intersections [32], and cooperative adaptive cruise control (CACC) [33].

Like the traditional adaptive cruise control (ACC), CACC is mainly applied in cruising scenarios. However, CACC utilizes V2V communication technologies, such as dedicated short-range communications (DSRC) [34], to facilitate vehicle platooning. With CACC, vehicles are able to cruise at shorter inter-vehicle distances compared to the cases with traditional ACC [35]. Shorter inter-vehicle distances lead to higher traffic throughput. In other words, the efficiency of the traffic systems can be increased. Furthermore, with the information of surrounding vehicles sent via V2V communication, unnecessary acceleration and braking can be avoided. Better fuel economy can be thus achieved. In addition, aerodynamic drag of the following vehicles (FVs) in a platoon can be potentially reduced if they are driven closely to the preceding vehicles (PVs). This further decreases the fuel consumption. As shown in [36] via the reduced-sized wind tunnel experiments with passenger car models of 0.619 m length, the air drag coefficient drops by more than 15% for the second vehicle in the platoon if the inter-vehicle distance reaches less than 3 vehicle length. Even more reduction in air drag coefficients happens for the third and forth vehicles in the experiment of four-vehicle platoon. In addition, vehicles forming a platoon in coordination with the traffic light can pass the road intersection with overall delay and stops reduced, thus leading to fuel saving and higher transportation efficiency [37]. As a result, CACC is believed to be a viable technology that increases traffic capacity and achieves better fuel economy.

Motivated by the above encouraging capabilities, we thus seek the possibility of further improving the fuel economy by the synergy of PnG and CACC. More specifically, realizing CACC through PnG is focused on in this study. The detailed literature review and the gaps identified in the literature are given in the following section.

1.2 Literature Review

1.2.1 Pulse-and-Glide Operations

The concept of alternately turning on and off the engine based on the characteristics of ICE engines to save fuel is introduced in 1976 [17]. In [18], simulation results show 30 to 77% MPG improvement for a 2007 Ford Focus and 24 to 90% for a 2004 Toyota Prius at low speeds (25 to 35 mph). Compared to the simulation results, roughly 4% reduction of MPG improvement is observed for the cases of Toyota Prius in the dynamometer experiment. It is also pointed out in [18] that further studies on the PnG operations for the hybrid vehicles are needed. In [38], an optimal control problem of the car-following scenario is formulated. In this problem, the FV is controlled to follow a constant-speed PV with the goal of minimizing the fuel consumption. The solution of the optimal control problem shows that as opposed to the usual driving strategy of constant-speed in cruising, PnG is the optimal control for low to medium speeds in terms of fuel saving. Roughly 35% to 15% fuel saving is achieved from 22 mph to 67 mph, with fuel saving percentage decreasing with the increase of speed. Further in [39], a rule-based switching strategy is developed to decide the timing of PnG switching in the car-following strategy. Up to 20% fuel economy improvement is achieved in simulations, and the same trend of decreased fuel saving with speed increase in [38] is also observed. In [40], the mechanism of PnG for saving fuel is further studied using the well-known Bittanti's π-test [41], which is a tool to estimate whether better performance is possible by periodic control compared to constant control inputs. Reference [40] constructs the theory basis of PnG that concludes that PnG operation is optimal in the concave region of the fuel-rate curve in Figure 1.3.

In [23], the PnG of a parallel hybrid vehicle is studied. The PnG operation with vehicle body for temporary energy storage is termed the Speed-PnG, while the one

using only the battery to store the energy is termed the SOC-PnG. Therefore, in SOC-PnG the battery state of charge (SOC) oscillates, rather than the vehicle speed in Speed-PnG. The numerical solutions obtained in [23] indicate that the fuel saving potential of both Speed-PnG and SOC-PnG decreases as the speed increases, but with SOC-PnG being less effective in saving fuel at every speed. In brief, the research efforts mentioned above establish the theory and analysis of PnG, and indicate the relationship between fuel saving potential and speed. However, the question of whether the ride comfort will be significantly influenced by PnG due to the speed oscillation is not addressed. Especially in autonomous vehicles, drivers may become more sensitive to the vehicle acceleration and deceleration and have lower levels of tolerance for motion oscillations [42].

As shown in [23], SOC-PnG may be more favorable in terms of ride comfort, but the fuel saving performance is much lower than that of Speed-PnG. Therefore, SOC-PnG may not be the most ideal solution to ride comfort concerns. In [43], the ride comfort issue caused by jerks in PnG is analyzed by applying the Pontryagin minimum principle to the formulated optimal control problem. It establishes an approach to determine the PnG period based on the requirement of jerk level. However, the impact of PnG acceleration on ride comfort is not considered in [43]. The influence of Speed-PnG on ride comfort with both jerk and acceleration considered is studied using numerical simulations in [44]. This research tries to quantify the relation between fuel saving and ride comfort based on the comfort index established from the experiment with different participants [45]. The suggested requirements for ride comfort are acceleration less than 0.3 m/s^2 and jerk between -6 to 4 m/s^3. This set of suggested ride comfort requirements corresponds to the level of "noticeable only to skeptical customers." With this set of requirements, 28.2% and 5.2% fuel savings are achieved respectively at 30 kph and 90 kph on a 2.0L ICE vehicle, and 22.3% and 2.2% on an ICE vehicle with 1.2L engine. However, Reference [45] does not propose a control

method to fulfill the ride comfort in PnG.

Based on this literature review, a control framework for PnG that is able to effectively leverage ride comfort limits for fuel saving is still necessary to advance the realization of PnG implementation in real world, especially given that ride comfort requirements are very subjective and the PnG benefits differ on different vehicles.

The influence of PnG on traffic smoothness and fuel saving performance in mixed traffic flow is studied in [46] via numerical simulations. The mixed traffic flow is composed of automated vehicles conducting PnG and manually driven conventional vehicles that follow the intelligent driver model [47] in simulations. The manually driven vehicles may save or waste fuel depending on the speed and acceleration of the lead PnG vehicle that they are following. Furthermore, it is pointed out in [46] that average speed and level of penetration of PnG vehicles are the two major factors affecting traffic smoothness and overall fuel consumption. The overall fuel benefit becomes larger if the penetration of PnG vehicles is higher [46]. In [48], the rule-based switching approach in [39] is extended to the case with PV also conducting Speed-PnG and applied to a platoon. It shows that in a homogeneous platoon the proposed PnG switching method can achieve overall 21.8% fuel saving around 45 mph, compared to the case with linear quadratic controllers. However, in the cases of heterogeneous platoon, where the heterogeneity is characterized as acceleration deviations, it is observed that undesired PnG switchings and range violations happen more frequently with the increase of heterogeneity. The rule-based PnG switching is further refined by the same group of researchers and applied to the heterogeneous platoon in [49]. It shows that the switching frequency and range violation are improved with larger range oscillation. However, this tends to enlarge the platoon length, which may reduce the overall traffic system efficiency that CACC originally aims to improve. Therefore, without degrading the traffic throughput, how to effectively platoon the PnG vehicles to maximize the fuel economy while maintaining the individual drivers' ride comfort

is still an open question.

As to the PnG experiments using real vehicles, a 2004 Toyota Prius is tested on the chassis dynamometer in [18]. For PnG cases oscillating between 20 to 30 mph and 30 to 40 mph, 44% and 87% MPG improvements are achieved respectively. However, the authors in [18] indicate that the SOC variations influence the results significantly, so the simulation results with multiple repeated PnG cycles aiming to average out the SOC influence are also reported, which reach 36% to 65% MPG improvements with the same speed ranges of the dynamometer tests. In [50], an ICE vehicle Renault Clio 3 Eco 2 with 5-speed manual gearbox is used to test the PnG on a test track. The test vehicle is operated by a well-trained driver to implement PnG in the ranges of 50 to 70 kph and 90 to 110 kph, from which roughly 12% and 13% fuel savings are achieved respectively. Reference [22] reports the results of an automated ICE vehicle Nissan X-trail tested on a test course. A fuel saving performance of 43.4% is achieved around 40 kph. For highway, the researchers resorted to numerical simulation instead and obtained roughly 8% fuel economy improvement. As such, the PnG performance of real vehicles under different speeds is still open for exploration.

1.2.2 Cooperative Adaptive Cruise Control

As an application of CAV technologies, CACC has attracted increasing attention from researchers. Many works are presented in the literature in this domain; however, most of them focus on string stability or safety, and less on improving fuel economy.

References [51] and [52] utilize the consensus control approach via V2V communication to control the distances between the vehicles. In these works, the target is to maintain desired platoon formations. In other words, in steady state the vehicles drive at the same speed. Therefore, these approaches intrinsically lose the potential for fuel saving by allowing flexible inter-vehicle ranges. In [53], a controller based on reinforcement learning is established. This controller takes through V2V communica-

tion the acceleration information of the PV as input and maintains the constant time headway. In [35], the acceleration information of PV is transmitted to the FV and constitutes the feedforward term of the controller in addition to the proportional-derivative control based on measured relative speed and inter-vehicle range. This research shows that by including the PV acceleration for the feedforward control, smaller time headway can be achieved without losing the string stability compared with the case with traditional ACC. Reference [54] further tackles the communication delay issue based on the control approach proposed in [35]. When the communication is less reliable, the acceleration information of the vehicle right in front of the PV is exploited additionally. This way, the string stability can still be maintained under the condition of communication delay. Moreover, some works adopt the model predictive control (MPC) approach for CACC. In [55], a robust MPC approach is proposed to maintain close to the minimum safety distance. A control method based on the sliding-mode control for CACC is presented in [56]. In this paper, the focus is on the impact of communication related parameters on the platoon performance, specifically the minimal inter-vehicle range that can be achieved. It is concluded that under realistic communication delay and actuator lag, message frequency of 10 Hz is suggested to maintain the vehicle platoon. Higher frequency might be unnecessary and could congest the communication channel. In [57], a data-driven CACC approach via on-line reinforcement learning is proposed to control the buses travelling on an exclusive bus lane. A 30% increase of bus service volume is achieved without sacrificing the travel time in simulations.

Communication issues may adversely influence the platoon string stability. In [58], the Kalman filter is used to estimate the PV acceleration. When temporary communication loss happens, this estimate is used to improve the car-following capability of the vehicles in a platoon. Similarly, for the issue of communication loss, in [59] a switching controller based on the H_∞ control is developed to robustly stabilize

the platoon when communication loss happens. To efficiently use the communication resources and avoid the channel congestion, the approach of event-triggered control is applied to stabilize the vehicle platoons, especially under actuator delays and disturbances [60, 61]. Reference [62] proposes an on-line method to exploit different communication topology to improve the string stability under imperfect communication.

The potential of CACC in vehicle platooning for fuel saving is explored in [63]. In the simulation with the leading vehicle following a modified FTP-75 driving cycle and the full knowledge of future speed profile of the PVs, it is shown that the fuel saving achieved ranges from 14.7% to 33.4% in a seven-vehicle platoon, depending on the position of the vehicles. Also demonstrated in [63] are the cases with different length of time horizons of knowledge for future speed information. It is shown that the longer the time horizons are, the closer the fuel saving approaches to that of the full knowledge case. This indicates the potential of V2V communication, which may provide the ability to better predict into the future to save the fuel. On the other hand, Reference [63] also shows that the larger the floating margins (the allowed variation of inter-vehicle distance) are, the higher the fuel saving potential is. This benefit of flexible range is directly pointed out in [64]. Reference [64] states that more flexible policies of inter-vehicle distances can create more degrees of freedom for fuel saving. However, similar to the case of increasing the inter-vehicle range for PnG operations, larger distances between vehicles would decrease the overall traffic throughput, which is against one of the original purposes of CACC. Therefore, proper coordination between the vehicles in platoons is required.

Even though the tasks under CAVs are often studied separately, the scenarios of CACC combined with other tasks have also been explored in literature. For example, CACC is combined with ecoAND at the road intersections in [65, 66]. In this case, the main purpose is to facilitate the vehicles to form platoons such that they can pass the

intersection efficiently in different directions, like Reference [37] introduced previously. Another example is combining CACC with the merging scenarios on highways [67]. For the combined tasks of CACC-ecoAND and CACC-merging, the communication in general involves both V2V and V2I communication. The infrastructures at the intersections or merging ramps can be controlled accordingly, as well.

Another important research topic of CACC in recent years is about cyber attack and security. Similar to other systems of internet of things, e.g. microgrids, the vehicles are connected and form a network in CACC. Any malicious behaviors intruding this network can lead to serious consequences. In this topic, researchers focus on how to detect the threats in a timely manner and try to avoid or mitigate the resultant damage [68, 69, 70, 71].

From this literature review, it can be seen that most of the research on CACC is devoted to keeping platoon formation and/or maintaining string stability. With these purposes, some works bring communication delays, communication losses, actuator lags, model uncertainties, and other disturbances into the scope. These works try to realize the goal of increasing traffic throughput, the benefit anticipated by platooning, with the help of CAV technologies. However, only quite limited number of works are dedicated to improving fuel economy. In [63] and [64], even though the concept of creating room for reducing fuel consumption by allowing variations of inter-vehicle ranges is introduced, directly bringing the PnG operations to CACC is not considered. To think from the opposite perspective, relaxing inter-vehicle ranges for fuel saving implies that those approaches invented for keeping platoon formation are not suitable for PnG platoons, since the flexibility that could be used for improving fuel economy will be lost. For example, if the whole platoon is controlled to travel with a rigid formation, the fuel saving performance of the FVs will be dictated by the lead vehicle. When the lead vehicle cruises at constant speed, the FVs cannot fulfill PnG under these control approaches. Even if the lead vehicle conducts PnG, the FVs need to

follow the same PnG pattern. This may cause the loss of some fuel saving potential and/or sacrifice the ride comfort for the FVs, especially given that PnG benefits differ from car to car and ride comfort requirements change from driver to driver. On the other hand, even though the PnG operation is applied to the platoons in [48] and [49], the problems of avoiding frequent PnG switching caused by heterogeneity and keeping the platoons compact for higher traffic throughput still persist.

1.3 Objectives, Scope of the Study, and Approaches

The overarching goal of this dissertation is to realize CACC through PnG to maximize the fuel saving potential of vehicles in a platoon. The literature survey above shows that in spite of numerous encouraging results, an on-line control framework for PnG that can effectively leverage ride comfort limits for fuel saving is missing, especially for HEVs. Also, the issue of undesired PnG switchings in heterogeneous platoons is still unresolved. Therefore, filling these gaps is necessary to achieve our goal.

First, the topic of PnG operations in car-following is studied. To develop a control framework that is flexible to include different requirements and is able to deal with uncertainties and disturbances in a more systematic manner, an MPC approach is adopted. The developed method must be able to effectively maximize the fuel saving potential from PnG under different ride comfort requirements. Moreover, this control needs to be on-line implementable. A series of convexification and simplification techniques are thus explored to solve MPC efficiently. For ride comfort, also for the purpose of reducing the computational load, we only consider the levels of acceleration and deceleration, rather than jerks. The ride comfort concern from jerks is assumed to be taken care of by the low-level actuator control and is not considered in this study.

For the platooning problem, we only concentrate on the development of strate-

gies for achieving the highest possible fuel saving potential, rather than on the string stability. Our rationale is that keeping safety is always the top priority. If the platoon encounters a situation where PnG may be risky, we simply deactivate the PnG function and let the approaches developed for maintaining safety distances take over. To tackle the challenges for platooning PnG vehicles pointed out in literature, we develop the idea of PnG synchronization, such that the vehicles in a platoon can preserve the freedom to pursue fuel saving while keeping the platoon compact. For the PnG synchronization in heterogeneous platoons, a control approach is developed based on the Kuramoto oscillator model [72]. The Kuramoto oscillator model provides a synchronization mechanism that only relies on local communication. The rich research outcomes of the Kuramoto model in literature also provides a strong theory basis for further study [73, 74].

After developing the control for PnG synchronization, we conduct the sensitivity analysis on one single PnG vehicle to study how different parameters influence the fuel savings. The results tell us that the amount of speed oscillations does not affect the fuel saving potentials significantly in practical applications. This finding simplifies our analysis on how to design the control gains, Kuramoto gain, and PnG period. Given these control parameters, designing proper range policies that can ensure safety while keeping the platoons compact is out of the scope of current research and is left for future study.

1.4 Contributions

The contributions of this dissertation can be summarized as follows.

- A control method based on minimum-time control is developed for PnG implementation on HEVs in car-following. This method is on-line implementable and helps balance the trade off between fuel saving and ride comfort, while achieving

SOC sustenance.

- Real driving data from Safety Pilot dataset [75] is analyzed to set the ride comfort requirement for PnG. The PnG fuel saving potential is also studied using the naturalistic driving data from Safety Pilot dataset.

- A decentralized control approach for PnG synchronization in heterogeneous platoons based on the Kuramoto oscillator model is presented. This approach only relies on local communication and is able to maintain the fuel saving potentials of different vehicles while keeping the platoons compact.

- The guidelines for designing control and platooning parameters for the proposed method for PnG synchronization are presented. These step-by-step design instructions ensure the successful implementation of the proposed control method.

- The PnG experiment is conducted using an automated Lincoln MKZ hybrid vehicle and 13% MPG improvement is observed at low speed.

1.5 Outline of the Dissertation

This dissertation is organized as follows. In Chapter II, the performance and features of PnG operations of HEVs are studied through the proposed control for car-following. The results of PnG synchronization in heterogeneous platoons are presented in Chapter III. The analysis on the proposed PnG synchronization method is then analyzed in Chapter IV. Chapter V summarizes the results of physical experiments of PnG using a Lincoln MKZ hybrid vehicle. Conclusions and future work are given in Chapter VI.

CHAPTER II

Pulse-and-Glide Operations in Car-Following

2.1 Introduction

As indicated in [23], Speed-PnG can achieve significant fuel savings, but it may cause ride comfort concerns. On the other hand, SOC-PnG, in which the battery SOC oscillates instead of the vehicle speed, can lead to better ride comfort. However, it is less efficient because of battery ohmic losses.

Motivated by these observations, in this chapter we present the concept of introducing speed oscillation into SOC-PnG to seek a balance between fuel saving and ride comfort, while meeting the SOC sustenance requirements. Specifically, a control framework for hybrid electric vehicles (HEVs) with step-gear transmission is developed. In this framework, the vehicle oscillates around a desired range to the preceding vehicle (PV) with limited acceleration/deceleration. The acceleration/deceleration limits are intended to be at the discretion of the drivers to select according to the ride comfort levels they desire. Given that ride comfort is subjective for individuals and the sense of discomfort can gradually increase over time [42], it is important to have this freedom for ride comfort selection. The proposed framework creates the basis for future product design in fulfilling this purpose.

To achieve this goal, we formulate the PnG operation as two minimum-time control problems, one for the gliding phase and one for the pulsing phase. In the gliding phase,

the motor may need to provide some torque to reduce the deceleration. Therefore, the battery SOC will decrease. Then in the pulsing phase, the battery SOC drop that happened in the gliding phase needs to be restored. Based on the linearized vehicle dynamics, the approximation of SOC dynamics and its convexification using the McCormick envelope [76], and the sparsity optimization approach in [77], the two minimum-time optimal control problems are transcribed into quadratic programming (QP) problems via the pseudo-spectral (PS) method. The resulting problems can be solved efficiently by existing solvers.

The rest of this chapter is organized as follows. The vehicle models and the parameters used in this work are introduced in Section 2.2. Section 2.3 explains in detail the formulated minimum-time control problems and the solution strategy. Simulation results are presented in Section 2.4. Finally, conclusions and future work are given in Section 2.5.

2.2 Vehicle Model

In this work, we focus on a parallel HEV with step-gear transmission. The key parameters of the vehicle used in this chapter are summarized in Table 2.1. The engine brake specific fuel consumption (BSFC) map and the motor efficiency map are shown in Figure 2.1 and Figure 2.2 respectively, and the vehicle and SOC dynamics are described below.

2.2.1 Vehicle Dynamics

In this study, only the longitudinal vehicle dynamics is considered for the car-following scenario with the following constant time headway range policy:

$$R_{\text{des}} = d_0 + h_\tau v_P, \tag{2.1}$$

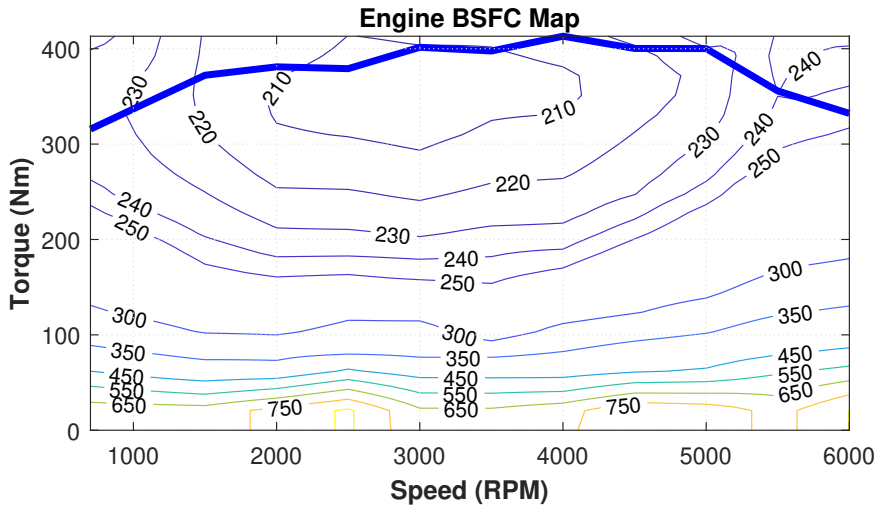

Figure 2.1: The engine map of the simulation studies.

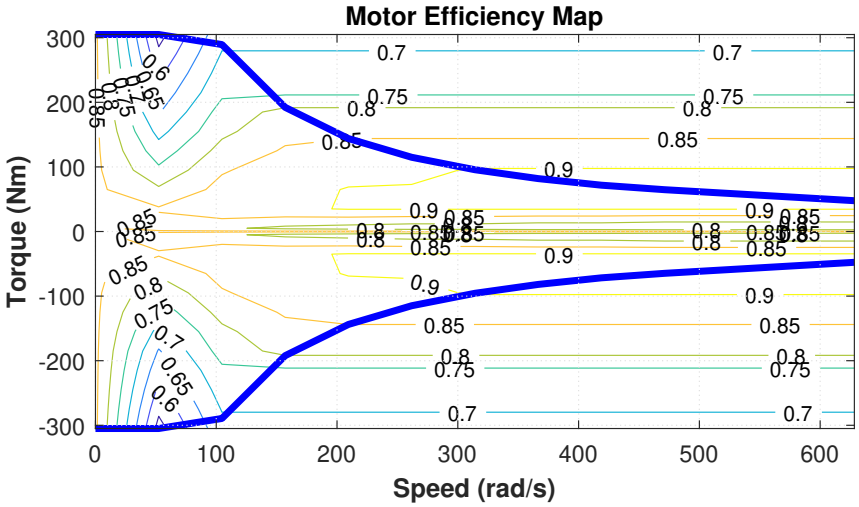

Figure 2.2: The motor efficiency map of the simulation studies.

where R_{des} is the desired range to the PV, d_0 is the standstill range, h_τ is the time headway, and v_P is the speed of PV. Then the dynamics of range error $dR := R - R_{\text{des}}$, where R is the range to the PV, is

$$d\dot{R} = -v + v_P + h_\tau a_P, \tag{2.2}$$

with a_P being the acceleration of PV. The dynamics of speed of the following vehicle (FV), which we control, is

$$\dot{v} = k_1 v^2 + k_2(T_e + T_m) - g f_r, \tag{2.3}$$

with $k_1 := -C_d \rho_a A_v/(2M_v)$ and $k_2 := \eta_T \eta_0 r_T r_0/(M_v r_w)$, where the vehicle parameters are as defined in Table 2.1. $T_e > 0$ and T_m are respectively the engine torque and motor torque, with $T_m > 0$ corresponding to battery discharging and $T_m < 0$ corresponding to battery charging.

2.2.2 SOC Dynamics

For the SOC dynamics, we adopt the widely-used open-circuit-voltage-resistance (OCV-R) model:

$$S\dot{O}C = \frac{-I_{\text{bat}}}{C_{\text{bat}}}, \tag{2.4}$$

where

$$I_{\text{bat}} = \frac{V_{\text{oc}} - V_{\text{oc}}\sqrt{1 - 4P_{\text{bat}}R_{\text{bat}}/V_{\text{oc}}^2}}{2R_{\text{bat}}} \tag{2.5}$$

is the battery current and C_{bat} is the nominal battery capacity. In addition, $P_{\text{bat}} = \eta_m P_m$ while charging and $P_{\text{bat}} = \eta_m^{-1} P_m$ while discharging. The motor efficiency η_m is obtained from Figure 2.2. The open-circuit voltage, V_{oc}, and the battery internal resistance, R_{bat}, are functions of SOC and defined as shown in Figure 2.3.

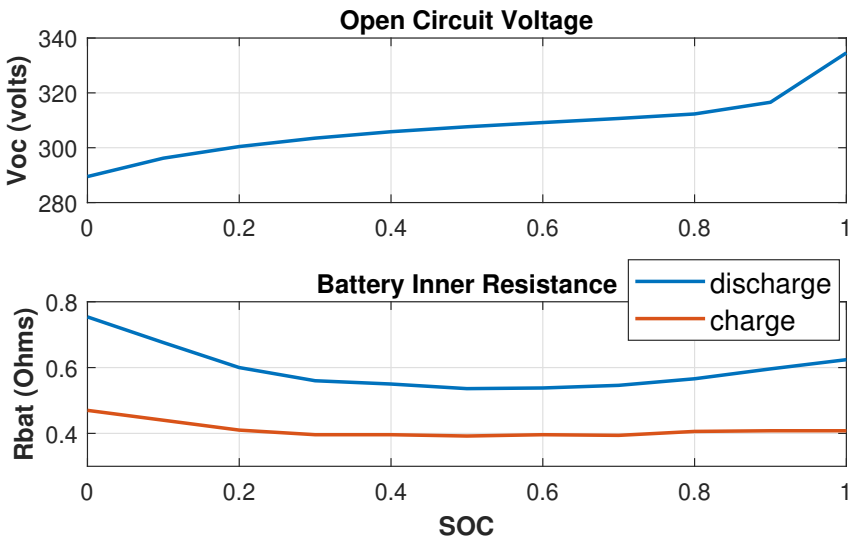

Figure 2.3: The open circuit voltage and battery inner resistance for the whole battery pack.

Parameter	Description	Value	Unit
M_v	vehicle weight	2948	kg
C_d	air drag coefficient	0.4	-
A_v	vehicle frontal area	3.26	m^2
ρ_a	air density	1.202	kg/m^3
f_r	rolling resistance	0.015	-
r_w	effective tire radius	0.3848	m
g	acceleration of gravity	9.81	m/s^2
r_T	gear ratio (gear 1-6)	[4.03, 2.36, 1.53, 1.15, 0.85, 0.67]	-
η_T	gear efficiency (gear 1-6)	[0.963, 0.971, 0.993, 0.993, 0.995, 0.993]	-
r_0	final drive ratio	3.23	-
η_0	final drive efficiency	0.966	-
C_{bat}	battery capacity	6	kWh

Table 2.1: The vehicle parameters of the simulation studies.

2.3 Methodology

In this section, the on-line implementation of the PnG operation is introduced. Two problems, one for the gliding phase and another for the pulsing phase, are formulated as minimum-time control problems. The longitudinal dynamics is linearized and the SOC dynamics is convexified. Then, with the adoption of the concept of sparsity optimization and convexification technique for minimum time problems in [77], the unknown variable of time to be minimized (the end time of these two individual problems) is avoided in the problem formulation. At last, the two problems are solved on-line in the MPC fashion via the pseudo-spectral method, which transcribes them into QP problems that can be solved very efficiently.

2.3.1 Problem Formulation

We assume the engine can be totally disengaged. Even though the engine sweet spot cannot be achieved at every speed as in the case of continuously variable transmission [39], the similar concave-convex shape of the fuel-rate curve can still be observed for a given engine speed, as shown in Figure 2.4 with 40 mph and 60 mph with gear 6 as examples, drawn from the engine map of Figure 2.1. Moreover, the gear is not changed in our PnG strategy. In other words, the engine will run at roughly the same speed. Therefore, PnG operation is still beneficial in terms of fuel saving for the vehicle with step-gear transmission used in this study.

Recall that the purpose of this work is to introduce speed oscillation to SOC-PnG, which originally can achieve constant speed for the FV when the PV is cruising at constant speed. The speed oscillation is introduced to recover some of the fuel saving potential from the Speed-PnG operations. To achieve this goal, we formulate two minimum-time control problems, one for the gliding phase and the other for the pulsing phase. The problems are solved every ΔT s using the MPC approach to counter the changing traffic environment. In the gliding phase, the vehicle glides to

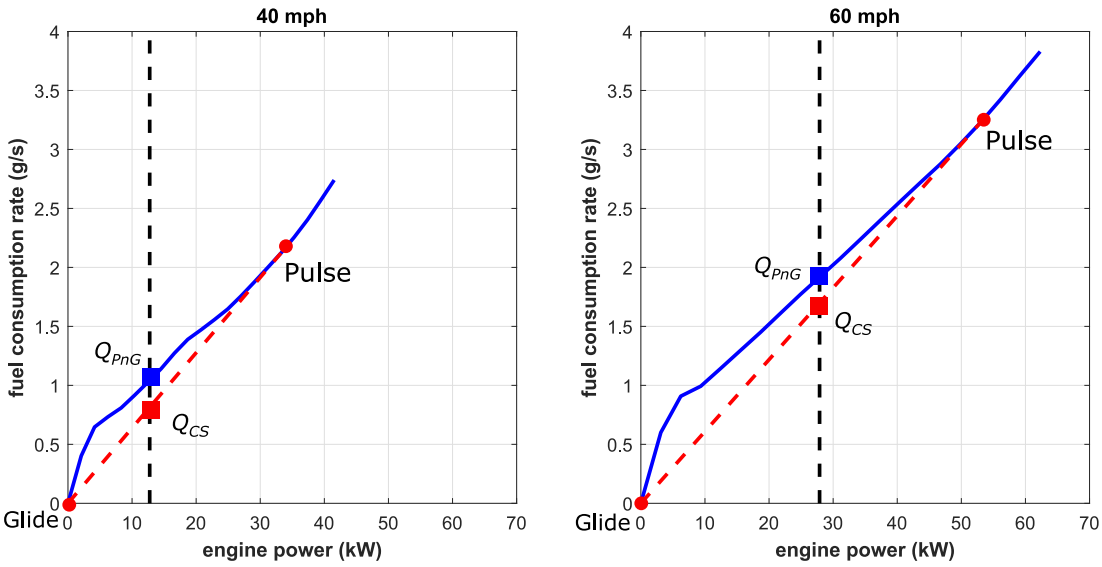

Figure 2.4: The fuel-rate curve for step-gear transmission at given speeds with gear 6. The fuel rate of constant-speed driving is denoted by Q_{CS} and that of PnG operation is by Q_{PnG}.

the preset minimum speed, $v_{\min}$, when it converges to R_{des}. On the other hand, in the pulsing phase the vehicle pulses to the preset maximum speed, $v_{\max}$, when it converges to R_{des} again. In the whole process, the range constraint (for safety) and the acceleration/deceleration constraints (for ride comfort) need to be satisfied. The problem formulations and how to solve them efficiently on-line are introduced next.

2.3.1.1 The Gliding Phase Problem

The purpose during the gliding phase is to minimize the battery power consumption while satisfying the constraints. The SOC drop resulting from this battery power consumption needs to be restored in the pulsing phase for the purpose of SOC sustenance. Therefore, less battery power consumption leads to better fuel economy in the whole PnG process. The battery power consumption is, however, directly linked to the deceleration constraint. Higher motor driving power leads to higher SOC drop and allows the vehicle glide to the minimum speed at a later time. On the contrary, with just enough motor driving power that can fulfill the deceleration constraint,

the battery power consumption can be reduced and the preset minimum PnG speed will be achieved earlier in this situation. With this rationale, we formulate the gliding phase problem as a minimum-time control problem such that the battery power consumption can be minimized while ensuring the satisfaction of constraints.

In the gliding phase, the constraint with respect to the minimum range error $dR_{\min}$ is more crucial compared to the one of $dR_{\max}$, since it may be easily violated if the initial gliding speed is too high or the PV is reducing its speed. The minimum-time control problem for the gliding phase is as follows:

$$\begin{aligned} \min_{T_m(t)} \quad & (t_{f,\mathrm{gld}} - t_{0,\mathrm{gld}}) \\ \text{s.t.} \quad & \text{vehicle longitudinal dynamics (2.2) and (2.3)} \\ & -d_{\lim} \leq a(t) \leq a_{\lim} \\ & 0 \leq T_m(t) \leq T_{m,\max}^{\mathrm{disch}} \\ & \dot{T}_{m,\min} \leq \dot{T}_m(t) \leq \dot{T}_{m,\max} \\ & dR_{\min} \leq dR(t) \leq dR_{\max} \\ & v_f(t_{f,\mathrm{gld}}) = v_{\min}. \end{aligned} \tag{2.6}$$

In (2.6), the time duration of gliding phase $(t_{f,\mathrm{gld}} - t_{0,\mathrm{gld}})$ is to be minimized. This optimal control problem needs to satisfy the vehicle dynamics and acceleration/deceleration limits, the constraint for motor torque variation, and the range error constraint.

Also, problem (2.6) needs to be solved every ΔT s until switching to the pulsing phase. The initial boundary conditions of dR and v are those at the current time $t_{0,\mathrm{gld}}$. The final boundary condition only includes the achieving of $v_{\min}$, since the vehicle will glide to lower speed such that R_{des} can be reached for sure. This can also help the convergence of problem solving, instead of adding too many constraints to problem (2.6).

2.3.1.2 The Pulsing Phase Problem

In the pulsing phase, the engine is turned on to drive the vehicle and charge the battery at the same time. The principle for achieving better fuel economy is now to operate the engine closer to the sweet spot. From Figure 2.1, we can see that the engine efficiency is higher with increased torque at any given engine speed. In practical applications, using the most efficient engine operating points at different engine speeds usually leads to high acceleration that will negatively influence the ride comfort. In other words, the efficiency of engine operation is limited by the acceleration constraint for ride comfort. Therefore, among the engine torques satisfying the acceleration limit, higher torque will result in faster convergence to the preset $v_{\max}$, which is also with higher engine efficiency. This leads to the formulation of the pulsing phase problem as the minimum-time problem as well. In the pulsing phase, the constraint with respect to the maximum range error dR_{max} is more crucial compared to that with respect to dR_{min}, since it may be easily violated if the initial pulsing speed is too low or the PV is increasing its speed. The optimal control problem for the pulsing phase is as follows:

$$
\begin{aligned}
\min_{T_m(t),\ T_e(t)} \quad & (t_{f,\text{pls}} - t_{0,\text{pls}}) \\
\text{s.t.} \quad & \text{vehicle longitudinal dynamics (2.2) and (2.3)} \\
& \text{SOC dynamics (2.4)} \\
& -d_{\text{lim}} \leq a(t) \leq a_{\text{lim}} \\
& T^{\text{ch}}_{m,\text{max}} \leq T_m(t) \leq 0 \\
& \dot{T}_{m,\text{min}} \leq \dot{T}_m(t) \leq \dot{T}_{m,\text{max}} \\
& 0 \leq T_e(t) \leq \bar{T}_{\text{sw}} \\
& \dot{T}_{e,\text{min}} \leq \dot{T}_e(t) \leq \dot{T}_{e,\text{max}} \\
& T_e(t) + T_m(t) \geq 0 \\
& dR_{\text{min}} \leq dR(t) \leq dR_{\text{max}} \\
& v_f(t_{f,\text{pls}}) = v_{\text{max}} \\
& SOC_f(t_{f,\text{pls}}) = SOC_{\text{target}}.
\end{aligned}
\tag{2.7}
$$

The objective function in (2.7) is to minimize the time duration of pulsing phase $(t_{f,\text{pls}} - t_{0,\text{pls}})$. The constraints in (2.7) are described as follows. The optimal control problem needs to satisfy the vehicle dynamics, acceleration/deceleration limits, and the range constraint. Both the engine torque and motor torque need to be within the desired range. The upper limit of T_e is set to $\bar{T}_{\text{sw}}$, the most efficient engine torque at the given engine speed. The motor torque for charging is also from the engine (here we do not consider regenerative braking), so $T_e + T_m$ needs to be greater than zero. In addition, in this phase, the SOC dynamics is considered for the purpose of SOC sustenance. In other words, the final SOC in this phase needs to achieve the target SOC, SOC_{target}, which is the SOC level at the beginning of the gliding phase. Similar to the gliding phase problem (2.6), the final boundary conditions only include the achieving of v_{max} in addition to that for the target SOC, since the vehicle will pulse to higher speed such that R_{des} can be reached surely.

Problem (2.7) also needs to be solved every ΔT s. The initial boundary conditions

of dR, v, and SOC are those at the current time $t_{0,\text{pls}}$. The final conditions are as just described above.

2.3.2 Solution Strategy

In this work, the Legendre pseudo-spectral method (PS) method with Legende-Gauss-Radau (LGR) collocation points [78] is adopted to solve the optimal control problems (2.6) and (2.7). However, if we directly apply the PS method to solve the whole PnG cycle, we need to use multi-interval PS due to the discontinuous nature of the PnG operation [79] and the time horizon of the problem will be too long for practical applications. The computation load will also be heavier and not ideal for real-time applications. In the following, a series of approximation strategies devoted to efficient on-line problem solving are introduced. Then the resultant quadratic problems are transcribed using the PS method to become QP problems.

2.3.2.1 Linearization and Approximation of the Dynamics

The longitudinal dynamics (2.3) is nonlinear, which will lead to a set of nonlinear constraints after applying the PS method. However, we can exploit the feature of small speed oscillation to linearize (2.3) around the average speed to obtain

$$\dot{v} = 2k_1\bar{v}v - k_1\bar{v}^2 + k_2(T_e + T_m) - gf_r, \tag{2.8}$$

where $\bar{v}$ is the average speed or the cruising speed of the PV.

The SOC dynamics (2.4) is also nonlinear. To solve the optimal control problem efficiently enough for a real-time application, the surface of $dSOC/dt$ is fitted with first order in both SOC and P_m as shown in Figure 2.5. Therefore, the SOC dynamics can be approximated as

$$\dot{SOC} \approx c_{00} + c_{10}SOC + c_{01}P_m, \tag{2.9}$$

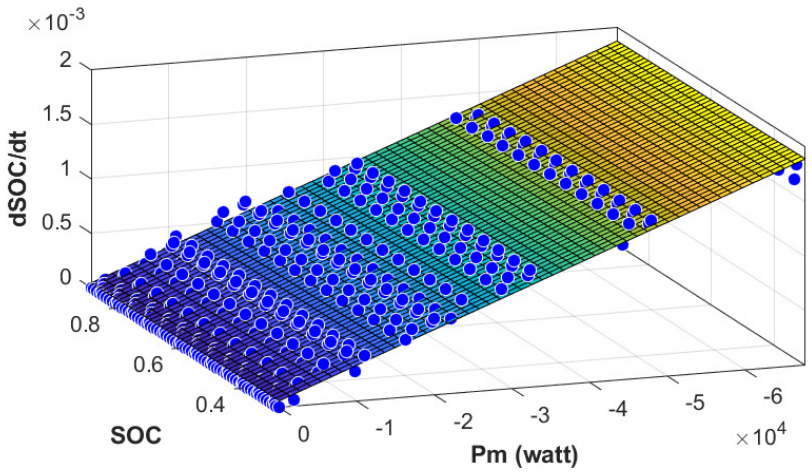

Figure 2.5: The fitting of the SOC dynamics during charging.

where $c_{00} = 7.919 \times 10^{-5}$, $c_{10} = -4.244 \times 10^{-5}$, and $c_{01} = -2.704 \times 10^{-8}$ for the vehicle model used in this study. However, due to the fact that $P_m = T_m \omega_m$, the SOC dynamics is not yet a linear constraint after being transcribed via the PS method. In addition, because there is no gear shifting in our PnG strategy, $P_m = c_{\omega v} T_m v$ with $c_{\omega v} := r_w r_T r_0$ being a constant. Therefore, P_m is a bilinear term in the state v and control T_m, both being unknown. We then adopt the conventional McCormick envelope approach [76] to convexify the bilinear term P_m as follows.

The underestimates of P_m are:

$$\begin{aligned} P_m &\geq (T^{\text{ch}}_{m,\min} v + T_m v_{\min} - T^{\text{ch}}_{m,\min} v_{\min})/c_{\omega v} \\ P_m &\geq (T^{\text{ch}}_{m,\max} v + T_m v_{\max} - T^{\text{ch}}_{m,\max} v_{\max})/c_{\omega v}, \end{aligned} \tag{2.10}$$

and the overestimates of P_m are:

$$\begin{aligned} P_m &\leq (T^{\text{ch}}_{m,\max} v + T_m v_{\min} - T^{\text{ch}}_{m,\max} v_{\min})/c_{\omega v} \\ P_m &\leq (T_m v_{\max} + T^{\text{ch}}_{m,\min} v - T^{\text{ch}}_{m,\max} v_{\max})/c_{\omega v}. \end{aligned} \tag{2.11}$$

As can be seen from (2.10) and (2.11), the constraints for P_m are linear. The tighter the upper and lower bounds of the variables are in the bilinear terms, the more

precise the convexification is. Because the speed oscillation is intended to be small in this work, the result of this approximation is acceptable, as will be seen from the simulation results.

2.3.2.2 Relaxing the Acceleration/Deceleration Constraints

For the gliding phase problem, to ensure feasible solutions, especially in the case of varying speed PV, the deceleration constraint is relaxed to become a soft constraint by adding a slack variable to it. This additional deceleration is achieved by a braking acceleration as an additional control variable. In this study, we simply assume this braking acceleration is provided by the friction brake. The slack variable of deceleration constraint and the braking acceleration will be penalized in the objective function.

Similarly, for the pulsing phase problem, a slack variable is added to the acceleration constraint such that it becomes soft. Then this slack variable is penalized in the objective function of the pulsing phase problem. This way, the control proposed can better handle the real traffic environment, especially with the fact that the subjective feeling of ride comfort does not abruptly change if the preset acceleration/deceleration limits are just slightly exceeded temporarily.

Therefore, the objective functions of (2.6) and (2.7) will become:

$$\min_{T_m(t),\ s_d(t),\ a_b(t)} \quad (t_{f,\mathrm{gld}} - t_{0,\mathrm{gld}}) + \int_{t_{0,\mathrm{gld}}}^{t_{f,\mathrm{gld}}} \Big[w_d s_d^2(t) + w_b a_b^2(t) \Big] dt, \tag{2.12}$$

and

$$\min_{T_m(t),\ T_e(t),\ s_a(t)} \quad (t_{f,\mathrm{pls}} - t_{0,\mathrm{pls}}) + \int_{t_{0,\mathrm{pls}}}^{t_{f,\mathrm{pls}}} w_a s_a^2(t) dt, \tag{2.13}$$

where s_a and s_d are respectively the slack variables of acceleration and deceleration

constraints, $a_b \leq 0$ is the braking acceleration, and w_a, w_d, and w_b are the associated weighting factors.

2.3.2.3 Sparsity Optimization Formulation for the Pulsing and Gliding Problems

In problems (2.6) and (2.7), the objects are respectively to minimize the gliding and pulsing duration by finding the unknown switching times, $t_{f,\text{gld}}$ and $t_{f,\text{pls}}$. If we directly apply the PS method, the unknown switching times will make the transcribed problems nonlinear because of the longitudinal vehicle dynamics and SOC dynamics. The objective functions (2.12) and (2.13) will also become non-quadratic due to the penalizing terms. Therefore, we adopt the strategy based on sparsity optimization in [77] to the pulsing and gliding phase problems.

The strategy in [77] for minimum-time control problem is summarized as follows. Consider a discrete minimum-time control problem:

$$\begin{aligned} \min_{u(0),\ldots,u(T-1)} \quad & T \\ \text{s.t.} \quad & x(t+1) = Ax(t) + bu(t), \\ & x(T) = 0 \text{ and } x(t) \neq 0,\ t = 0, 1, ..., T-1, \\ & u(t) \in \mathcal{U},\ t = 0, 1, ..., T-1. \end{aligned} \tag{2.14}$$

It is equivalent to the sparsity optimization problem:

$$\begin{aligned} \min_{u(0),\ldots,u(T-1)} \quad & |\{t : \|x(t)\|_2 \neq 0\}| \\ \text{s.t.} \quad & x(t+1) = Ax(t) + bu(t), \\ & \exists T_1 \leq T : x(t) = 0,\ t = T_1, ..., T, \text{ and} \\ & x(t) \neq 0,\ t = 0, 1, ...T_1 - 1, \\ & u(t) \in \mathcal{U},\ t = 0, 1, ..., T-1, \end{aligned} \tag{2.15}$$

where the operator $\|(.)\|_2$ is the 2-norm and $|(.)|$ means the carnality. Then in [77] (2.15) is convexified to

$$\begin{aligned} \min_{u(0),\ldots,u(T-1)} \quad & \sum_{t=1}^{T} w(t)\,\|x(t)\|_2 \\ \text{s.t.} \quad & x(t+1) = Ax(t) + bu(t), \\ & u(t) \in \mathcal{U},\ t = 0, 1, ..., T-1, \end{aligned} \tag{2.16}$$

where $w(t)$ is an increasing function. The problem of (2.16) is then solved using the MPC approach, of which the MPC horizon in fact does not need to cover the minimum time [77].

To apply this approach of sparsity optimization for our minimum-time problems, we need to have the target states be at the origin. With the new states defined as $\epsilon_v := v - v_{\min}$ in the gliding phase and $\epsilon_v := v - v_{\max}$ and $\epsilon_{\text{soc}} := SOC - SOC_{\text{target}}$ in the pulsing phase, together with the simplification and convexification techniques introduced above, problems (2.6) and (2.7) become:

$$\begin{aligned} \min_{T_m(t),\ s_d(t),\ a_b(t)} \quad & \int_{t_{0,\text{gld}}}^{t_{0,\text{gld}}+\Delta T_{\text{gld}}} \Big[w(t)\epsilon_v(t)^2 + w_d s_d^2(t) + w_b a_b^2(t) \Big] dt \\ \text{s.t.} \quad & d\dot{R}(t) = -(\epsilon_v(t) + v_{\min}) + v_P + h_\tau a_P \\ & \dot{\epsilon}_v(t) = 2k_1\bar{v}(\epsilon_v(t) + v_{\min}) - k_1\bar{v}^2 + k_2(T_e(t) + T_m(t)) - gf_r \\ & -d_{\lim} - s_d(t) \le a(t) \le a_{\lim} \\ & 0 \le T_m(t) \le T_{m,\max}^{\text{disch}} \\ & \dot{T}_{m,\min} \le \dot{T}_m(t) \le \dot{T}_{m,\max} \\ & dR_{\min} \le dR(t) \le dR_{\max} \\ & s_d(t) \ge 0 \\ & a_b(t) \le 0, \end{aligned} \tag{2.17}$$

and

$$
\begin{aligned}
\min_{T_m(t),\ T_e(t),\ s_a(t)} \quad & \int_{t_{0,\mathrm{pls}}}^{t_{0,\mathrm{pls}}+\Delta T_{\mathrm{pls}}} \Big\{ w(t)\big[\epsilon_v^2(t) + w_{\mathrm{soc}}\epsilon_{\mathrm{soc}}^2(t)\big] + w_a s_a^2(t) \Big\} dt \\
\text{s.t.} \quad & d\dot{R}(t) = -(\epsilon_v(t) + v_{\max}) + v_P + h_\tau a_P \\
& \dot{\epsilon}_v(t) = 2k_1\bar{v}(\epsilon_v(t) + v_{\max}) - k_1\bar{v}^2 + k_2(T_e(t) + T_m(t)) - g f_r \\
& \dot{\epsilon}_{\mathrm{soc}}(t) = c_{00} + c_{10}(\epsilon_{soc} + SOC_{\mathrm{target}}) + c_{01}P_m(t) \\
& P_m(t) \geq \Big[T_{m,\min}^{\mathrm{ch}}(\epsilon_v(t) + v_{\max}) + T_m(t)v_{\min} - T_{m,\min}^{\mathrm{ch}}v_{\min}\Big]/c_{\omega v} \\
& P_m(t) \geq \Big[T_{m,\max}^{\mathrm{ch}}(\epsilon_v(t) + v_{\max}) + T_m(t)v_{\max} - T_{m,\max}^{\mathrm{ch}}v_{\max}\Big]c_{\omega v} \\
& P_m(t) \leq \Big[T_{m,\max}^{\mathrm{ch}}(\epsilon_v(t) + v_{\max}) + T_m(t)v_{\min} - T_{m,\max}^{\mathrm{ch}}v_{\min}\Big]/c_{\omega v} \\
& P_m(t) \leq \Big[T_m(t)v_{\max} + T_{m,\min}^{\mathrm{ch}}(\epsilon_v(t) + v_{\max}) - T_{m,\max}^{\mathrm{ch}}v_{\max}\Big]/c_{\omega v} \\
& -d_{\mathrm{lim}} \leq a(t) \leq a_{\mathrm{lim}} + s_a(t) \\
& T_{m,\max}^{\mathrm{ch}} \leq T_m(t) \leq 0 \\
& \dot{T}_{m,\min} \leq \dot{T}_m(t) \leq \dot{T}_{m,\max} \\
& 0 \leq T_e(t) \leq \bar{T}_{\mathrm{sw}} \\
& \dot{T}_{e,\min} \leq \dot{T}_e(t) \leq \dot{T}_{e,\max} \\
& T_e(t) + T_m(t) \geq 0 \\
& dR_{\min} \leq dR(t) \leq dR_{\max} \\
& s_a(t) \geq 0,
\end{aligned}
\tag{2.18}
$$

where ΔT_{gld} and ΔT_{pls} are respectively the MPC horizons of the gliding and pulsing problems, and w_{soc} in the objective function of (2.18) is the weighting factor for balancing the magnitudes of ϵ_v and ϵ_{soc}. For the $w(t)$ in the objective functions, we simply define it as

$$
w(t) = \alpha(t - t_{0,i}), \tag{2.19}
$$

with α a positive constant and $t_{0,i}$ being $t_{0,\mathrm{gld}}$ or $t_{0,\mathrm{pls}}$, the current time.

2.3.2.4 Problem Solving Using the Pseudo-Spectral Method

Problems (2.17) and (2.18) are solved using the PS method. The constraints in these two problems are now all linear and the objective functions are quadratic. Therefore, after the application of the PS method, the two problems will become QP problems, which can be solved very efficiently.

In this study, we assume that the PV speed and PV acceleration in the MPC horizons are known. In practical applications, they can be estimated by proper prediction methods, such as those in [80, 81]. The proposed method in this study can be further integrated with any methods able to predict the PV behaviors, which have already been explored extensively in literature and are out of the scope of our study.

2.3.3 The Ride Comfort Requirement

As discussed previously, vehicle bodies are more efficient energy buffers compared with batteries for storing the energy from engine in PnG. However, using the vehicle body as the energy buffer means that speed oscillation will occur, which may influence the ride comfort negatively. Therefore, it is necessary to consider ride comfort in the practical PnG implementation.

Here we assume that jerks can be properly handled by the design of low-level actuator control. Therefore, only the feelings of drivers caused by the pulsing acceleration and gliding deceleration are considered. The cycles of PnG in real applications are at the order of ten seconds. In literature, however, most of the research efforts for studying motion sickness under different excitation frequency only reach to 0.1 Hz or is not for longitudinal direction [82][83]. In other words, the research of human body reactions to very low frequency has not yet been well-established. As a result, we resort to the Safety Pilot dataset [75] to see what is the level of acceleration that people encounter in everyday driving. With the PnG experiment using real vehicle that will be presented in Chapter V, we can have better idea about the influence of

ride comfort by PnG.

From the Safety Pilot dataset, first the events in car-following scenario are chosen. Then we further extract those recorded in cruising scenario. If an event is with speed variation less than 10% of its average speed, it is defined as in the cruising scenario. The average root-mean-square acceleration of those selected cruising events ranges from 0.17 to 0.2 m/s^2 at different speeds (30 to 80 mph). Therefore, we choose 0.2 m/s^2 as the acceleration/deceleration limits for ride comfort, close to a suggested maximum acceleration 0.3 m/s^2 in [44]. However, the level of acceleration 0.2 m/s^2 from the analysis of Safety Pilot dataset is the one that people encounter everyday in traditional cruising, which may be very conservative. More systematic study for ride comfort in PnG is needed, which would need to involve numerous experiments with different subjects and is thus not in the scope of this study.

2.4 Simulation Results and Discussions

In this work, it is assumed that the road is flat without any grade variation. First, the cases with constant-speed PV are simulated with different speeds. A case with varying-speed PV is then considered to further validate the control of the proposed method. At last, the Safety Pilot dataset is exploited to define the PV speed to gain more comprehensive idea about the potential of fuel saving using the proposed method in real traffic. All simulations are started with the FV at the desired range to the PV. Except for some cases with constant-speed PV, all the other cases with varying-speed PV are with gear 6. The MPC horizons for all cases are set as 6 s. In simulations, the computation time for solving each problem on a laptop with Intel® i5 CPU in MATLAB using the built-in quadprog solver is roughly less than 0.1 s. Therefore we choose $\Delta T = 0.5$ s, i.e., solving the QP problems every 0.5 s, which is sufficient for normal driving situations.

2.4.1 Constant-Speed Preceding Vehicle

Figure 2.6 shows the MPG for CS driving at different speeds in engine mode, and Figure 2.7 summarizes the MPG improvements of SOC-PnG without speed oscillation. In this study, the baseline cases for MPG improvement are those of CS driving in engine mode with gear 6, because gear 6 renders the least fuel consumption in every speed of CS driving. It can be seen that due to high vehicle weight and not very efficient motor, pure SOC-PnG cannot save fuel for the vehicle studied. On the other hand, for Speed-PnG without involving the electrical path of the powertrain, high MPG improvements can be achieved as summarized in Figure 2.8. The MPG improvements of Speed-PnG range roughly from 8% to 35%, following the trend of decreased fuel saving with speed increase. However, this achievement might be at the expense of ride comfort. The root-mean-square accelerations at different speeds of pure Speed-PnG are also shown in Figure 2.8. We can see that they can reach beyond 0.3 m/s^2 at higher speeds, even with gear 6 that leads to lower accelerations. Nevertheless, if we introduce 10% speed oscillation to the SOC-PnG, some fuel saving potential can be regained using the proposed control method, as shown in Figure 2.9. Meanwhile, the root-mean-square accelerations are about 0.2 m/s^2, the preset level of the acceleration/deceleration limits for ride comfort. Figure 2.10 plots the simulation trajectories of the case of 40 mph as an example. We can see that the range and acceleration/deceleration constraints are satisfied and the battery SOC is also maintained.

In this simulation study, we see that partial fuel saving capability can be recovered if speed oscillations are allowed to the SOC-PnG. This is because the vehicle body is a more efficient energy buffer than the battery. Furthermore, we can also observe the performance of different PnG operations, with the feature that pure Speed-PnG and pure SOC-PnG serve respectively the upper bound and lower bound of the fuel saving potential. Next, we will apply the proposed method to a case with varying-speed PV

to further check its performance.

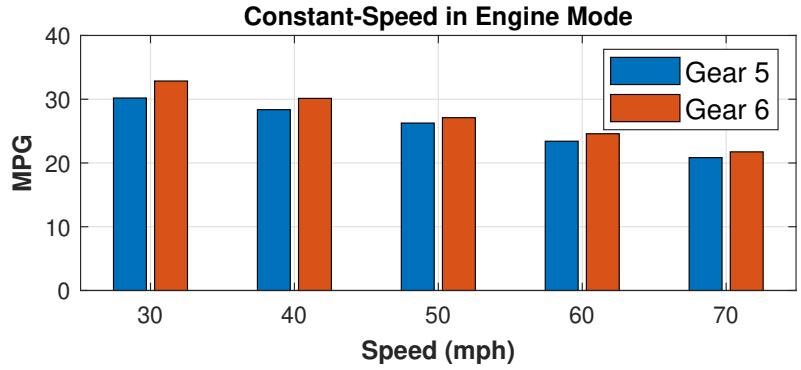

Figure 2.6: The MPG of constant-speed driving at different speeds in engine mode.

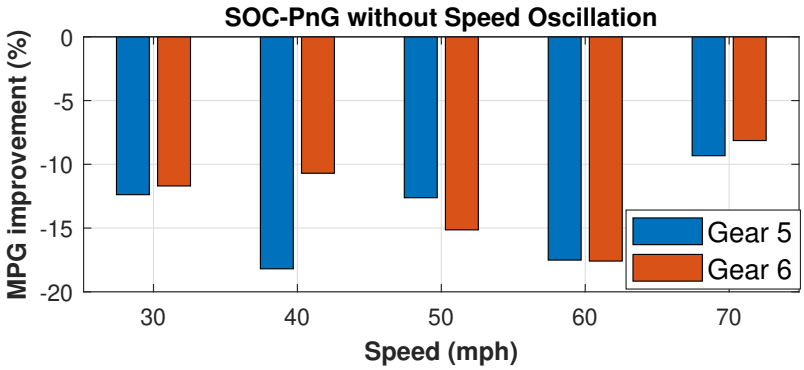

Figure 2.7: The MPG improvements of constant-speed driving at different speeds with pure SOC-PnG.

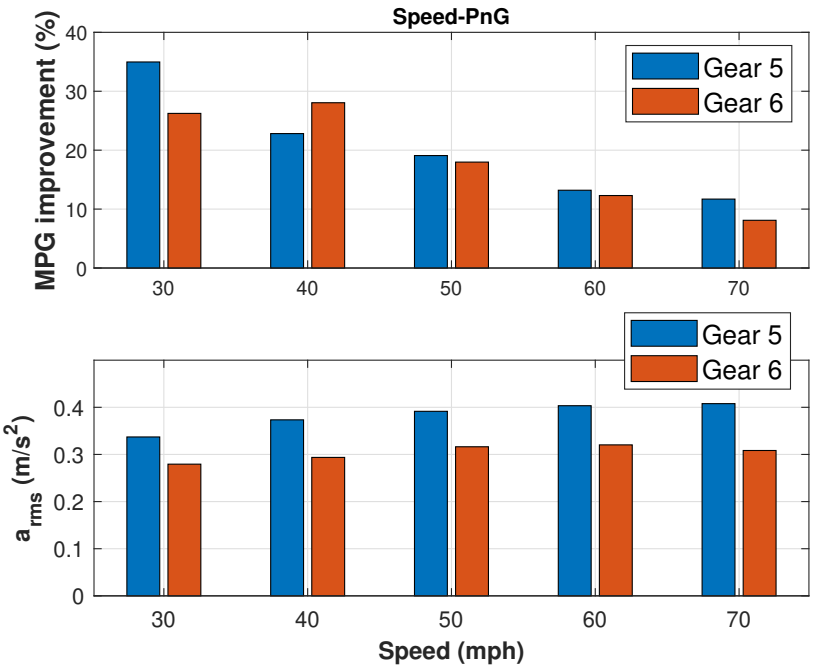

Figure 2.8: The MPG improvements and root-mean-square accelerations of Speed-PnG with 10% speed oscillation at different speeds.

2.4.2 Varying-Speed Preceding Vehicle

To examine the control performance of the proposed method, a speed profile with 0.06 m/s^2 root-mean-square acceleration, shown in Figure 2.11, is used as the speed of PV. Two cases are simulated, one starting in pulsing phase and another starting in gliding phase. The simulation results are shown in Figure 2.12 and Figure 2.13 respectively. We can see that in both cases, the range constraint is satisfied. However, the limits of acceleration and deceleration for ride comfort are sometimes exceeded. Due to the varying speed of PV, the FV may need to temporarily increase the acceleration or deceleration to meet the range constraint. For example, in Figure 2.12 at $t = 32$ s, the FV raises its acceleration beyond the preset limit 0.2 m/s^2 according to the speed increase of PV, such that the range error is still within the bounds later around $t = 38$ s. Furthermore, at $t = 46$ s, also in Figure 2.12, the FV applies brake to reduce its speed in response to the speed reduction of PV, which leads to the temporary

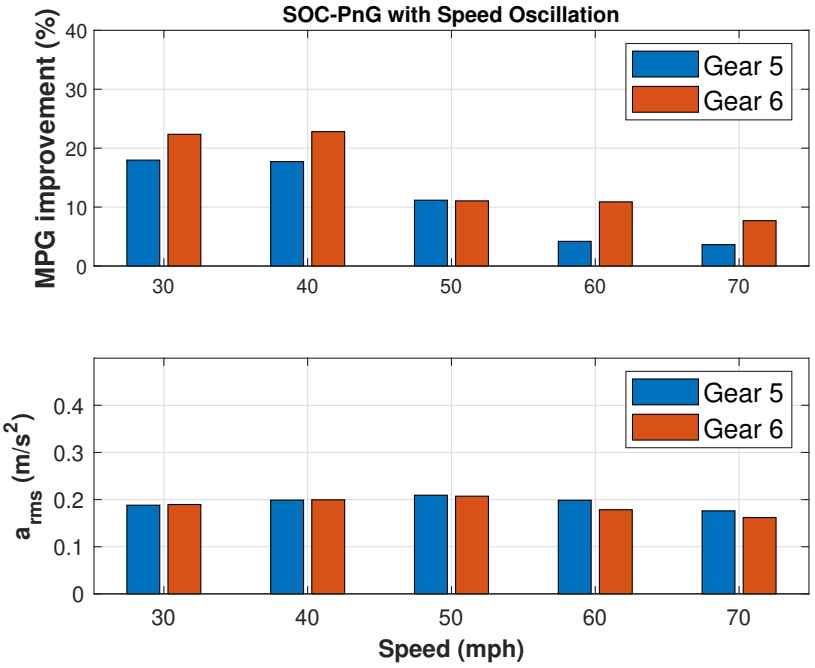

Figure 2.9: The MPG improvements and root-mean-square accelerations of SOC-PnG with 10% speed oscillation at different speeds.

exceeding of deceleration from the preset limit. This phenomenon is also reflected in the root-mean-square acceleration, 0.22 m/s^2 for the case starting in pulsing and 0.23 m/s^2 for the one starting in gliding. The fuel economy for these two cases are 36.6 MPG and 40.9 MPG, respectively. It also indicates the fact that for short runs, starting with pulsing tends to have slightly lower MPG because larger proportion of time is with engine turned on. If driven in engine mode without PnG operation, the fuel economy is 29.3 MPG. Therefore, roughly 32.1% MPG improvement is achieved if the average of MPG from the cases in Figure 2.12 and Figure 2.13 is considered.

The simulations here show that the proposed method is able to deal with the cases where the PV has varying speed. Further study using naturalistic driving data is presented next.

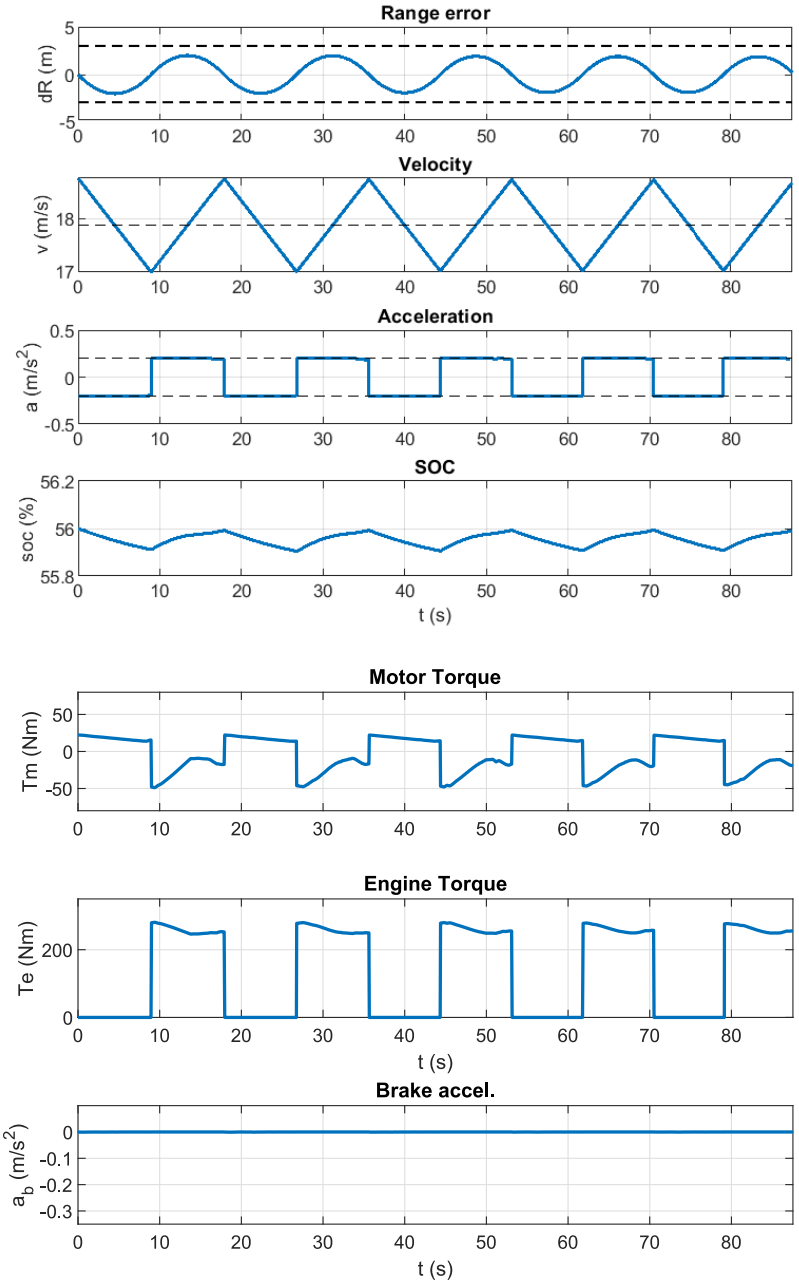

Figure 2.10: The simulation results of constant-speed PV at 40 mph with gear 6. The dashed lines indicate the allowed range error, PV speed, and acceleration/deceleration limits for ride comfort.

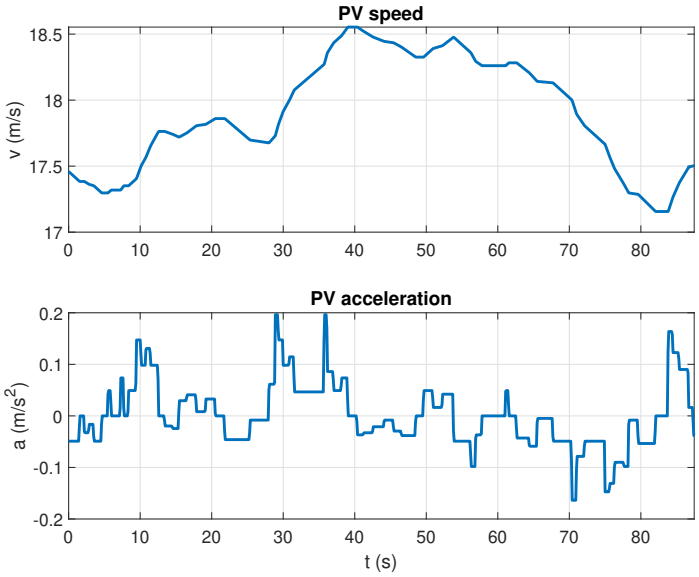

Figure 2.11: The speed and acceleration trajectories used in the case of varying-speed PV.

2.4.3 Preceding Vehicle with Speed from the Safety Pilot Dataset

Using the Safety Pilot dataset, we extract the cruising events from those in the car-following scenario. Similar to the ride comfort analysis presented previously, if the speed of an event in the car-following scenario is with variation less than 10% of its average speed, we assign it as the speed of PV. There are in total 1,161 events of local roads and 507 events of highways adopted in this simulation study. The total driving durations are 8.5 and 11.4 hours for the local and highway events respectively. The detailed distributions of these events are shown in Figure 2.14 and Figure 2.16. For each event, the initial position of FV is at the desired range and two simulations are implemented, one starting in pulsing and another starting in gliding. The average MPG of these two simulations is then considered as the MPG result of this event.

Figure 2.15 and Figure 2.17 are the results for local roads and highways respectively. For the local events, the root-mean-square acceleration is higher, on average slightly over 0.2 m/s^2. Therefore, the weighting factor for penalizing the slack variable

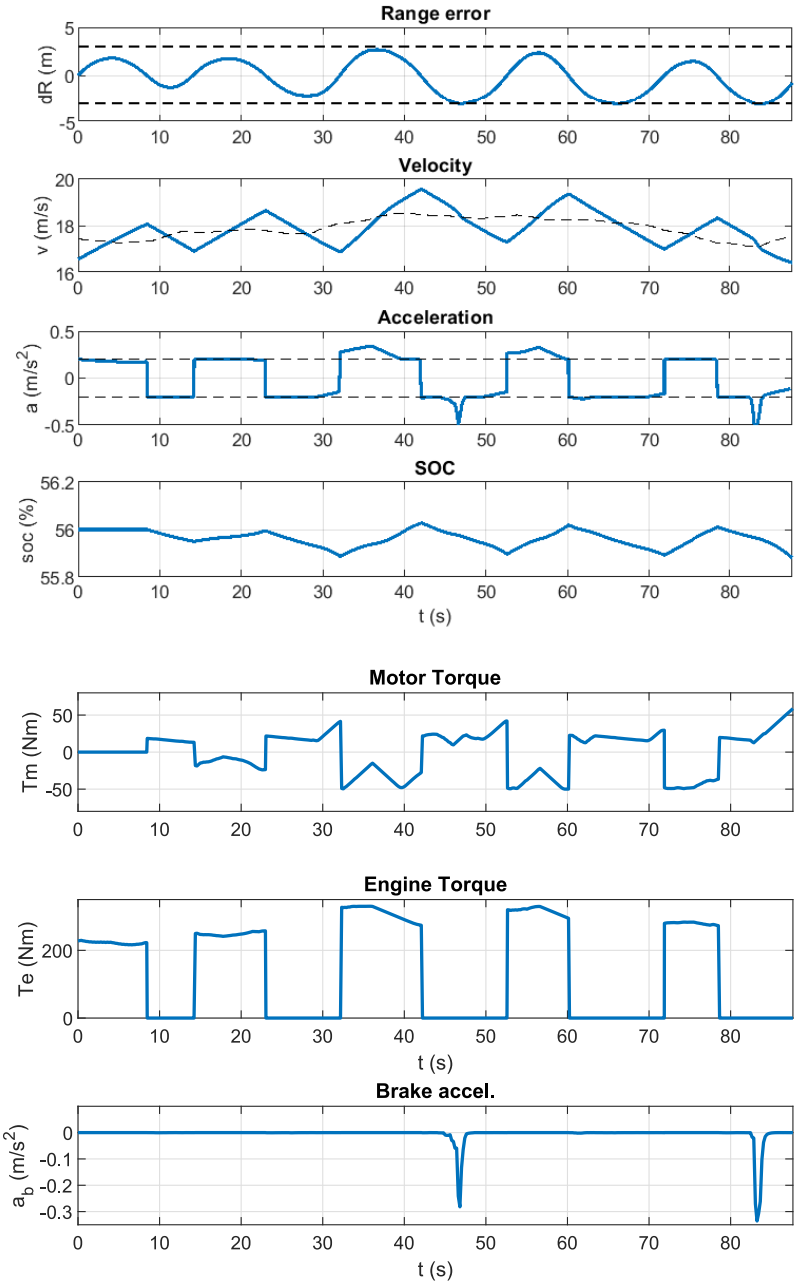

Figure 2.12: The simulation results of varying-speed PV at 40 mph with gear 6 and starting in pulsing. The dashed lines indicate the allowed range error, PV speed, and acceleration/deceleration limits for ride comfort.

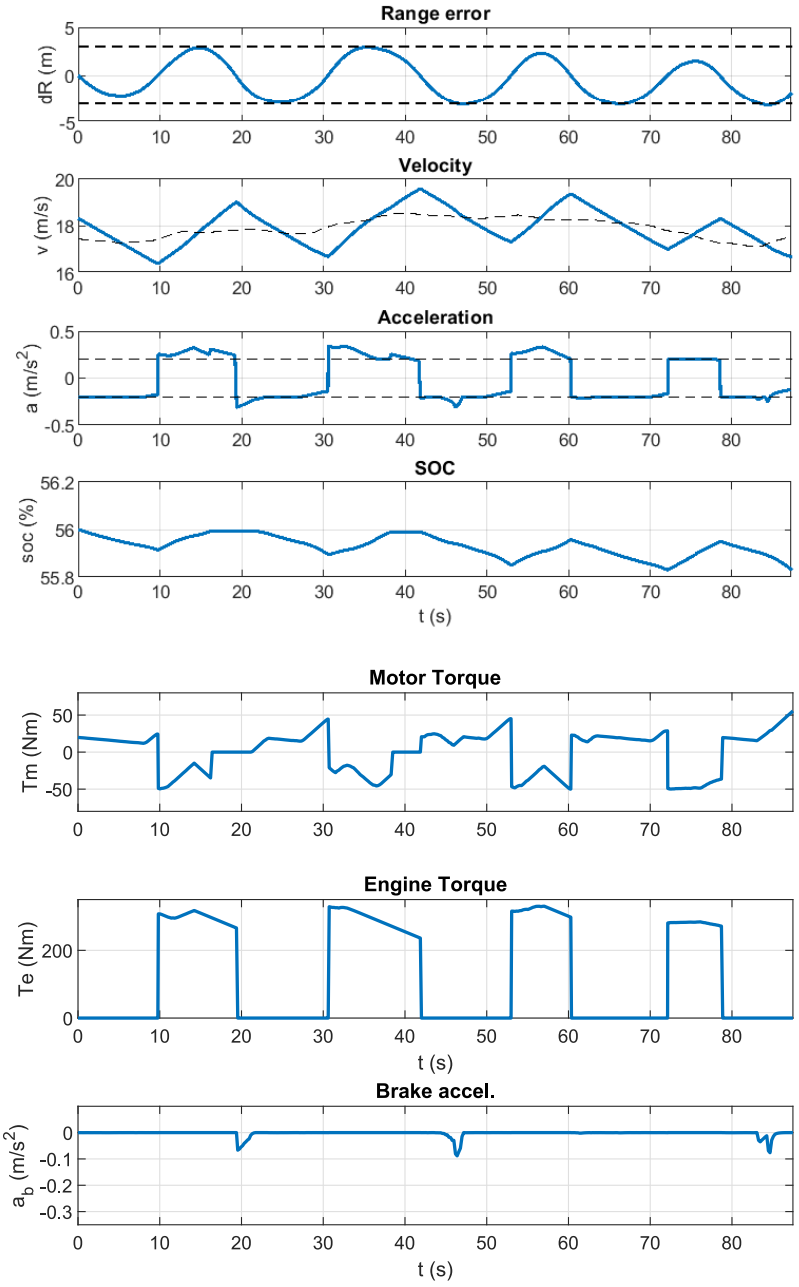

Figure 2.13: The simulation results of varying-speed PV at 40 mph with gear 6 and starting in gliding. The dashed lines indicate the allowed range error, PV speed, and acceleration/deceleration limits for ride comfort.

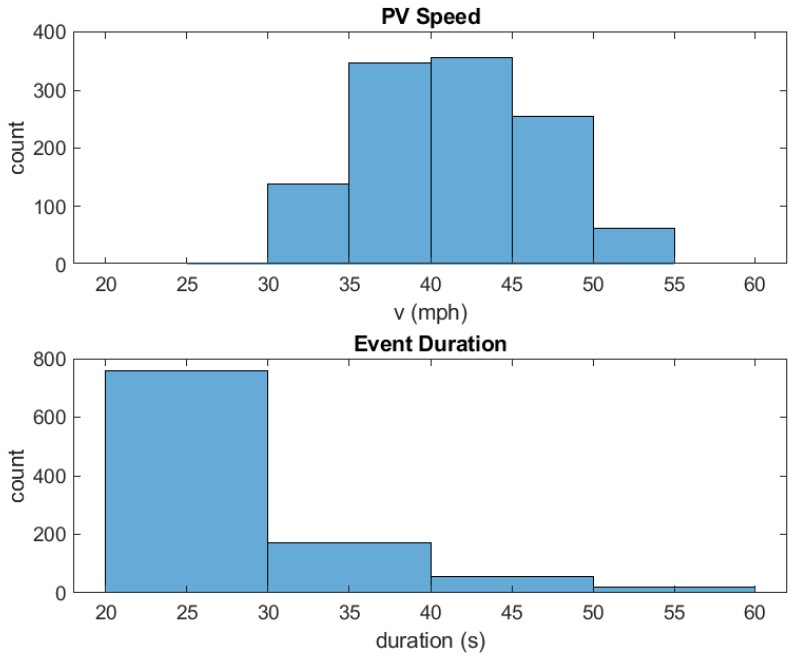

Figure 2.14: The statistics of Safety Pilot data on local roads used in the simulations.

of the acceleration constraint is reduced from 1×10^6 to 100, such that the fuel saving potential will not be degraded by the PV. Even so, we can see that the distribution of FV acceleration is still highly overlapped with that of the PV acceleration in Figure 2.15. From our experience of PnG experiment, which will be presented in Chapter V, this level of acceleration is very mild and does not cause discomfort. For the highway events, the FV accelerations are on average lower and the MPG improvements are less compared with the outcomes of local events, which follows the general trend of PnG that fuel saving potential decreases as the speed increases.

However, we can that there are some cases where PnG actually leads to more fuel consumption, either on local roads or on highways. The average of MPG improvements for local events is 17.1% with standard deviation 19.9%. For highway events, the average of MPG improvements is 5.1% with standard deviation 5.5%. In order to dive further into the individual cases, the MPG improvements against the root-mean-square accelerations of PV are plot in Figure 2.18. It can be seen that

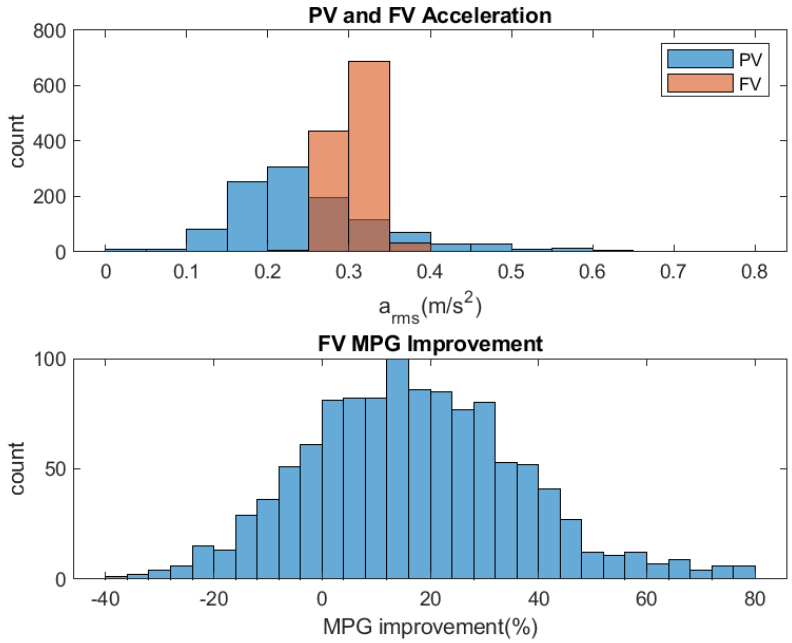

Figure 2.15: The simulation results using the Safety Pilot data on local roads.

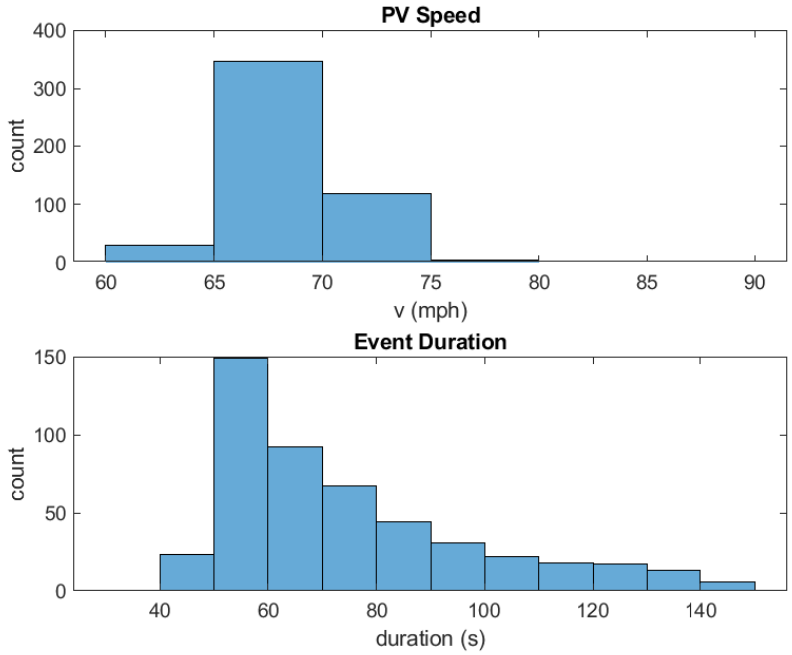

Figure 2.16: The statistics of Safety Pilot data on highways used in the simulations.

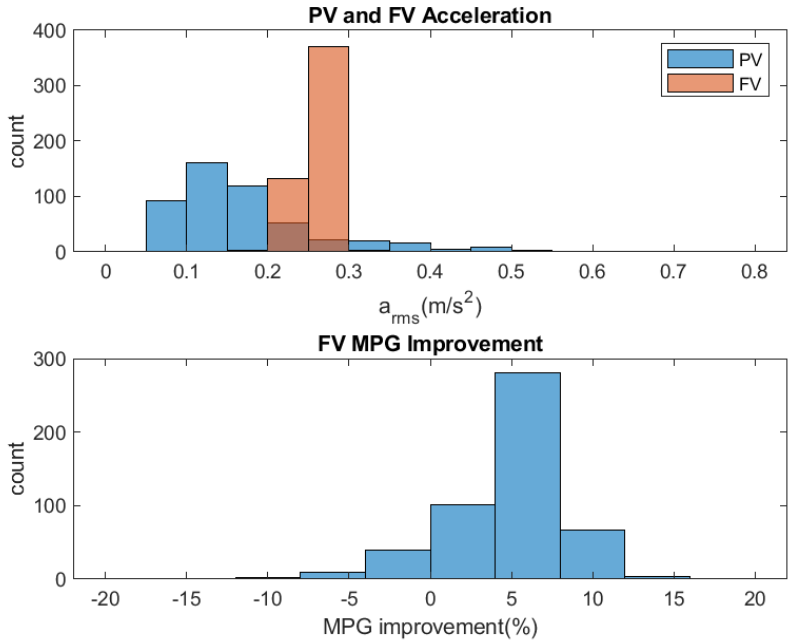

Figure 2.17: The simulation results using the Safety Pilot data on highways.

the MPG improvements are roughly inversely proportional to the PV accelerations, which suggests that the benefits of fuel saving by PnG tend to be smaller when the PV accelerations are large. In orther words, if the PV is driving relatively aggressively, following it tightly may end up burning more fuel. In this case, if the driver of FV is willing to trade off ride comfort for fuel savings, higher fuel saving potentials are still possible.

We further rerun the simulations using the Safety Pilot dataset with increased a_{lim}, from 0.2 m/s^2 in previous cases to 0.3 m/s^2. Figure 2.19 and Figure 2.20 show the simulations results of local roads and highways respectively, where the results of 0.2 m/s^2 acceleration limit from Figure 2.15 and Figure 2.17 are also added for comparison. It can be seen that on local roads, using $a_{\text{lim}} = 0.2$ m/s^2 or $a_{\text{lim}} = 0.3$ m/s^2 does not lead to very different results, for both the MPG improvements and FV accelerations. It is because smaller penalizing factor was previously used already in the simulations with $a_{\text{lim}} = 0.2$ m/s^2. However, for the highway cases, significant

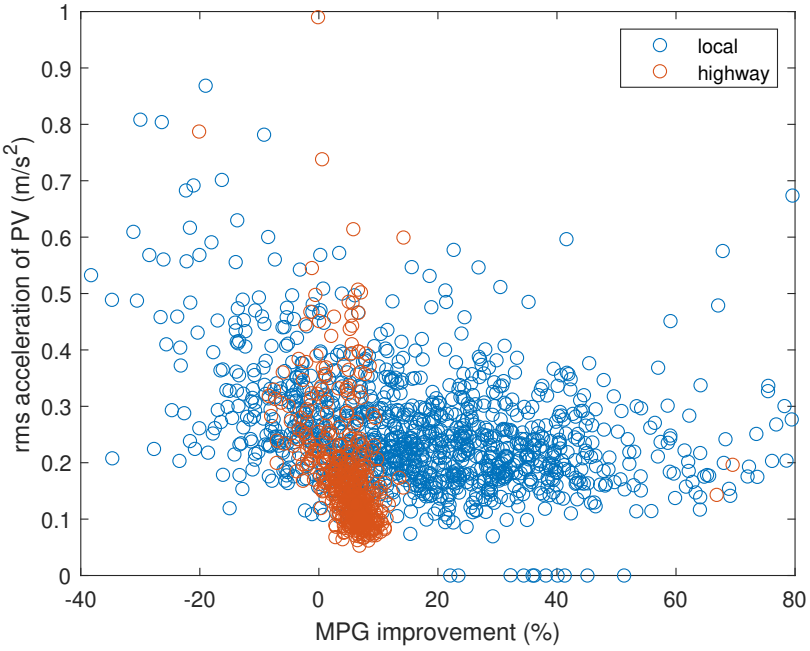

Figure 2.18: The results of MPG improvements and the PV accelerations using the Safety Pilot data.

MPG improvements are obtained $a_{\text{lim}} = 0.3$ m/s^2. The average root-mean-square accelerations of FV increases from about 0.25 m/s^2 to 0.31 m/s^2, and the average of MPG improvements is 7.4% with standard deviation 4.6%, slightly improved from 5.1% with standard deviation 5.5% in the cases with $a_{\text{lim}} = 0.2$ m/s^2.

From the the simulations using the Safety Pilot dataset, we discover that there are some situations where PnG might lead to more fuel consumption, especially when the PV is with larger accelerations. This also motivates the research in the next chapter about PnG synchronization in platoons, since in PnG platoons, the PVs might have considerable acceleration levels.

2.5 Conclusions and Future Work

In this chapter, a control approach for PnG operations of HEVs in car-following scenario is presented. This framework is developed to achieve a balance between the

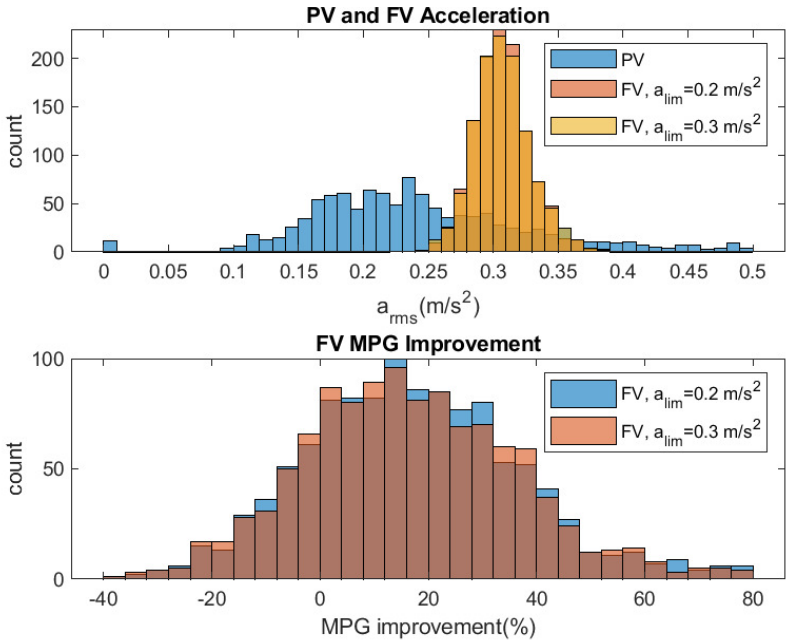

Figure 2.19: The simulation results using the Safety Pilot data on local roads with different acceleration limits.

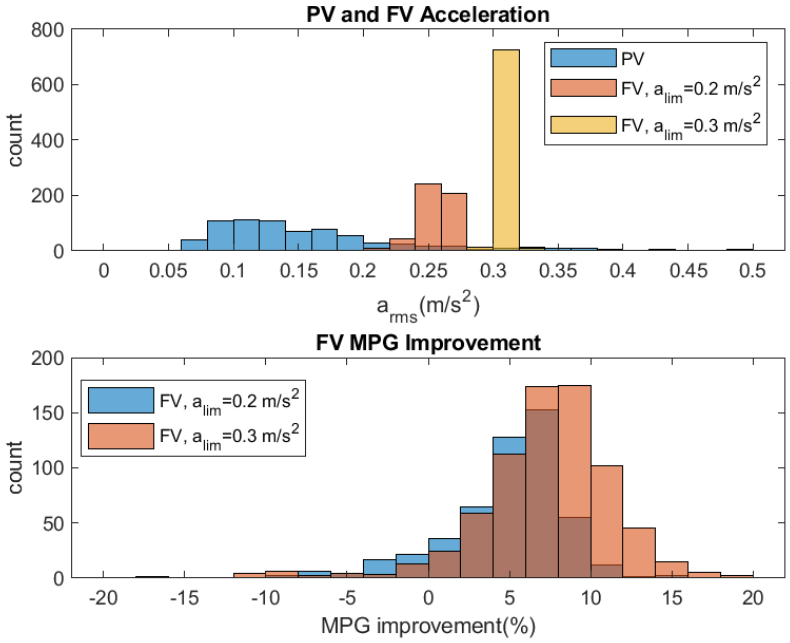

Figure 2.20: The simulation results using the Safety Pilot data on highways with different acceleration limits.

fuel saving potential of pure Speed-PnG and the ride comfort of pure SOC-PnG while maintaining SOC.

In the proposed framework, two minimum-time control problems are formulated, one for the gliding phase and one for the pulse phase. With the linearization of vehicle dynamics, the approximation of SOC dynamics with the convexification by the McCormick envelope, and the convexification approach for sparsity optimization in [77], these two problems become QP problems after being transcribed by the PS method. Therefore, the proposed method can be solved efficiently. In the numerical simulations of constant-speed PV, the improvements of fuel economy achieved range from about 8% to 23%, corresponding to speed decreasing from 60 mph to 30 mph. It is a significant improvement compared with the operation of SOC-PnG without speed oscillation for the vehicle used in this study. For the simulations of naturalistic PV speed using Safety Pilot dataset, we observe on average about 17% and 5% MPG improvements on local roads and highways, respectively.

The conclusion is that the proposed framework is a promising approach to balance the benefits of Speed-PnG and SOC-PnG, i.e., fuel saving and ride comfort respectively. The results encourage the further development of the proposed strategy of SOC-PnG with speed oscillation.

In this study, we simply assume that the allowed range oscillation and time headway of range policy are given. The proper values of these parameters are actually related to the characteristics of the ego vehicle itself, the driver's preferences, and how the PV is driven. Based on the behaviors of PV, these parameters may need be adjusted accordingly. For example, if the PV is driven aggressively with more drastic acceleration and deceleration such that the acceleration/deceleration constraints need to be adjusted often to fulfill the range constraints, it might be a good idea to increase the inter-vehicle range. This higher level of design and control can be further studied in the future to make the proposed PnG control more comprehensive.

CHAPTER III

Pulse-and-Glide Synchronization for Heterogeneous Platoons

3.1 Introduction

Pulse-and-glide (PnG) is an eco-driving technique that is promising in saving fuel [18, 39]. In this study, we seek to achieve more fuel saving potential in vehicle platooning by introducing PnG into CACC. However, as shown in [48], a rule-based PnG switching method developed based on homogeneous platoons may lead to undesired PnG switchings in heterogenous platoons. Increasing the inter-vehicle ranges can improve this issue as pointed out in [49]. However, it may not be ideal in terms of traffic throughput.

Motivated by the need for a control method that is capable of handling heterogeneity in the platoons of PnG vehicles while keeping the platoon compact, we propose the synchronization of PnG vehicles as a solution. This chapter focuses on the PnG synchronization in heterogeneous platoons via V2V communication. By synchronization, the individual vehicles are able to complete their desired PnG cycles while forming a platoon. On the other hand, with synchronized PnG, the amount of range oscillations can be reduced and thus a more compact platoon can be formed.

In the proposed method, the vehicles with different acceleration limits for ride

comfort are synchronized to have the same PnG period and to reach the maximum and minimum distance errors at the same time. The synchronization of PnG vehicles is achieved via the synchronization of their virtual oscillators based on the Kuramoto model, which provides a simple yet effective mechanism for synchronization with local coupling [73].

Range keeping is achieved by adjusting the reference speeds and positions that the PnG vehicles oscillate around to make the vehicles compensate the range errors. The entire process is decentralized. Numerical simulations show that the method can synchronize a PnG platoon of vehicles with different acceleration limits as the requirements of ride comfort. Also, the amplitudes of range oscillations are reduced after synchronization. The vehicles with higher acceleration limits are able to maintain higher fuel economy as a result of their uninterrupted PnG operations due to synchronization. Therefore, the method provides a promising approach to increase the overall fuel saving potential of PnG platoons while maintaining the desired range with small amount of range oscillations.

The rest of this chapter is organized as follows. The problem setup is given in Section 3.2, including the vehicle model used in this study. In Section 3.3 we present a preliminary study on homogeneous platoons, which shows the potential of PnG synchronization. Section 3.4 presents the proposed PnG synchronization method for heterogeneous platoons, which is the main contribution of this chapter. Simulation results are given in Section 3.5. Finally, conclusions and future work are given in Section 3.6.

3.2 Problem Setup

3.2.1 The Vehicle Platoon

Consider a series of N connected automated vehicles (CAVs) forming a platoon. The vehicles implement PnG simultaneously around a desired speed $\bar{v}_c$ with a desired PnG period. Both the desired speed and PnG period are assumed to be given constants. The desired speed can, for example, be set according to the speed limit of the road. The desired PnG period could, for example, be determined via optimization approaches to maximize the platoon performance. The desired speed and PnG period are shared via V2V communication to every vehicle in the platoon. For the cases of heterogeneous platoons, the heterogeneity in the PnG accelerations is assumed to be due to the different ride comfort preferences of the individual drivers instead of due to different vehicle types. Hence, all vehicles in the platoon are characterized with the vehicle parameters given in Table 3.1, which correspond to a vehicle with conventional powertrain and step-gear transmission. The engine brake specific fuel consumption (BSFC) map is shown in Figure 3.1. Note that because in the presented method vehicle accelerations are controlled, variations of vehicle parameters, even though not considered in this study, can be easily accommodated as long as the target acceleration can be achieved by the controlled vehicles.

3.2.2 Vehicle Dynamics

Only the longitudinal vehicle dynamics are considered. The dynamics of the ith vehicle are given as

$$\begin{aligned} \dot{x}_i &= v_i, \\ \dot{v}_i &= a_i = \tfrac{1}{M_v}(F_{d,i} - \tfrac{1}{2}C_d\rho_a A_v v_i^2 - M_v g f_r), \end{aligned} \tag{3.1}$$

where x_i, v_i, and a_i are respectively the position, speed, and acceleration, and $F_{d,i}$ is the driving force. $F_{d,i} < 0$ means braking. The definitions and values of the other parameters are given in Table 3.1.

The constant time headway range policy is adopted; i.e.,

$$R_{\text{des}} = d_0 + h_\tau \bar{v}_c, \tag{3.2}$$

where R_{des} is the desired range to the immediate PV, d_0 is the standstill range, and h_τ is the time headway. Unlike the usually used instantaneous speed of the ego vehicle in the range policy (3.2), here the desired speed $\bar{v}_c$ is used.

Parameter	Description	Value	Unit
M_v	vehicle weight	2948	kg
C_d	air drag coefficient	0.4	-
A_v	vehicle frontal area	3.26	m^2
ρ_a	air density	1.202	kg/m^3
f_r	rolling resistance	0.015	-
r_w	effective tire radius	0.3848	m
g	acceleration of gravity	9.81	m/s^2
r_T	gear ratio (gear 1-6)	[4.03, 2.36, 1.53, 1.15, 0.85, 0.67]	-
η_T	gear efficiency (gear 1-6)	[0.963, 0.971, 0.993, 0.993, 0.995, 0.993]	-
r_0	final drive ratio	3.23	-
η_0	final drive efficiency	0.966	-

Table 3.1: The vehicle parameters of the simulation studies.

3.3 A Preliminary Study on the Potential of PnG Synchronization

Before the presentation of the proposed method for heterogeneous platoons, a preliminary study on the benefit of PnG synchronization is conducted using homogeneous platoons to motivate this research.

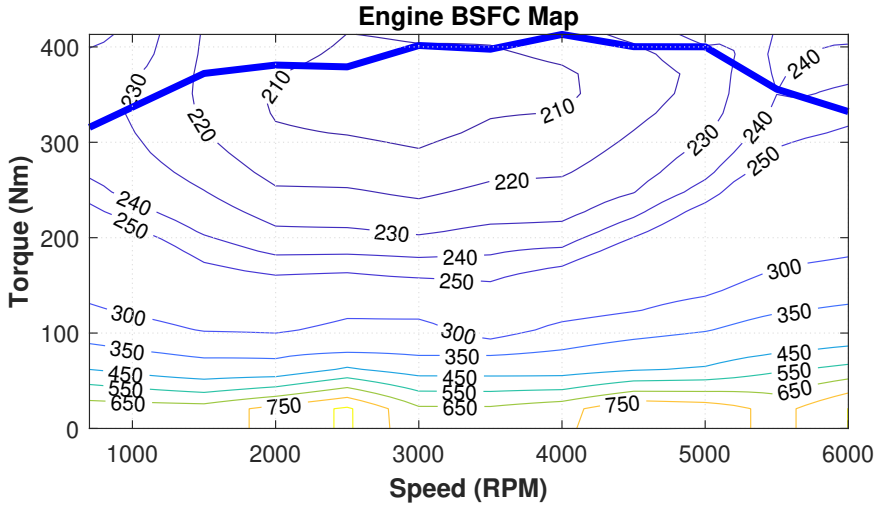

Figure 3.1: The engine map of the simulation studies.

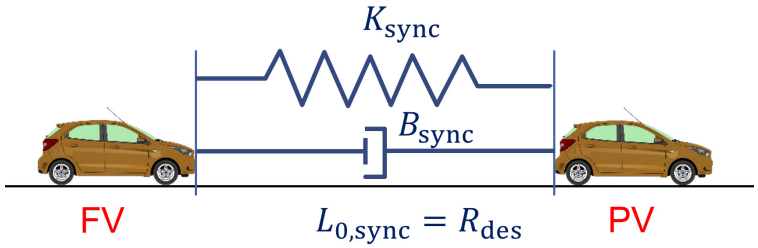

Figure 3.2: The schematic diagram of the virtual spring-damper approach for homogeneous platoons.

A virtual spring-damper system is introduced to provide the coupling mechanism to synchronize the homogeneous platoons, as shown in Figure 3.2. The driving force of the FVs is determined by the virtual spring-damper system, the acceleration of their immediate PV, a_P, and the speed difference $(v_P - v_F)$ as follows:

$$F_F = M_v a_P + \left[K_{\text{sync}}(R - R_{\text{des}}) + B_{\text{sync}}(v_P - v_F)\right], \tag{3.3}$$

where M_v is the mass of the vehicles, K_{sync} and B_{sync} are respectively the spring and damping constants, and R_{des} is the desired range, which is equal to the natural length of the virtual spring $L_{0,\text{sync}}$.

In this simulation study of homogeneous platoons, three levels of traffic volumes are adopted. They are low, medium, and high traffic volumes with 150, 200, and 250 vehicles passing through a 2.7 km straight and flat road. The initial speeds of the vehicles in the three traffic volumes range from 30 to 40 mph, with randomized initial inter-vehicle ranges. In the baseline cases, the vehicles are controlled by the intelligent driver model [47]. In the PnG cases, the vehicles implement Speed-PnG around 40 mph with 0.2 m/s^2 acceleration limit. A parameter called critical range $R_c = 53$ m is introduced. Only when the inter-vehicle range is within R_c does the FV implement the approach of (3.3) to catch up with its PV and maintain the desired range. As a benchmark, the rule-based method for PnG platoons proposed in [48] is also implemented, with the same critical range assigned. This approach decides the PnG switching timing based only on the current speed difference and range to the PV, without any synchronization mechanism.

The average MPG improvements are summarized in Figure 3.3, where the results of the benchmark method proposed in [48] is referred to as without synchronization. We can see that even though significant MPG improvements can be obtained with or without synchronization, the performance of fuel saving is better with PnG synchro-

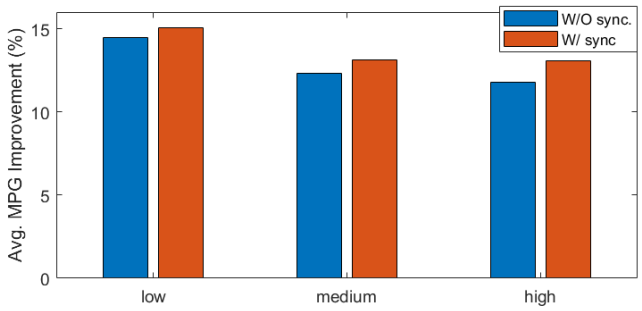

Figure 3.3: The MPG improvements of the study of PnG synchronization for homogeneous platoons under different traffic volumes.

nization. Such performance improvement is more obvious with higher traffic volumes. It is because with denser traffic, the PnG behaviors tend to be interfered by the nearby vehicles such that the target fuel saving potential cannot be achieved. However, with synchronization, the vehicles are able to fulfill the desired PnG patterns. Therefore, better fuel saving performance is obtained.

From this preliminary study, we can understand the benefit of PnG synchronization for fuel saving. However, the approach of virtual spring-damper system (3.3) is not suitable for heterogeneous platoons, since it will impose the same PnG pattern for all the vehicles in the platoon. Some fuel saving potential and/or ride comfort will be lost accordingly. Therefore, we develop a PnG synchronization method specifically for heterogeneous platoons, which is the main contribution of this chapter and is presented in the following.

3.4 Methodology

3.4.1 The Pulse-and-Glide Strategy

During PnG, we keep the same gear without shifting as in Chapter II. The engine turns on and off periodically, complying with the acceleration limit during the pulsing phase. This acceleration limit is assumed to have been determined by the driver of

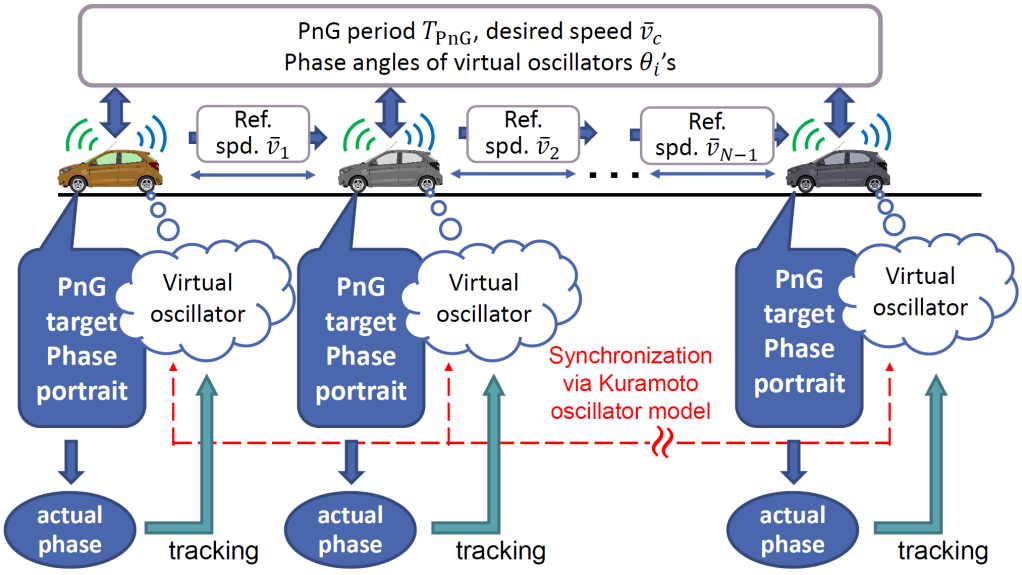

Figure 3.4: Illustration of the control concept.

each vehicle according to the preferred ride comfort. The reference speed $\bar{v}_i$ of the ith vehicle is equal to $\bar{v}_c$, the desired speed for the platoon, except when it needs to adjust the range to its immediate PV. The vehicle speed is equal to the reference speed $\bar{v}_i$ at the boundaries of the maximum and minimum allowable distance errors. The distance error is defined as the deviation from the distance that would be covered if the vehicle were to cruise at a constant speed of $\bar{v}_i$. The upper and lower bounds for the speed and distance error are determined from the acceleration limit as explained in the next section.

3.4.2 Solution Strategy

The basic control concept is illustrated in Figure 3.4 and summarized as follows. Each vehicle maintains its own virtual oscillator and establishes its PnG target phase portrait, which is parameterized with the phase angle. Synchronizing the virtual oscillators is achieved via the Kuramoto model [73], and the vehicles are controlled to track their own virtual oscillators. This way, the PnG oscillations are also synchronized after the virtual oscillators are synchronized. The information that needs to

be shared includes the PnG period T_{PnG}, the desired speed $\bar{v}_c$, and the phase angles of the virtual oscillators. The reference speed of the PV, $\bar{v}_{i-1}$, also needs to be transmitted to the vehicle i. An adaptive cruise controller (ACC) is implemented in parallel for safety considerations. The whole control strategy is explained in detail in the remainder of this section.

3.4.3 Safety Monitoring

For safety considerations, an ACC controller with proportional-derivative (PD) control is implemented to monitor the status of the ego vehicle. With the range error defined as $\Delta R_i := R_i - R_{\text{des}}$ based on the range policy (3.2), where R_i is the range to the PV, the acceleration demanded by the ACC controller is given by

$$a_{\text{ACC},i} = K_{P,i} \cdot \Delta R_i + K_{D,i} \cdot (v_{i-1} - v_i). \tag{3.4}$$

If the deceleration (when $a_{\text{ACC},i} < 0$) demanded by the ACC controller is larger than the deceleration of free gliding by a preset tolerance, it is judged that the current situation is not suitable for PnG operations due to safety concerns. In this work, a brake force is provided according to the ACC controller to mitigate the possible collision. If this situation happens during the pulsing phase, the engine also stops providing any driving force. In practical applications, the monitoring of this ACC controller can be referenced to advise the drivers whether to activate the PnG or not.

3.4.4 Synchronization of Pulse-and-Glide Operation

3.4.4.1 The Target Phase Portrait and Definition of Phase Angle of the Virtual Oscillators

The first step for a vehicle is to create the target phase portrait of the PnG operation that fulfills the desired PnG period. For the ith vehicle, with the distance

traveled with $\bar{v}_i$ given as

$$\bar{x}_i(t) = \int_0^t \bar{v}_i(\tau) d\tau, \tag{3.5}$$

the current distance error Δx_i is obtained as

$$\begin{aligned} \Delta x_i(t) &= \Delta x_i(0) + \bar{x}_i(t) - x_i(t), \\ x_i(t) &= \textstyle\int_0^t v_i(\tau) d\tau. \end{aligned} \tag{3.6}$$

Here $\Delta x_i(0)$ is the initial distance error, determined by the initial speed, depending on whether the vehicle is in pulsing or gliding phase initially. The speed difference between the reference speed and actual speed is

$$\Delta v_i(t) = \bar{v}_i(t) - v_i(t). \tag{3.7}$$

With the assumption of small amount of speed oscillation, the air drag and rolling resistance are assumed to be constant and represented with the values calculated using $\bar{v}_i$, the reference around which the vehicle speed oscillates. Then, similar to [39], the target phase portrait of PnG based on Δx_i and Δv_i is obtained, which are given by

$$\begin{aligned} \Delta v_i &= -\bar{a}_{\mathrm{pls},i} \cdot t \\ \Delta x_i &= \Delta x_{\max,i} - \tfrac{1}{2} \bar{a}_{\mathrm{pls},i} \cdot t^2, \ t \in (-\infty, +\infty) \end{aligned} \tag{3.8}$$

for pulsing, and

$$\begin{aligned} \Delta v_i &= -\bar{a}_{\mathrm{gld},i} \cdot t \\ \Delta x_i &= \Delta x_{\min,i} - \tfrac{1}{2} \bar{a}_{\mathrm{gld},i} \cdot t^2, \ t \in (-\infty, +\infty) \end{aligned} \tag{3.9}$$

for gliding. In the pulsing curve (3.8), $\bar{a}_{\mathrm{pls},i}$ is a constant acceleration for pulsing, and the $\Delta x_{\max,i}$ is the designed maximum distance error. On the other hand, in the gliding curve (3.9), $\bar{a}_{\mathrm{gld},i}$ is also constant, and the $\Delta x_{\min,i}$ is the designed minimum distance

error. The pulsing acceleration $\bar{a}_{\text{pls},i}$ is set equal to $a_{\text{lim},i}$, the acceleration limit for ride comfort, while the gliding acceleration $\bar{a}_{\text{gld},i}$ is the free gliding acceleration (negative) for $\bar{v}_i$. With (3.8) and (3.9), the time required to travel to every point from any other point on the target phase portrait can be calculated for a given set of $\bar{a}_{\text{pls},i}$, $\bar{a}_{\text{gld},i}$, $\Delta x_{\text{max},i} > 0$, and $\Delta x_{\text{min},i} < 0$. In this study, $\bar{a}_{\text{gld},i}$ is not controllable in the stage of target phase portrait generation, because braking or using the engine to control the deceleration would be against the philosophy of PnG. Recall, however, if braking is necessary for safety at any time, it is applied by the ACC as described in Section 3.4.3 above. If braking is needed for range keeping, it is applied according to the range keeping algorithm that is described in Section 3.4.5 below. Therefore, adjusting $\Delta x_{\text{max},i}$ and $\Delta x_{\text{min},i}$ is the only way to change the PnG period. For simplicity, we let $\Delta x_{\text{max},i} = -\Delta x_{\text{min},i}$. When a target PnG period is given, each vehicle finds its target PnG curve iteratively by updating the $\Delta x_{\text{max},i}$. Convergence can be achieved in 0.3 s on a laptop with Intel® i5 CPU in MATLAB, and once solved, it can be used for all future times if the PnG acceleration and/or the PnG period do not change. For example, the target phase portraits for $\bar{a}_{\text{pls},i} = 0.3$ m/s^2 and $\bar{a}_{\text{pls},i} = 0.5$ m/s^2 are plotted in Figure 3.5. The dashed lines are derived from (3.8) and (3.9), which then define the target phase portraits denoted with circles. These two target phase portraits both fulfill the PnG period of 25 s; i.e., the vehicles will go along the phase portraits counterclockwise and finish one PnG period in 25 s if they switch to pulsing or gliding phase according to the intersections of pulsing and gliding curves. Note that the distance error is enlarged to accommodate the larger pulsing acceleration for preserving the same PnG period.

Once the target PnG phase portrait that fulfills the target PnG period is obtained, it is parameterized with the phase angle. Figure 3.6 shows an example. The phase angle is assigned proportionally to the traveling time on the target phase portrait from $-180°$ to $180°$. The point where Δx_{max} is achieved is chosen as $0°$, while Δx_{min}

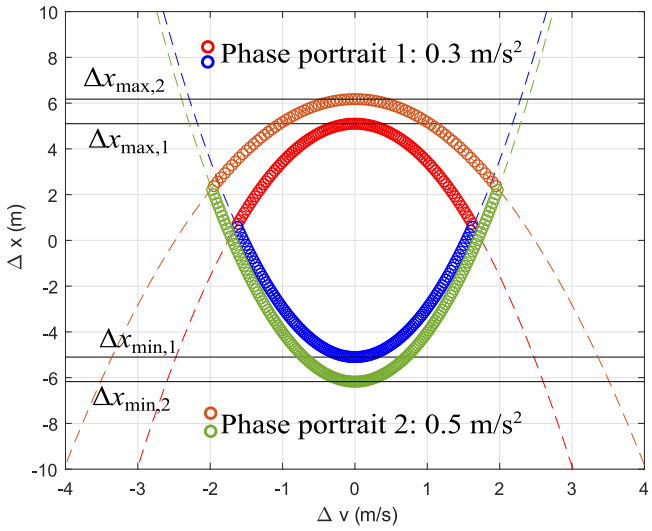

Figure 3.5: The target phase portraits for (1) $\bar{a}_{\text{pls},i} = 0.3$ m/s^2 and (2) $\bar{a}_{\text{pls},i} = 0.5$ m/s^2, both fulfilling PnG period 25 s. The dashed lines are pulsing and gliding curves. The red (orange) circles indicate the pulsing phase and the blue (green) circles indicate the gliding phase, and together they form the target phase portrait for $\bar{a}_{\text{pls},i} = 0.3$ m/s^2 ($\bar{a}_{\text{pls},i} = 0.5$ m/s^2).

corresponds to $\pm 180°$. The other locations of phase angles depend on the pulsing and gliding durations of the specific PnG operation.

3.4.4.2 The Coupling of Virtual Oscillators

The proposed method for PnG synchronization is based on the Kuramoto oscillator. Assuming there are N virtual oscillators, one for each vehicle in the platoon, the dynamics of the Kuramoto model is as follows:

$$\dot{\theta}_i = \omega_i + \frac{K}{N} \sum_{j=1}^{N} \sin(\theta_j - \theta_i), \tag{3.10}$$

where θ_i and ω_i are respectively the phase angle and natural frequency of the ith oscillator, and $K > 0$ is the coupling gain. The coupling gain K can be different for every pair of oscillators, but here we assign the same K to provide a uniform coupling strength for the vehicles.

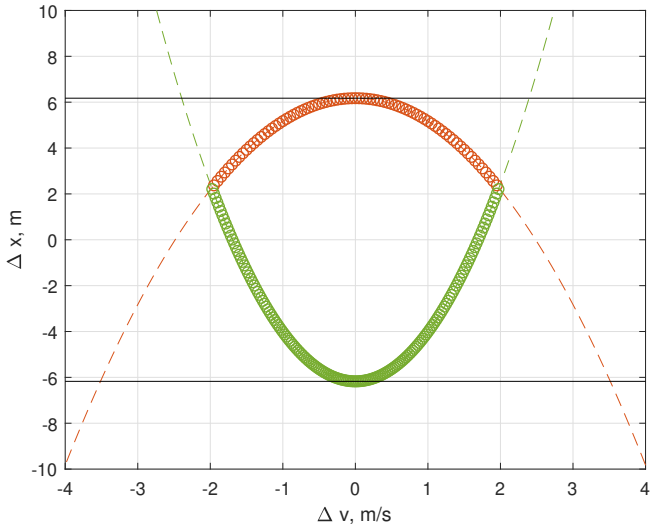

Figure 3.6: The parameterization of the target phase portrait for an example of PnG period $T_{\text{PnG}} = 25$ s, pulsing duration $T_P = 8$ s, and gliding duration $T_G = 17$ s.

An important property of Kuramoto oscillators is that when the natural frequencies of all the oscillators are the same, they will converge to the same phase angle without any phase difference. In our case, the natural frequency is defined by the PnG period, which is common for all the vehicles, and thus converging to the same phase angle in all vehicles is theoretically guaranteed.

3.4.4.3 The Tracking Controller

With the target phase angle from the Kuramoto oscillator (3.10), the target states are interpolated from the phase-angle-parameterized target phase portrait. Then, a state feedback tracking controller is designed so that the vehicle states converge to the target states.

In the following discussion, the superscript $\mathcal{K}$ denotes the values from the Kuramoto oscillator. Assuming the initial time is zero, the Kuramoto oscillator of a vehicle is initialized with the current phase angle, i.e., $\theta_i^{\mathcal{K}}(0) = \theta_i(0)$. This implies

$\Delta x_i^{\mathcal{K}}(0) = \Delta x_i(0)$. From (3.6) and (3.7) we know that

$$\begin{aligned} d\Delta x_i/dt &= \Delta v_i, \\ d\Delta v_i/dt &= \bar{a}_i - a_i. \end{aligned} \tag{3.11}$$

Similarly, because the values of $\bar{x}_i$, $\bar{v}_i$, and $\bar{a}_i$ are shared between the vehicle and virtual oscillator, we have

$$\begin{aligned} d\Delta x_i^{\mathcal{K}}/dt &= \Delta v_i^{\mathcal{K}}, \\ d\Delta v_i^{\mathcal{K}}/dt &= \bar{a}_i - a_i^{\mathcal{K}}. \end{aligned} \tag{3.12}$$

Define the error vector

$$e_i := [\Delta x_i^{\mathcal{K}} - \Delta x_i \ , \ \Delta v_i^{\mathcal{K}} - \Delta v_i]^T. \tag{3.13}$$

The error dynamics can be expressed as

$$\dot{e}_i = \begin{bmatrix} 0 & 1 \\ 0 & 0 \end{bmatrix} e_i + \begin{bmatrix} 0 \\ 1 \end{bmatrix} (-a_i^{\mathcal{K}} + a_i), \tag{3.14}$$

where the target acceleration $a_i^{\mathcal{K}}$ is from the Kuramoto oscillator (3.10):

$$a_i^{\mathcal{K}} = C_i^{\mathcal{K},j} \cdot \dot{\theta}_i, \tag{3.15}$$

where j is an index for pulsing or gliding. The constant coefficient $C_i^{\mathcal{K},j}$ is from the relation between the phase angle and vehicle speed defined during the parameterization of the target phase portrait, which is linear, but the coefficients are different for pulsing and gliding phases:

$$v_i^{\mathcal{K}} = C_i^{\mathcal{K},j} \cdot \theta_i^{\mathcal{K}} + D_i^{\mathcal{K},j}, \tag{3.16}$$

where the coefficients are solved from the parameterized target phase portrait directly.

Then, a state feedback controller is designed to control a_i so that the error dynamics (3.14) can converge to zero:

$$a_i = -K_{s,i} \cdot e_i - C_i^{\mathcal{K},j} \cdot \theta_i^{\mathcal{K}}, \tag{3.17}$$

where $K_{s,i}$ is the controller gain. When implementing the control, if the vehicle is currently in pulsing phase, then (3.17) is used to control the engine torque. If the vehicle is in gliding phase, brake is applied according to (3.17) if it demands a deceleration that is beyond the deceleration of free gliding. After synchronization, this brake due to (3.17) will vanish, because the target phase portrait is established based on the free gliding deceleration.

3.4.5 Range Keeping

Due to the different PnG accelerations, the range between two consecutive vehicles oscillates even after the PnG synchronization is successfully achieved. If a PD controller with feedforward of PV's acceleration based on measured range and speed difference (e.g. [35]) is used for range keeping, it will interfere with the synchronization because of the phase difference between this force for range keeping and the force for synchronization.

To still keep the desired range, an approach integrated into the above tracking control of synchronization is designed as follows. The ego vehicle records the range to the PV at the time when it reaches its minimum distance error $\Delta x_{\min,i}$, denoted as $t_{x,\min,i}$. If the range violation exceeds a certain tolerance, it attempts to compensate the range violation in the following PnG period(s). The reason for picking this time instance as the reference is safety, since the ego vehicle reaches the foremost position of PnG at this time instance. The reference speed $\bar{v}_i$ and position $\bar{x}_i$ are then manipulated to facilitate the range compensation as explained below. Performing

these manipulations once in every PnG period is suitable given that safety is already guaranteed with the monitoring ACC given in Section 3.4.3.

Denote the range error at $t_{x,\min,i}$ as $\Delta R_{e,i}$. If $\Delta R_{e,i} > 0$, it means the ego vehicle needs to catch up. Then, the reference speed $\bar{v}_i$ is temporarily changed by the ego vehicle in the following PnG period to guide the ego vehicle to travel more distance by the amount of $\Delta R_{e,i}$. On the contrary, if $\Delta R_{e,i} < 0$, $\bar{v}_i$ is changed temporarily in the same way to increase the range. The reference trajectory is designed using a 5th-order polynomial:

$$\bar{x}_i(t) = c_{5,i}t^5 + c_{4,i}t^4 + c_{3,i}t^3 + c_{2,i}t^2 + c_{1,i}t + c_{0,i}. \tag{3.18}$$

The coefficients of (3.18) are solved with the final boundary conditions

$$\begin{aligned} \bar{x}_i(t_{x,\min,i} + T_{\text{PnG}}) &= \bar{x}_i(t_{x,\min,i}) + \bar{v}_c T_{\text{PnG}} + \Delta R_{e,i}, \\ \bar{v}_i(t_{x,\min,i} + T_{\text{PnG}}) &= \bar{v}_c, \\ \bar{a}_i(t_{x,\min,i} + T_{\text{PnG}}) &= 0, \end{aligned} \tag{3.19}$$

and the initial boundary conditions as $\bar{x}_i$, $\bar{v}_i$, and $\bar{a}_i$ at $t_{x,\min,i}$. This way, the speed at which the PnG operation switches is also adjusted, since $\bar{v}_i$ is changed. For the case of $\Delta R_{e,i} > 0$, the switching speed increases, which increases the distance traveled in the next PnG cycle. For $\Delta R_{e,i} < 0$, the switching speed is lowered such that the averaged speed and distance traveled in the next PnG cycle are reduced.

We can also exploit V2V communication in the range keeping in the following way. If $\bar{v}_{i-1}$ is transmitted to vehicle i, vehicle i can take action earlier to catch up.

This way, (3.18) becomes

$$\begin{aligned} \bar{x}_i(t) &= \bar{v}_{i-1} \cdot \Delta t \\ &\quad + c_{5,i}t^5 + c_{4,i}t^4 + c_{3,i}t^3 + c_{2,i}t^2 + c_{1,i}t + c_{0,i} \\ \bar{v}_i(t) &= (\bar{v}_{i-1} - \bar{v}_c) + d\bar{x}_i/dt, \end{aligned} \tag{3.20}$$

where Δt is the sample time period.

This range keeping approach, although described separately from the PnG synchronization, happens simultaneously under the tracking control (3.17) introduced previously for synchronization.

3.5 Simulation Results and Discussions

In the simulation study, a four-vehicle platoon traveling around the desired speed $\bar{v}_c = 40$ mph is set up. The target PnG period is chosen as $T_{\text{PnG}} = 25$ s. The four vehicles, labeled in sequence as PV, FV1, FV2, and FV3, are driven with gear 5 without any gear shifting. Since $\bar{v}_c$ is constant, the desired range R_{des} is also constant, chosen as 20 m. Initially, the ranges between each pair of consecutive vehicles are all 25 m, while the speeds are 40, 42, 38, 36 mph for PV, FV1, FV2, and FV3, respectively. The acceleration limits are given as 0.3, 0.4, 0.5, and 0.6 m/s^2 for the four vehicles in the same order. The Kuramoto coefficient is $K = 0.1$, while the natural frequencies for all virtual oscillators are $\omega_i = 2\pi/T_{\text{PnG}}$. The control gains $K_{s,i}$ in (3.17) are $[0.05,\ 0.3]$ for all four vehicles.

The trajectories of ranges, speeds, and accelerations are plotted in Figure 3.7. The synchronization is achieved at around $t = 50$ s, earlier than the completion of range keeping, which happens around $t = 150$ s. The ranges are maintained roughly within 1.5 m of the desired range of 20 m. From the trajectories of accelerations it is seen that, except for the early transients, the accelerations satisfy the preset

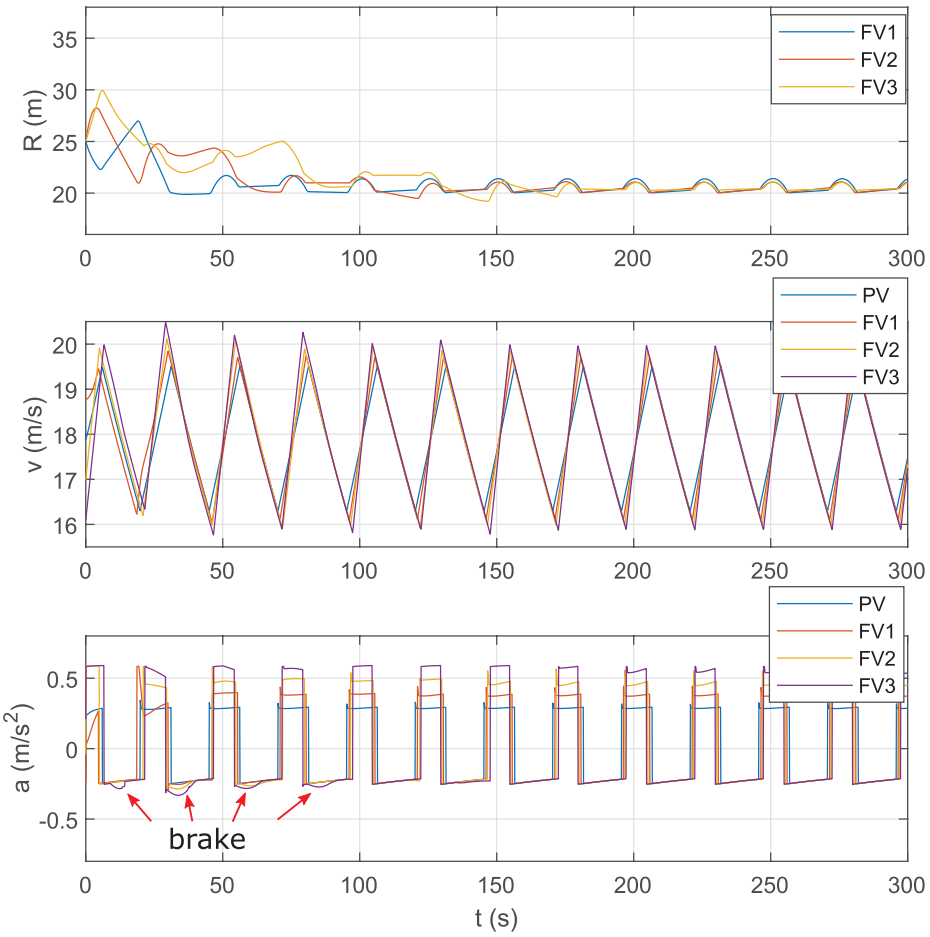

Figure 3.7: The trajectories of the case with synchronization.

limits. Note that before $t = 100$ s, FV2 and FV3 slightly apply the brake to facilitate synchronization and/or range keeping, as indicated by the red arrows in Figure 3.7. The trajectories of the phase angles of the virtual oscillators are shown in Figure 3.8. Initially, the phase angles are distributed in the range of roughly 75°, which are initialized to the phase angles corresponding to their vehicles' initial states. However, based on the Kuramoto model, the virtual oscillators are synchronized within 10 s, setting the target for the vehicles to track to be synchronized.

The phase portraits of the four vehicles for $t \in [250, 300]$ s are plotted in Figure 3.9 and converge to the target phase portraits defined by the pulsing curve (3.8) and gliding curve (3.9). Also note the gradual expansion of the target phase portraits to accommodate the given PnG period as the acceleration limits of the vehicles increase

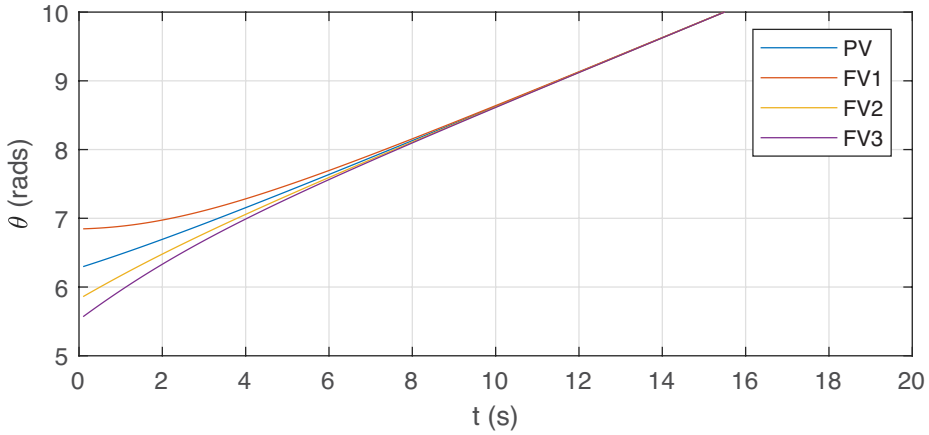

Figure 3.8: The synchronization of the phase angles of the virtual oscillators.

towards the end of the platoon. The bounds of the distance error slightly increase, as well.

Taking FV1 as an example, the deviations of its reference speed $\bar{v}_2$ from $\bar{v}_c$ and reference position $\bar{x}_2$ from the distance traveled by $\bar{v}_c$, which is equal to $\bar{v}_c \cdot t$, are plotted in Figure 3.10. To keep the desired range, the reference speed of FV1 is temporarily increased. Also, the reference position gradually deviates from $\bar{v}_c \cdot t$, and the amount of deviation finally converges close to 5 m, compensating the initial range error of 5 m.

To show the benefits of PnG synchronization, the same parameters and settings are reused in another simulation run without synchronization. The four vehicles in the platoon still keep the same PnG period $T_{\text{PnG}} = 25$ s and carry out their target accelerations as in the synchronization case. The results are shown in Figure 3.11. As expected, the vehicles never achieve phase synchronization. Even though a steady state is achieved, the range oscillations are larger than those with synchronization, which leads to a longer platoon. In particular, the total oscillation of inter-vehicular distance reaches 18 m without synchronization as opposed to 5 m with synchronization. In addition, as seen in the acceleration trajectories, more frequent brake intervention and PnG switching are observed, which may negatively influence the ride

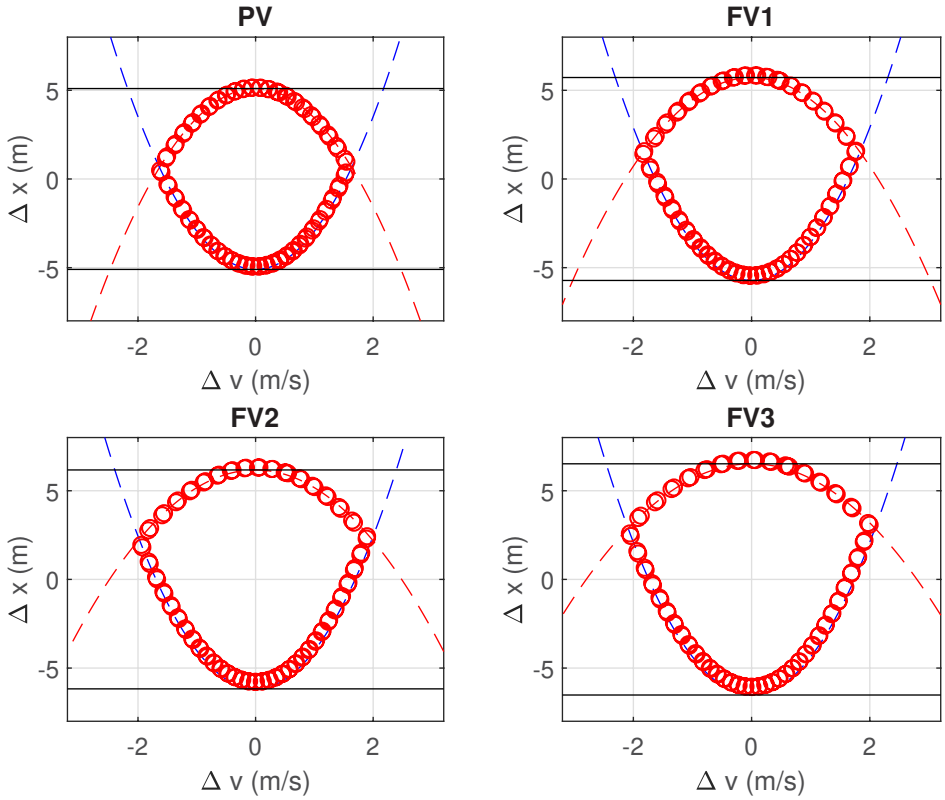

Figure 3.9: The phase portraits of all four vehicles at steady state ($t \in [250, 300]$ s). The red and blue dashed lines are the pulsing curve (3.8) and gliding curve (3.9), respectively. The black lines correspond to the allowed position deviations.

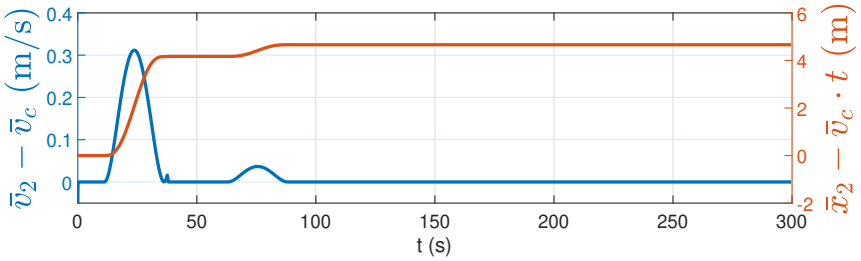

Figure 3.10: The deviations of the reference speed and position of FV1 from the desired trajectories. The distance traveled by $\bar{v}_c$ is equal to $\bar{v}_c \cdot t$.

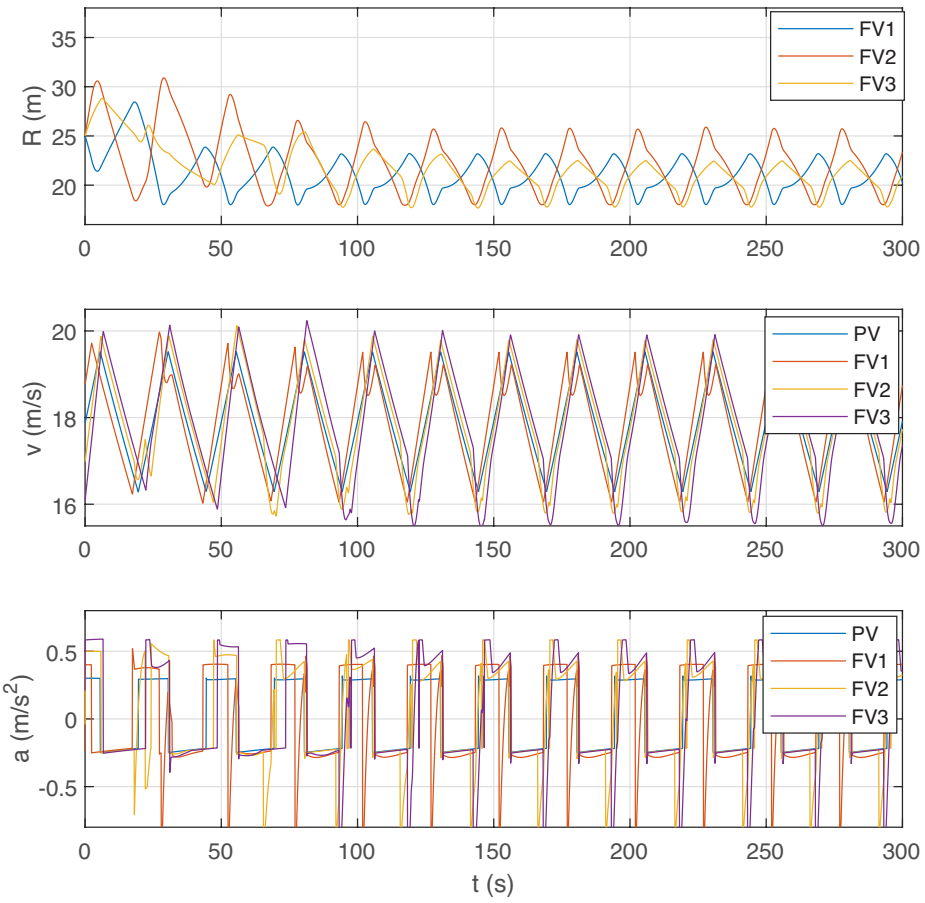

Figure 3.11: The trajectories of the case without synchronization.

comfort and fuel economy.

Finally, the fuel economy improvements in steady state during $t \in [200, 300]$ s are summarized in Figure 3.12. For PV and FV1, the MPG improvements are almost the same for both the cases with and without synchronization. Those for FV2 and FV3, however, increase significantly with synchronization. For example, when synchronization is used, an MPG improvement of 31% is observed for FV3 compared to the best fuel economy possible at constant speed. Without synchronization, this improvement drops down to 22%, leading to a 29% loss in MPG improvement. The frequent braking and PnG switching that are observed when synchronization is not used further raises concerns about ride comfort. The fuel economy improvements increase roughly linearly with the increase of the acceleration limits when synchronization is

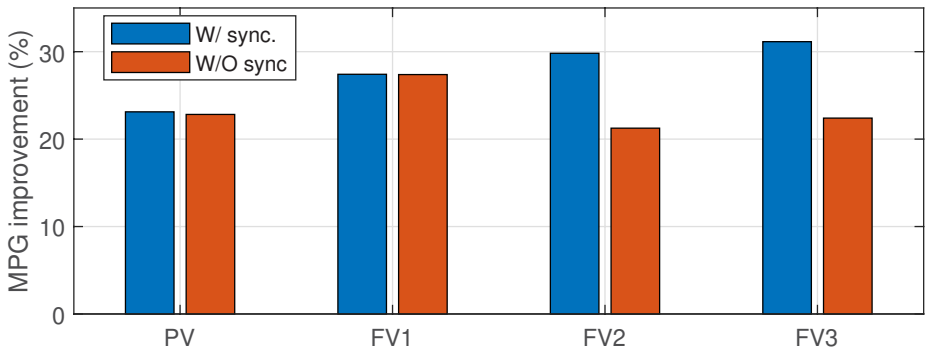

Figure 3.12: The MPG improvements in steady state during $t \in [200, 300]$ s. The baseline: constant-speed driving with gear 6 (30.4 MPG, best fuel economy possible for constant speed at 40mph).

used, highlighting that the trade-off between fuel economy and ride comfort is better balanced with synchronization.

3.6 Conclusions and Future Work

In this study, a decentralized control method is proposed that synchronizes PnG vehicles with different acceleration requirements in a platoon. Using this method, vehicles with different acceleration of PnG, which lead to different fuel saving potentials, can still form a platoon and complete their PnG cycles while remaining close to their desired ranges.

Specifically, the PnG synchronization happens via the synchronization of a series of virtual oscillators, each of them maintained by a vehicle. Given a PnG period, every vehicle in the platoon individually creates and parameterizes with the phase angle its own target phase portrait fulfilling the target PnG period. Then, the target vehicle states given by the virtual oscillator are tracked using a state feedback controller. The PnG vehicles are gradually synchronized after the synchronization of the virtual oscillators based on the coupling mechanism of the Kuramoto model. A platoon of four vehicles traveling around 40 mph with different PnG accelerations is numerically simulated. With the proposed method, the PnG vehicles are synchro-

nized successfully, reaching a total oscillation of inter-vehicle range of roughly 5 m, compared to 18 m of the case without synchronization. Hence, a more compact platoon is achieved with synchronization. In steady state, MPG improvements reach up to 31% with synchronization, whereas without synchronization these benefits drop by up to 29%. Without synchronization, more frequent braking and PnG switching are observed, raising concerns about ride comfort.

In conclusion, the proposed method is a promising approach for platooning of PnG vehicles with heterogeneous acceleration, allowing the vehicles to improve fuel economy while maintaining the desired range and ride comfort.

In this study, the focus is on developing a mechanism of PnG synchronization for heterogeneous platoons. The proposed synchronization method based on the Kuramoto model is flexible such that more advanced and sophisticated methods for controlling individual vehicles can be easily integrated. On the other hand, in this study we do not work on string stability but simply propose the deactivation of PnG if the traffic environment is risky. Nevertheless, a proper design and control for platooning PnG vehicles can avoid frequent PnG deactivation, which increases the potential of fuel saving. This leads to the focus of the next chapter. In addition, the suitable and flexible range policies are also very important in ensuring safety in driving environment while maintaining the platoon compactness. Developing such range policies compatible with the proposed PnG synchronization method is thus a topic for future research.

CHAPTER IV

Analysis on Pulse-and-Glide Platoons

4.1 Introduction

In the last chapter, a control method based on virtual oscillators was proposed to achieve synchronization in PnG platoons. This method is decentralized and scalable, only requiring local communication. In particular, the Kuramoto model [72] is exploited to synchronize the virtual oscillators, which provide the target vehicle states for individual vehicles to track. Threfore, PnG vehicles in a platoon can be synchronized after the synchronization of virtual oscillators. More detailed information on the Kuramoto model can be found in [73, 74]. Simulation results showed that PnG synchronization can help fulfill the target PnG cycles so that the desired fuel saving potentials can be maintained. On the other hand, it was pointed out that more compact platoons are possible using the proposed synchronization method, because the oscillations of inter-vehicle range could be reduced.

This chapter is devoted to analyzing the proposed PnG synchronization method, which is important since we introduce the Kuramoto model for the virtual oscillators. The interaction between it and the PnG operations need further study to ensure the success of the proposed method. Specifically, the questions that are intended to be answered via the analysis include: How does the PnG period influence the PnG platoons and how can it be properly determined? How do we design the individual

controllers? How do the Kuramoto oscillators affect the PnG synchronization and how can we design them such that the desired synchronization behaviors can be achieved?

The analysis conducted to answer the above questions starts from the sensitivity analysis of a single PnG vehicle. Since the speed oscillations form the key challenge in PnG synchronization, only Speed-PnG is focused. From the sensitivity analysis of a single PnG vehicle, it is discovered that different amounts of speed oscillations do not influence the fuel saving potentials as long as they are small, which is practically the case in general. This finding helps us narrow down our scope to only concentrate on the platoon compactness, without worrying about the fuel economy. As will be explained later, the PnG period influences the platoon compactness via the tracking capabilities of individual controllers of vehicles.

For safety, in this research it is assumed that properly assigned range policies can create enough safety distance between vehicles based on the tracking capabilities and behaviors of surrounding vehicles. As to how to design the range policies, it is left for the future work. We then summarize the key findings of the analysis by proposing the guidelines for choosing the PnG period and the design of control gains and Kuramoto gain. A series of simulation studies are also presented to validate these ideas and arguments.

The rest of this chapter is organized as follows. The sensitivity analysis for a single PnG vehicle is given in Section 4.2. In Section 4.3, the results of analysis on PnG platoons are presented, which is summarized with the guidelines for the design of related parameters. Section 4.4 shows the simulations that validate the findings from the analysis for our proposed PnG synchronization method. In Section 4.5 some analysis results are further discussed. Finally, conclusions and future work are given in Section 4.6.

4.2 Sensitivity Analysis of a Single PnG Vehicle

The sensitivity analysis of one single vehicle conducting Speed-PnG is implemented. First the assumption of constant acceleration and deceleration in PnG operations is made and validated to be reasonable in our research. Based on this assumption, analytical expressions for the sensitivity coefficients of average required power in one PnG cycle are presented. These results help us gain the insights about the influences from different parameters. Furthermore, the MPG results under the variations of parameters of interest by simulations are given, which directly provide us with the ideas of how the fuel savings will be affected by those parameters.

4.2.1 The Assumption of Constant Acceleration and Deceleration

In the case where the acceleration and deceleration limits for ride comfort, a_{lim} and d_{lim}, are active, the PnG operation can be seen as with constant acceleration during pulsing and constant deceleration during gliding and they are equal to the accelerations at the average speed, $\bar{a}_{\text{pls}}$ and $-\bar{a}_{\text{gld}}$, respectively. On the other hand, when the acceleration/deceleration limits are not active, strictly speaking the accelerations are not constant due to the fact that the aerodynamic drag is quadratic in the vehicle speed. However, in practical PnG operations, they can still be viewed as constant as shown below.

The validity of the assumption of constant acceleration and deceleration is confirmed numerically using the vehicle model in Chapter III with the parameters defined in Table 3.1. Here the cases with 10% and 30% speed oscillations of the average speeds are simulated with inactive constraints of acceleration/deceleration limits. The average speeds range from 30 mph to 70 mph. In Figure 4.1 to Figure 4.4 the simulated speed trajectories and those approximated using constant accelerations at the average speeds are compared. We can see that the relative errors of the approximated speeds against the actual speeds are very small, less than 0.15 % in the case of 10% cases

and less than 1.5% in the 30% cases. However, the 30% speed oscillations might be too large and thus are not ideal in practical applications. For example, the speed of the case of 30% speed oscillation around 70 mph can be between 60 mph and 80 mph.

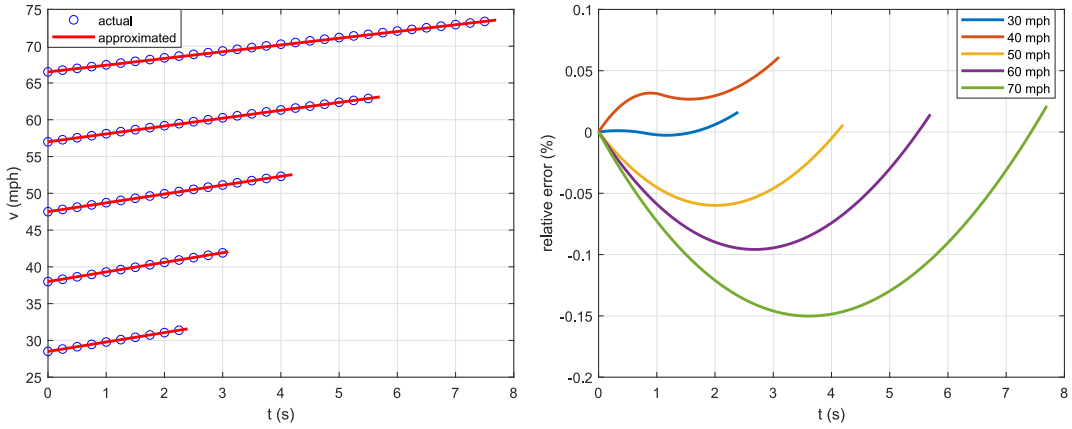

Figure 4.1: Validation of the constant acceleration assumption in pulsing with 10% speed oscillation.

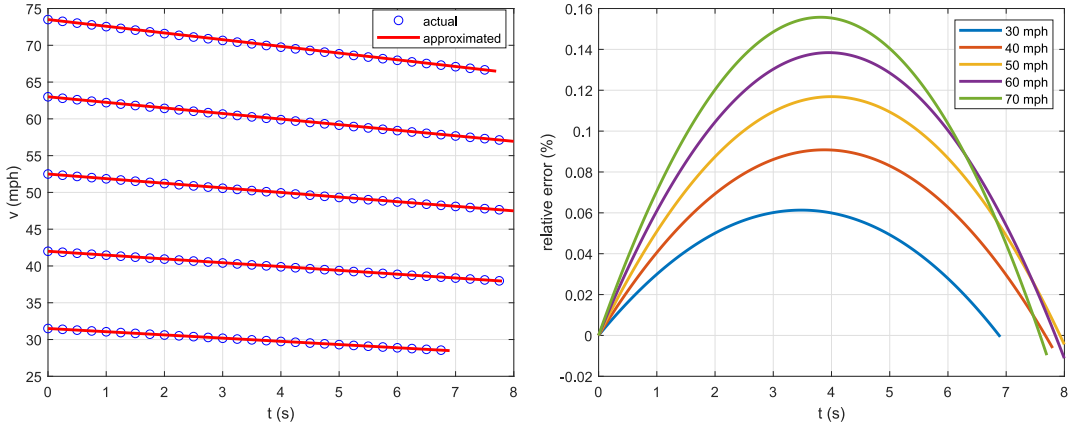

Figure 4.2: Validation of the constant acceleration assumption in pulsing with 10% speed oscillation.

From the above analysis, we can conclude that the PnG operations can be viewed as with constant acceleration and deceleration during pulsing and gliding phases, respectively, as long as the speed oscillations are sufficiently small. Practically, the amount of speed oscillations are indeed small enough to make this assumption valid.

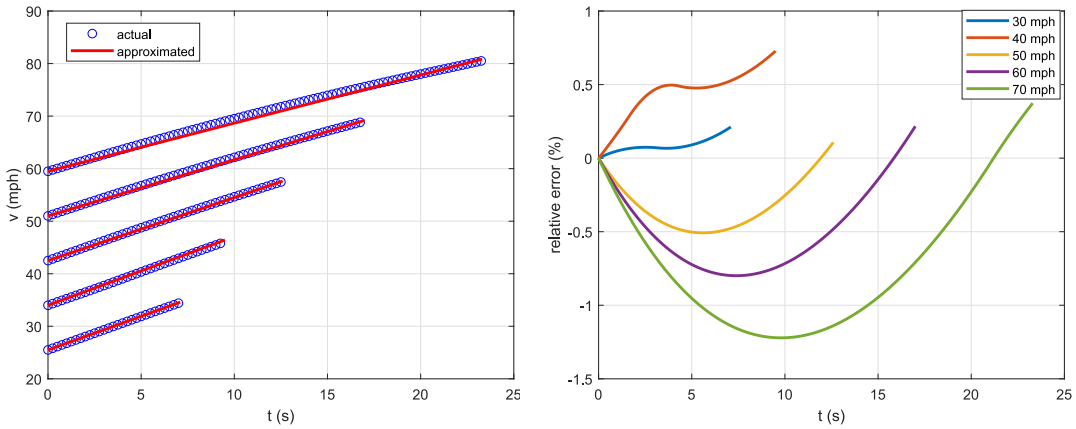

Figure 4.3: Validation of the constant acceleration assumption in pulsing with 30% speed oscillation.

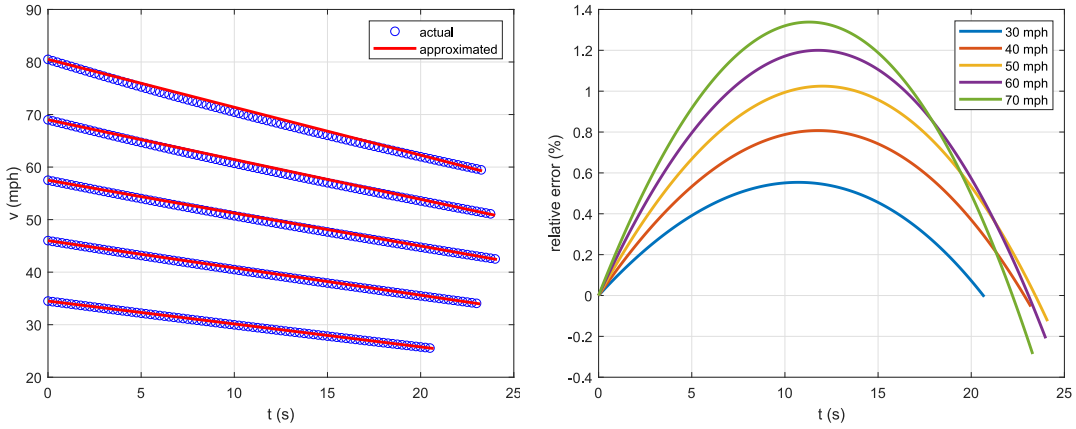

Figure 4.4: Validation of the constant acceleration assumption in pulsing with 30% speed oscillation.

This assumption further simplifies the analysis presented in the following sections.

4.2.2 The Sensitivity Analysis of Speed-PnG

The sensitivity analysis of Speed-PnG is presented here. The effects of variations of specific parameters on the fuel economy of PnG operations hinge on the changes of average power required in PnG cycles and the characteristics of engines that are illustrated by the concave-convex fuel rate curves as shown in Figure 1.3. Specifically,

if the concave regions of the fuel rate curves are larger, the influences of variations of vehicle parameters on the fuel savings tend to be small. On the contrary, if the concave regions are small, we might easily fall into the convex regions and PnG is no longer beneficial.

4.2.2.1 The Sensitivity Coefficients of Required Power in Speed-PnG

To begin with, the required power of PnG is focused. We denote P_{PnG} as the average power required in one PnG cycle and it can be expressed as

$$P_{\mathrm{PnG}} = \frac{E_{d,\mathrm{pls}} + E_{d,\mathrm{gld}}}{T_{\mathrm{PnG}}}, \tag{4.1}$$

where $E_{d,\mathrm{pls}}$ and $E_{d,\mathrm{gld}}$ are energy dissipated due to road load in the pulsing and gliding phases and T_{PnG} is the PnG period. The vehicle will return to its initial states when it completes one PnG cycle. Therefore, the required average power can be expressed as the dissipated energy in one cycle divided by the PnG period, which is equal to $T_{\mathrm{pls}} + T_{\mathrm{gld}}$, the addition of durations of pulsing and gliding phases. In addition, based on the assumption of constant acceleration and deceleration, the durations of pulsing and gliding phases can be expressed respectively as

$$T_{\mathrm{pls}} = \frac{\Delta v_{\mathrm{PnG}}}{\bar{a}_{\mathrm{pls}}} = \frac{v_{\max} - v_{\min}}{\bar{a}_{\mathrm{pls}}}, \tag{4.2}$$

and

$$T_{\mathrm{gld}} = \frac{-\Delta v_{\mathrm{PnG}}}{\bar{a}_{\mathrm{gld}}} = \frac{v_{\min} - v_{\max}}{\bar{a}_{\mathrm{gld}}}, \tag{4.3}$$

with $\Delta v_{\mathrm{PnG}} = v_{\max} - v_{\min}$ the amount of speed oscillation. The energy dissipated due to the road load in gliding is nothing but the change of kinetic energy during the gliding phase:

$$E_{d,\mathrm{gld}} = \frac{1}{2} M_v (v_{\max}^2 - v_{\min}^2) = M_v \bar{v} \Delta v_{\mathrm{PnG}}, \tag{4.4}$$

while that during the pulsing phase is

$$E_{d,\text{pls}} = \int_0^{T_{\text{pls}}} F_r(t)v(t)dt = \frac{\bar{v}\Delta v_{\text{PnG}}^2}{8\bar{a}_{\text{pls}}}\left[C_d\rho_a A_v \bar{v}^2 + 2M_v g \cdot \sin(\theta_r) + 2M_v f_r g \cdot \cos,(\theta_r)\right], \tag{4.5}$$

where $F_r = \frac{1}{2}C_d\rho_a A_v v^2 + M_v g \cdot \sin(\theta_r) + M_v g \cdot \cos(\theta_r)$ is the road load, with θ_r the road grade and other parameters defined in Table 3.1.

The analytical expression of average power required in one PnG cycle derived from (4.1) to (4.5) can then be used for sensitivity analysis. Here the vehicle mass M_v, aerodynamic drag coefficient C_d, rolling resistance coefficient f_r, speed oscillation Δv_{PnG}, and road grade θ_r are studied using the one-at-a-time technique for the local sensitivity analysis [84]. The sensitivity coefficients defined as the normalized partial derivatives of $P_{\mathbf{PnG}}$ with respect to the parameters of interest are as follows:

$$\phi_{M_v}^S := \frac{\partial P_{\text{PnG}}}{\partial M_v}\left(\frac{M_v}{P_{\text{PnG}}}\right) = \frac{2M_v g[\sin(\theta_r) + f_r\cos(\theta_r)]}{C_d\rho_a A_v\bar{v}^2 + 2M_v g\sin(\theta_r) + 2M_v g f_r\cos(\theta_r)}, \tag{4.6}$$

$$\phi_{C_d}^S := \frac{\partial P_{\text{PnG}}}{\partial C_d}\left(\frac{C_d}{P_{\text{PnG}}}\right) = \frac{C_d\rho_a A_v\bar{v}^2}{C_d\rho_a A_v\bar{v}^2 + 2M_v g\sin(\theta_r) + 2M_v g f_r\cos(\theta_r)}, \tag{4.7}$$

$$\phi_{f_r}^S := \frac{\partial P_{\text{PnG}}}{\partial f_r}\left(\frac{f_r}{P_{\text{PnG}}}\right) = \frac{2M_v g f_r\cos(\theta_r)}{C_d\rho_a A_v\bar{v}^2 + 2M_v g\sin(\theta_r) + 2M_v g f_r\cos(\theta_r)}, \tag{4.8}$$

$$\phi_{\Delta v_{\text{PnG}}}^S := \frac{\partial P_{\text{PnG}}}{\partial \Delta v_{\text{PnG}}}\left(\frac{\Delta v_{\text{PnG}}}{P_{\text{PnG}}}\right) = 0, \tag{4.9}$$

sensitivity coefficient w.r.t.	30 mph	40 mph	50 mph	60 mph	70 mph
vehicle mass (4.6)	0.75	0.63	0.53	0.43	0.36
aerodynamic drag coefficient (4.7)	0.25	0.37	0.47	0.57	0.64
rolling resistance coefficient (4.8)	0.75	0.63	0.53	0.43	0.36
amount of speed oscillation (4.9)	0	0	0	0	0

Table 4.1: Values of the sensitivity coefficients of average power required for Speed-PnG at nominal parameter values.

and

$$\phi^S_{\theta_r} := \frac{\partial P_{\mathrm{PnG}}}{\partial \theta_v}\Big(\frac{\theta_r}{P_{\mathrm{PnG}}}\Big) = \frac{2M_v g\theta_r[\cos(\theta_r) - f_r \sin(\theta_r)}{C_d\rho_a A_v \bar{v}^2 + 2M_v g\sin(\theta_r) + 2M_v g f_r \cos(\theta_r)}. \tag{4.10}$$

We can immediately observe that the sensitivity coefficient with respect to speed oscillation is always zero (4.9). It is due to the fact that varying the amount of speed oscillation does not change the ratio of durations between pulsing and gliding phase if the acceleration and deceleration are kept the same in cases of different speed oscillations. This is also the outcome of the assumption of constant acceleration and deceleration, which is valid when Δv_{PnG} is sufficiently small as described in Section 4.2.1. On the other hand, we can see that in (4.10) the sensitivity coefficient with respect to road grade is with θ_r in the numerator. If we evaluate $\phi^S_{\theta_r}$ at $\theta_r = 0$, the nominal value of road grade, the result will be always zero at different speeds. Therefore, direct simulations are applied to understand how the road grade influences the PnG performance and will be presented in Section 4.2.2.2.

The values of the sensitivity coefficients for different average speeds $\bar{v}$ obtained using the parameters in Table 3.1 as the nominal values are summarized in Table 4.1, The nominal value for road grade is assumed to be zero and the nominal speed oscillation is assumed to be 10% for all cases, since the sensitivity with respect to it is negligible as suggested by (4.9).

From Table 4.1, it is observed that sensitivity coefficients with respect to the

vehicle mass are exactly the same as those with respect to the rolling resistance coefficient. It can be known from (4.6) and (4.8) that they are identical when the road is totally flat. In addition, the values of sensitivity coefficients with respect to vehicle mass (or rolling resistance coefficient) and those with respect to aerodynamic drag coefficient sum up to one at every speed. It is because they respectively represent the components of rolling resistance and aerodynamic drag and these two components together constitute the total road load if the road grade is zero. We can also see that the sensitivity with respect to aerodynamic drag coefficient is more and more significant when speed increases. It is due to the fact that the aerodynamic drag is quadratic in the vehicle speed. When speed is higher, aerodynamic drag plays a more important role.

The above analysis gives the idea that which parameters are more influential at different speeds, as indicated by the sensitivity coefficients of average power required in one PnG cycle. Nevertheless, in order to obtain the MPG variations due to variations of specific parameters, we need to take into considerations the fuel rate curves derived from the engine map, which is relatively difficult to analytically expressed. Therefore, numerical simulations are resorted to. In the following, vehicle mass and road grade, two parameters that might relatively important in real applications, are studied using the simulation approach. The simulations with different amounts of speed oscillations are also conducted to validate the argument drawn from (4.9) that MPG is not affected by the amounts of speed oscillations.

4.2.2.2 The Influences on Fuel Saving Potentials

Here the numerical simulations of Speed-PnG are conducted to examine the MPG variations due to the variations of some parameters of interest. The chosen parameters include vehicle mass and road grade. The simulations with different speed oscillations are also conducted to confirm the argument that the amount of speed oscillation does

not affect the fuel economy, as implied by (4.9). For all cases, the transmission is set to gear 6 and the acceleration limit for ride comfort is 0.2 m/s^2. The parameter values in Table 3.1, again, are the nominal values. The simulation results of 40 mph and 60 mph are respectively shown in Figure 4.5 and Figure 4.6 as examples.

First we can see that different speed oscillations do not change the MPG results, which confirm the argument that the amount of speed oscillation does not affect the fuel economy. Then, from Figure 4.5 and Figure 4.6, the MPG does drop as total mass increases. If we assume that one driver/passenger is 80 kg (176 lbs) and there are totally five people onboard, the additional mass added to the vehicle mass is 400 kg (880 lbs), which is almost 15% of the nominal vehicle mass. This 15% additional mass leads to roughly 5.9% drop in MPG in the case of 40 mph and 4.5% drop in the case of 60 mph. Even so, the PnG operation is still able to provide fuel savings as compared with the constant-speed driving, the MPG of which is also provided in Figure 4.5 and Figure 4.6 as well.

The fuel economy is, however, more sensitive to road grade. We can see that for driving only slightly uphill with the vehicle in this research, the MPG drops significantly. Nevertheless, driving slightly downhill can increase the MPG by PnG even more, compared with the constant-speed driving. Practically, on average roads are flat. This fact implies that we may encounter downhill driving after being uphill, which is supported by the road grade statistics in Figure 4.7 from [85]. From Figure 4.7, roughly 25% of the time the road is flat, and 85% of the time the road grade is within ± 5 percent (2.86 degrees). More importantly, it can be observed that the road grade distribution is almost symmetric around 0% road grade. Statistically, under the influence of road grade variations, PnG might save even more fuel compared with PnG on perfectly flat road, since the MPG curves are "convex" in road grade in Figure 4.5 and Figure 4.6.

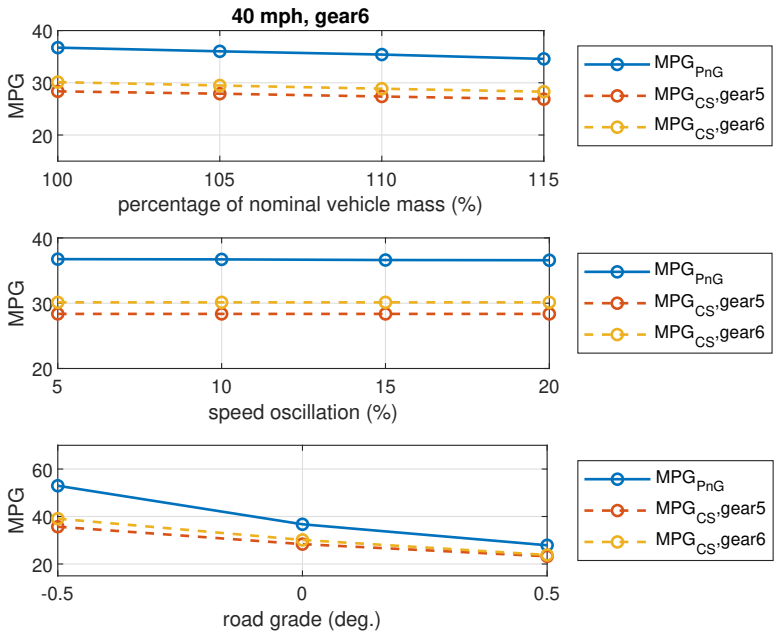

Figure 4.5: Variations of MPG with respect to the variations of vehicle mass, speed oscillation, and road grade: 40 mph. The MPG for constant-speed driving with gear 5 and gear 6 are also shown for reference.

4.2.2.3 Road Grade and Fuel Saving Potentials

In Section 4.2.2.2, it is argued that road grade variations might even increase the fuel economy of PnG, compared with PnG on totally flat road. Here we present the simulation results based on the profile of Sutton Road in Michigan, the road that we also used to conduct PnG experiments, to show this phenomenon.

Figure 4.8 is the road grade profile of Sutton Road. Also shown is the distribution of its road grade. We can see that almost 30% of the time the road is flat but with slightly more downhill in this direction. Therefore, in the simulations we conceptually make round trips such that the road grade distribution is symmetrical with respect to zero degree. On the other hand, a round trip also removes the influence of potential energy in computing the MPG. Also, in order to study the case with larger road grade variations, we manually adjust the road grade profile of Sutton Road by increasing

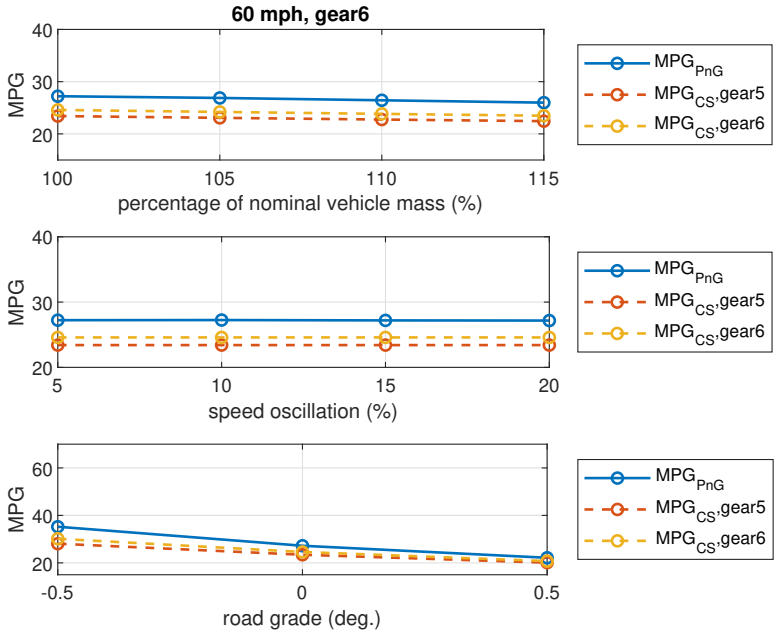

Figure 4.6: Variations of MPG with respect to the variations of vehicle mass, speed oscillation, and road grade: 60 mph. The MPG for constant-speed driving with gear 5 and gear 6 are also shown for reference.

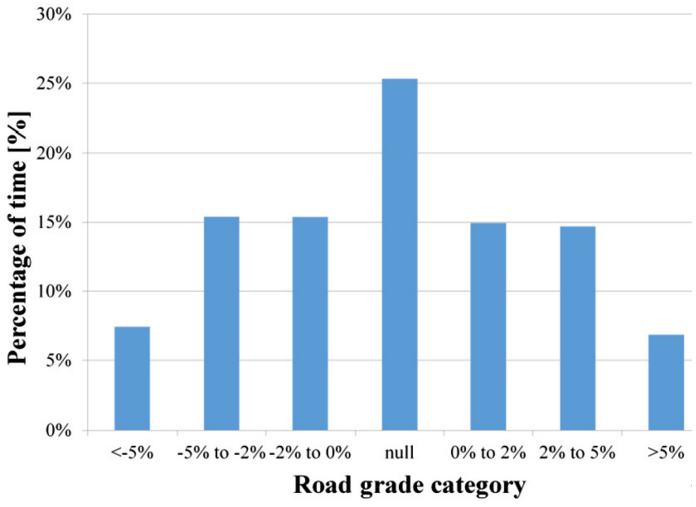

Figure 4.7: Road grade statistics from [85].

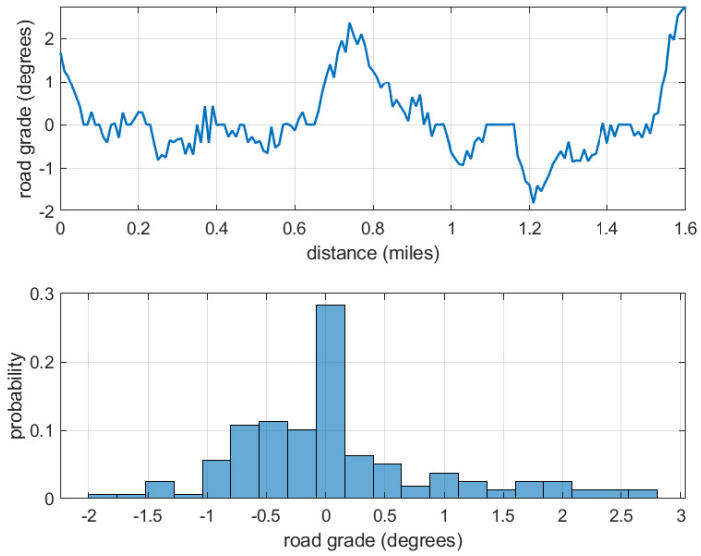

Figure 4.8: The road grade profile and statistics of Sutton Road in Ann Arbor.

the road grade by 1.5 times but limiting it within ±3 degrees, The original and adjusted road grade profiles in one round trip are plotted in Figure 4.9 and Figure 4.10, respectively.

In the simulations, gear 5 is used and the acceleration limit for ride comfort is 0.2 m/s^2. For each grade profile four round trips are implemented. The MPG trajectories along the distance travelled are shown in Figure 4.11. We can see that, even though the MPG trajectories fluctuate, the ones with road grade converge to higher MPG, with the adjusted profile rendering higher values. Therefore, this simulation study validates the argument that statistically road grade variations are possible to lead to better fuel saving results, compared with PnG on flat roads.

4.3 Analysis on the Proposed Approach for PnG Platooning

4.3.1 The Role of the PnG Period

In Section 4.2.2, it is shown that the amount of speed oscillation does not change the fuel saving potentials of PnG, as long as it is sufficiently small. It is because when

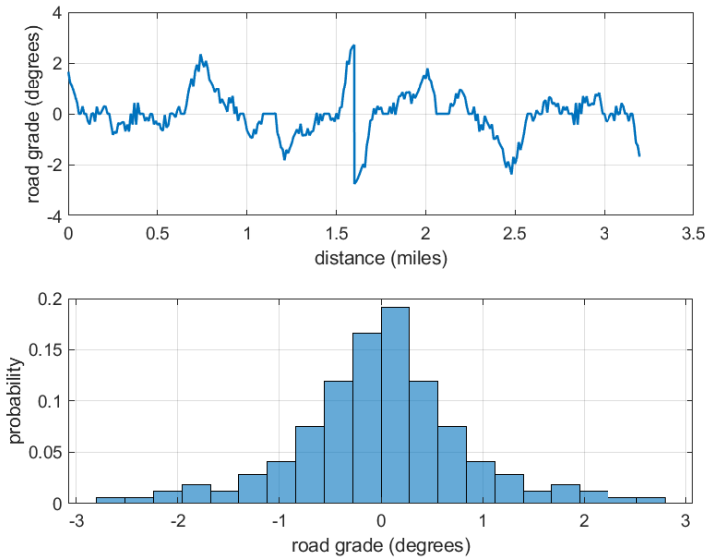

Figure 4.9: The road grade profile and statistics of Sutton Road in Ann Arbor in one round trip.

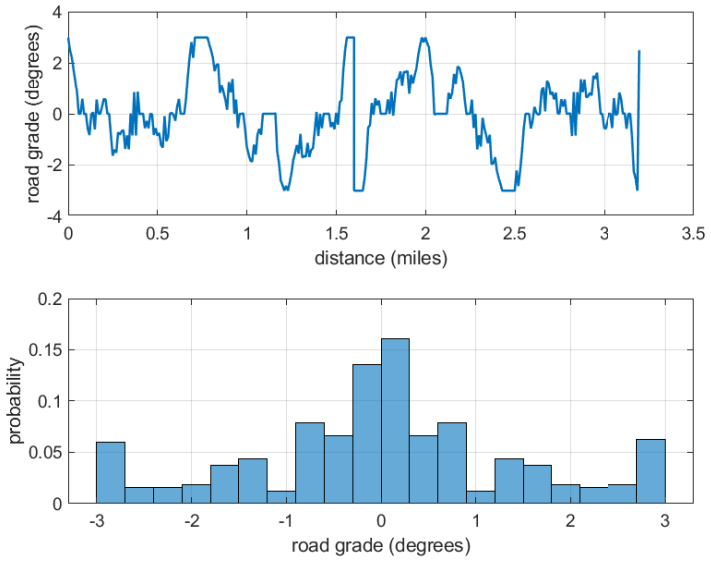

Figure 4.10: The adjusted road grade profile and statistics in one round trip.

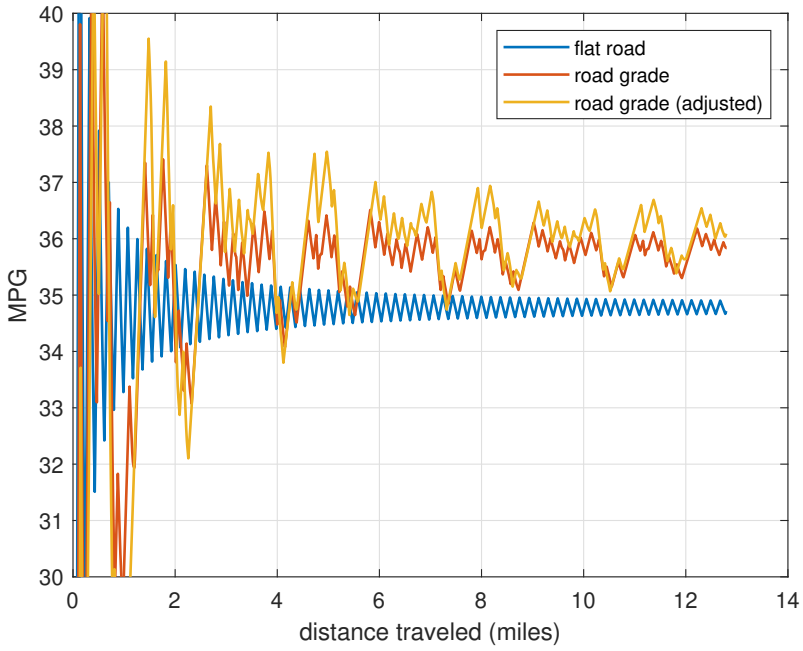

Figure 4.11: The MPG results for different road grade profiles.

the speed oscillation is small, the aerodynamic drag can be viewed as linear in the PnG process. The PnG synchronization approach proposed in Chapter III modulates this speed oscillation such that the heterogeneous PnG vehicles in a platoon are able to achieve the same PnG period and be synchronized, even given different pulsing accelerations for individual fuel saving purposes. In other words, in the proposed method, fuel saving potentials by PnG are not influenced by the PnG period. What PnG period affects is the platoon compactness.

In heterogeneous platoons, if with longer PnG period larger inter-vehicle ranges may be required for safety, because longer PnG period tends to result in larger amount of speed oscillations as just mentioned, and thus larger position oscillations. On the other hand, shorter PnG period may put more requirements on the tracking performance of individual controllers, otherwise the vehicles might not be able to track the target states in time and synchronization cannot be achieved. Therefore, in our proposed method, PnG period will influence the vehicle following ranges, which

further influence the compactness of the platoons. The individual tracking controllers tailored to be compatible with the individual vehicle response, also play a role here as well, in deciding a proper PnG period to use.

4.3.2 The Influence of Virtual Oscillators on Platooning

In our proposed method for PnG platooning presented in Chapter III, each vehicle maintains its own virtual oscillator and the virtual oscillators are coupled via the Kuramoto model. Recall the Kuramoto oscillator for the ith vehicle in a N-vehicle platoon:

$$\dot{\theta}_i = \omega_i + \frac{K}{N}\sum_{j=1}^{N}\sin(\theta_j - \theta_i). \tag{4.11}$$

Using the Kuramoto coupling mechanism, PnG synchronization can be achieved after the virtual oscillators are synchronized to evolve with identical phase angles. Therefore, we can say that the influence of Kuramoto oscillators happens during transient, since after synchronization the sinusoidal terms in (4.11) will vanish. Similar to determining a proper PnG period, the decision of the coupling strength characterized by K in (4.11) also needs to take into considerations the controller tracking capabilities and vehicle response.

4.3.3 The Individual Tracking Controllers

In Chapter III, a full state-feedback control was adopted for tracking the target states given by the Kuramoto oscillators. Here the analysis and design of individual tracking controllers with actuator dynamics considered are presented.

Recall in Chapter III the error dynamics of tracking the target vehicle state $[\Delta x_i^{\mathcal{K}},\ \Delta v_i^{\mathcal{K}}]^T$ for the ith vehicle is defined as

$$\dot{e}_i = \begin{bmatrix} 0 & 1 \\ 0 & 0 \end{bmatrix} e_i + \begin{bmatrix} 0 \\ 1 \end{bmatrix} (-a_i^{\mathcal{K}} + a_i), \tag{4.12}$$

where $e_i := [\Delta x_i^{\mathcal{K}} - \Delta x_i \ , \ \Delta v_i^{\mathcal{K}} - \Delta v_i]^T$ is the error vector and $a_i^{\mathcal{K}} = C_i^{\mathcal{K},j} \cdot \dot{\theta}_i$ with $\dot{\theta}_i$ following (4.11) and $C_i^{\mathcal{K},j}$ the constant from the parameterization of the target phase portrait. The control input is the acceleration command a_i to the vehicle. In this Section the actuator dynamics and disturbance are considered and the control loop for the ith vehicle is shown in Figure 4.12. The transfer function G_i corresponds to the error dynamics (4.12) but with the input defined as

$$u_i = a_{a,i} + d_i - a_i^{\mathcal{K}}, \tag{4.13}$$

where d_i is the disturbance while $a_{a,i}$ is the vehicle acceleration after actuator dynamics. The actuator dynamics is modeled as

$$P_i(s) = \frac{1}{\tau_i s + 1}, \tag{4.14}$$

where τ_i is the actuator time constant for vehicle i and s is the Laplace variable. In constructing the control, we "feedforward" the signal $a_i^{\mathcal{K}}$ and use a proportional-integral-derivative (PID) controller to ensure converging to zero errors. The reason to involve an integral term in the control is to eliminate the steady-state errors in pulsing and gliding phases, while the derivative term provides us the degree-of-freedom to place the closed-loop poles at desired locations. Therefore, the controller K_i is

$$K_i(s) = [k_{P1,i} \ k_{P2,i}] + [k_{I1,i} \ k_{I2,i}]/s + s[k_{D1,i} \ k_{D2,i}]. \tag{4.15}$$

In the following, the output of a signal $u(t)$ fed into a transfer function $G(s)$ is denoted as $G(s)[u(t)]$. The relationship between disturbance and the tracking errors

can be expressed via the transfer functions as

$$e_i = \begin{bmatrix} \frac{\tau_i s^2 + s}{p_c(s)} \\ \frac{\tau_i s^3 + s^2}{p_c(s)} \end{bmatrix} [d_i], \tag{4.16}$$

with

$$p_c(s) := \tau_i s^4 + (1 + k_{D2,i})s^3 + (k_{P2,i} + k_{D1,i})s^2 + (k_{P1,i} + k_{I2,i})s + k_{P1,i} \tag{4.17}$$

the characteristic polynomial. Similarly, the relationship between the signal $a_i^{\mathcal{K}}$ due to the virtual oscillator and the tracking errors can be expressed as

$$e_i = \begin{bmatrix} \frac{\tau_i s^2 + 2s}{p_c(s)} \\ \frac{\tau_i s^3 + 2s^2}{p_c(s)} \end{bmatrix} [a_i^{\mathcal{K}}]. \tag{4.18}$$

It can be seen that the transfer functions in (4.16) and (4.18) are all with the same characteristic polynomial (4.17), which is of 4th-order. Then proper design of the PID gains ensures the stability and convergence of the system in Figure 4.12. We choose the dominant poles $s_{\mathrm{dom},i}$ as a complex conjugate pair, the real parts of which are determined based on the actuator dynamics as $\mathrm{Re}(s_{\mathrm{dom},i}) = -1/5\tau_i$. Conceptually, we want the controller to be five times slower than the actuator, such that the actuator is able to achieve the control command given by the controller.

As explained in Section 4.3.1, the PnG period needs to be compatible with the performance of tracking controllers. If the PnG period is too short, then the controllers may not have sufficient time to converge. In determining a suitable PnG period, we assume that the closed-loop system in Figure 4.12 is dominantly a 2nd-order system by proper design of the PID controller. Then the 5% settling time for this system with a unit step input is $T_{s,i} = -3/\mathrm{Re}(s_{\mathrm{dom},i})$. With this design criterion and the assumption that the actuator dynamics is the same during both pulsing and gliding

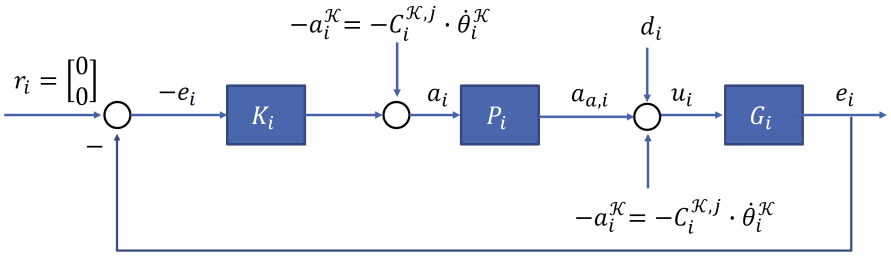

Figure 4.12: The control loop of target state tracking in PnG synchronization with disturbance and actuator dynamics.

phases, the requirement for PnG period is

$$T_{\text{PnG}} \geq 2 \cdot T_{s,i} = -2 \cdot \frac{3}{\text{Re}(s_{\text{dom},i})} = 30\tau_i, \tag{4.19}$$

with $\text{Re}(s_{\text{dom},i}) = -1/5\tau_i$. In a PnG platoon, the vehicles need to achieve the same PnG period in order to by synchronized, so (4.19) needs to be satisfied by every vehicle in the platoon.

4.3.4 The Influence of Communication Topology

Previously, an all-to-all communication (A2A) topology was assumed in the simulations in Chapter III. Actually synchronization can be achieved as long as the communication graph is connected, meaning for each node in the graph (each vehicle), there is a path linking to all the other nodes (other vehicles) [73]. Therefore, other types of communication topology that are with connected communication graph are also feasible. For example, some connected communication topology in CACC that has been studied in literature include predecessor-follower communication (PF) [86, 87], bidirectional communication (BD) [88, 89], two-predecessor-follower communication (2PF) [90, 91], and predecessor-leader-follower communication (PLF) [92, 93].

For undirected communication topology, e.g., BD and A2A [94, 95], a theorem in

[96] can be used to estimate the convergence rate of Kuramoto oscillators. Before the introduction of this theorem, some related background knowledge about the graph theory is introduced [97]. Consider an undirected graph $\mathcal{G}(N, e)$ with N vertices and e edges. An orientation σ can be applied to turn $\mathcal{G}$ into a directed graph $\mathcal{G}^\sigma$. Then the incidence matrix B is an $N \times e$ matrix defined on $\mathcal{G}^\sigma$ with entries $B_{ij} = 1$ if the edge j is incoming to vertex i, $B_{ij} = -1$ if the edge j is outcoming from vertex i, and $B_{ij} = 0$ otherwise. Furthermore, the symmetric matrix defined as: $L = BB^T$ is called the Laplacian of $\mathcal{G}$ and is independent of the choice of orientation σ. The second smallest eigenvalue of L, denoted as $\lambda_2(L)$, is called the algebraic connectivity or the Fiedler eigenvalue, which is greater than 0 if and only if graph $\mathcal{G}$ is a connected and is a measure of how well-connected the graph is [98]. In this formulation of graph, the N number of Kuramoto oscillators (4.11) can be rewritten as

$$\dot{\theta} = \omega - \frac{K}{N} B \sin(B^T \theta), \tag{4.20}$$

with $\theta = [\theta_1, \theta_2, ..., \theta_N]^T$ and $\omega = [\omega_1, \omega_2, ..., \omega_N]^T$.

Theorem 1 in [96] is summarized as follows. Consider the Kuramoto model (4.11) defined over an arbitrary undirected connected graph with incidence matrix B. For any value of the coupling $K > 0$, all trajectories will converge to the set of equilibrium solutions. In particular the synchronized state is locally stable and the rate of approaching to the synchronized state is no worse than $(2K/\pi N)\lambda_2(L)$ exponentially, where $\lambda_2(L)$ is the Fiedler eigenvalue or the algebraic connectivity of the graph. Therefore, if we have a desired time constant of the Kuramoto oscillators $\tau^{\mathcal{K}}$, the corresponding Kuramoto gain can be computed as

$$K = \frac{\pi N}{2\lambda_2(L)\tau^{\mathcal{K}}}. \tag{4.21}$$

A reasonable choice in our research here is $\tau^{\mathcal{K}} = T_{\mathrm{PnG}}$.

Conceptually, if the communication topology is less connected, like the BD communication, the Kuramoto oscillators will converge slower. However, the Kuramoto gain can also be tuned to adjust the convergence speed. Using the theorem in [96], a proper Kuramoto gain can be determined for a given communication topology if it is undirected. A proper Kuramoto gain is also important for transient behaviors, which will be further explained next in presenting the guidelines for the designing control gains and the Kuramoto gain.

4.3.5 The Guidelines for Control Design

In the proposed method for platooning PnG vehicles, there are three time scales, which correspond to actuator dynamics, tracking controller dynamics, and virtual oscillator dynamics. A proper design shall separate these three dynamics such that the PnG synchronization can happen successfully. Conceptually, the control command from the tracking controller should not be too fast to be realized by the actuator, and similarly the virtual oscillator should not be too fast such that the target states can be tracked by the vehicle. Here the discussions on the analysis above are summarized and presented as the guidelines for deciding the related control parameters.

- Figure out the time constants of the actuator dynamics τ_i's.
- Design the dominant poles of the characteristic polynomial (4.17) such that the dynamics of the close-loop system in Figure 4.12 is slow enough compared with the individual actuator dynamics. In this research the dominant poles of vehicle i are designed to be a complex conjugate pair with $\mathrm{Re}(s_{\mathrm{dom},i}) = \frac{-1}{5\tau_i}$, five times slower than the actuator dynamics. Therefore, this combined system of actuator and controller behaves like a 2nd-order system.
- Assign a suitable damping ratio to the combined system of actuator and controller. In this research a damping ratio of 0.78 is applied. Then together with

$\mathrm{Re}(s_{\mathrm{dom},i}) = \frac{-1}{5\tau_i}$, the locations of the dominant poles are decided.

- Choose the locations of the other remaining poles and solve for the PID control gains in (4.15). In this research, it is designed such that the real parts of the remaining two poles are at least 5 times away from the dominant poles and render the least summation of the absolute values of the PID gains. We wish to use smaller gains that can achieve the desired locations of the poles yet preventing too drastic control.

- Decide a settling time $T_{s,i}$ for the PID controller of the ith vehicle. Here the 5% settling time under the unit step input for a 2nd-order system is adopted, i.e. $T_{s,i} = 15\tau_i$.

- The PnG period T_{PnG} should be compatible with the settling time $T_{s,i}$'s for all the vehicles. By assuming the same actuator dynamics for both the pulsing and gliding phases for each vehicle, we set the criterion for deciding PnG period: $T_{s,i} \geq 30\tau_i$ for all i.

- Assuming the communication topology is undirected, e.g. A2A or BD, we use the theorem in [96] to estimate the convergence rate for the Kuramoto model as $\frac{2K}{\pi N}\lambda_2(L)$, where $\lambda_2(L)$ is the second smallest eigenvalue for the graph Laplacian of the communication topology, Then by assuming the time constant of the Kuramoto oscillators equal to the PnG period, i.e., $\tau^{\mathcal{K}} = T_{\mathrm{PnG}}$, the Kuramoto gain can be determined as

$$K = \frac{\pi N}{2\lambda_2(L)T_{\mathrm{PnG}}}. \tag{4.22}$$

Next, a series of studies are presented to support some key arguments discussed above using the guidelines to design the related parameters.

4.4 Simulation Studies

4.4.1 Actuator Dynamics and PnG Platooning

The goal of this study is to see how a vehicle with relatively slow actuator dynamics will influence the whole PnG platoon. Practically, sometimes there are heavy vehicles in the traffic, e.g. heavy duty trucks. These vehicles may lead to less compact platoons, which will be shown in the following.

Assume there are 4 identical vehicles, PV, FV1, FV2, and FV3, travelling around 40 mph but with different acceleration limits for ride comfort. From PV to FV3, a_{lim} is 0.2, 0.3, 0.4, and 0.5 m/s^2 respectively. The vehicle models and parameters are the same as those used in Chapter III except for the actuator dynamics, which was not considered previously. In the first case of this study of actuator dynamics, the actuator time constants τ_i's are 0.5 s for all four vehicles, while in the second case that of PV is increased to 1 s.

We choose the PnG period based on the criterion (4.19). Therefore, T_{PnG} is 15 s and 30 s for the first case and second case respectively. The corresponding target phase portraits are plotted in Figure 4.13 and Figure 4.14. It can be seen that in order to fulfill $T_{\text{PnG}} = 30$ s, even only due to one single vehicle (PV), the position deviations are larger, as denoted by the black lines in Figure 4.13 and Figure 4.14. The position deviation $\Delta x_{\max} - \Delta x_{\min}$ for FV4 in the second case almost reaches 19 m, significantly increased from roughly only 5 m in the first case. Due to the large position deviations in PnG, the inter-vehicle ranges may need to be larger in order to maintain safety. Therefore, the platoon in the second case will be longer than that in the first case, even though the number of vehicles are the same in both cases.

The outcome from this study of influence of actuator dynamics on platooning suggests that synchronizing PnG vehicles with too different actuator dynamics may not be a good idea. The other faster response vehicles need to have unnecessarily

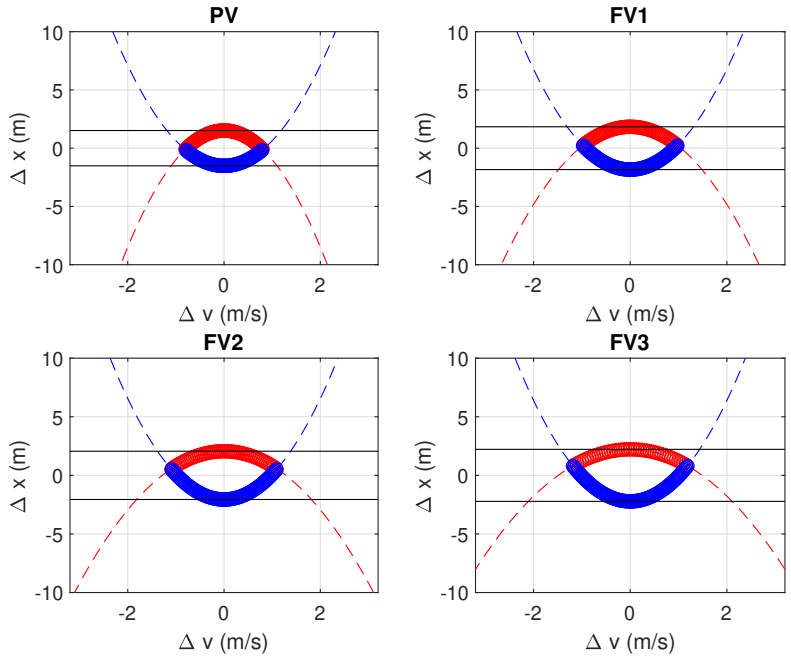

Figure 4.13: The target phase portraits of the case with $\tau_{\mathrm{PV}} = 0.5$ s, the same as all the other vehicles. The black lines indicate the maximum and minimum position deviations.

long PnG period and thus they tend to have large position oscillations especially if they wish to save more fuel by choosing less constrained accelerations. Practically, we can group vehicles with similar actuator dynamics to form a platoon. This will reduce the degree of sacrificing for some vehicles in a platoon and optimize the whole performance, which is a topic worth exploring in the future.

4.4.2 All-to-All and Bidirectional Communication Topology

In this study of communication topology, it is intended to validate the theory used to design the Kuramoto gain (4.22) and see whether it can accommodate A2A and BD topology.

Here four PnG vehicles try to form a platoon. The simulation setup is the same as that in the first case in Section 4.4.1, with identical actuator dynamics $\tau_i = 0.5$ s. However, the first case in this study of communication topology is with A2A

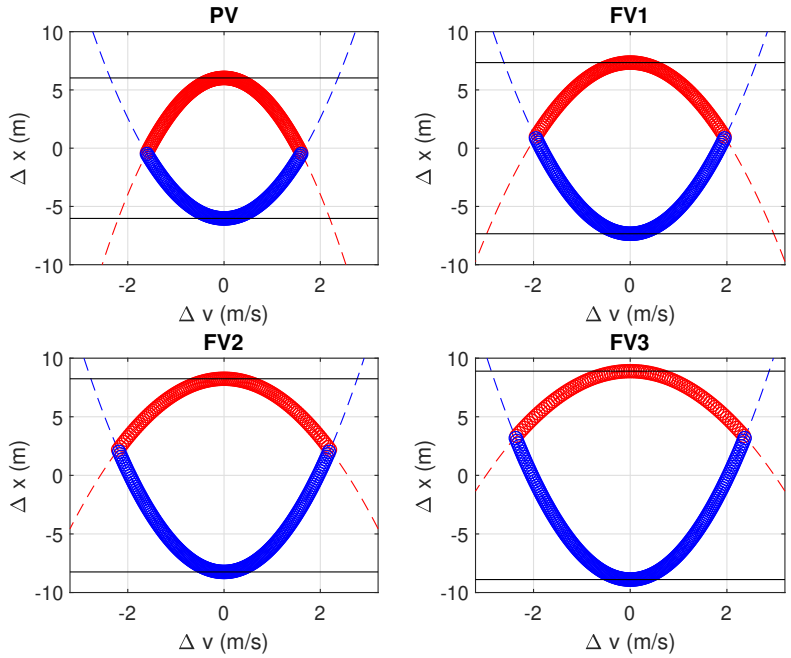

Figure 4.14: The target phase portraits of the case with $\tau_{\mathrm{PV}} = 1$ s, while the other vehicles are with $\tau_{\mathrm{PV}} = 0.5$ s. The black lines indicate the maximum and minimum position deviations.

communication and the second case with BD communication. For four vehicles ($N = 4$) the second smallest eigenvalues $\lambda_2(L)$ for the communication graph Laplacian are 4 and 0.5858 respectively for A2A and BD topology. From (4.22) we obtain the Kuramoto gain $K = 0.1047$ for the A2A case and $K = 0.7151$ for the BD case.

The trajectories from simulations of these two cases are presented in Figure 4.15 and Figure 4.16. It can be observed that both cases achieve steady state around $t = 60$ s to $t = 70$ s and there is not obvious difference between the two after synchronization. The results of MPG improvements are summarized in Figure 4.17 and there is not significant difference between these two cases also.

From this study, we can see that by using the guideline of designing the Kuramoto gain based on the theorem in [96], similar performance can be achieved in spite of different communication topology.

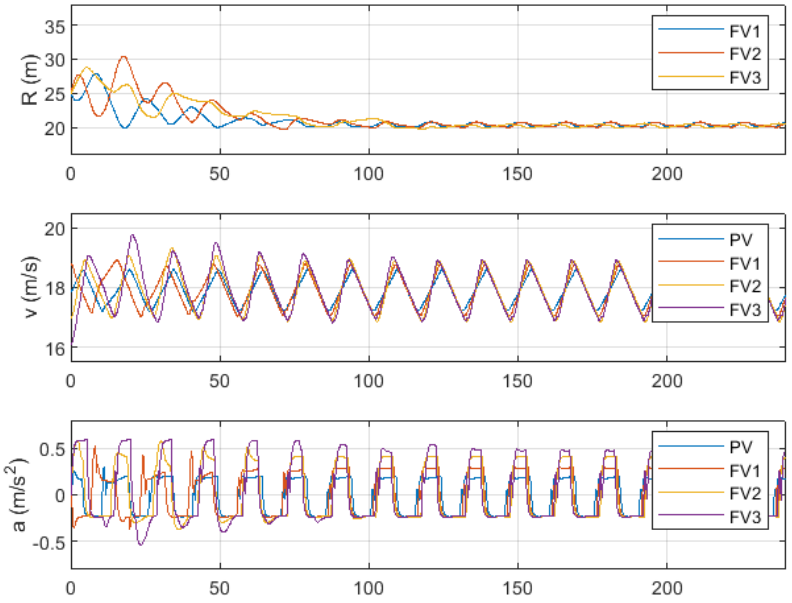

Figure 4.15: The trajectories of the case with all-to-all communication.

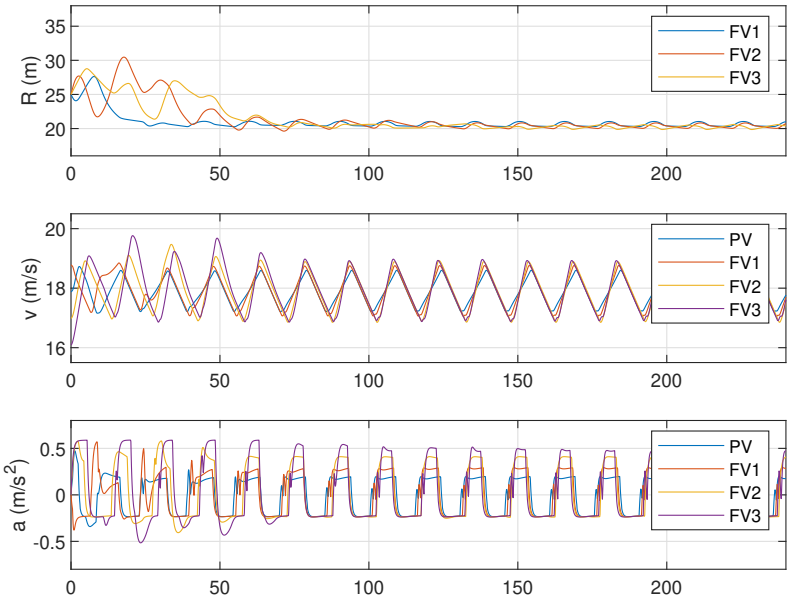

Figure 4.16: The trajectories of the case with bidirectional communication.

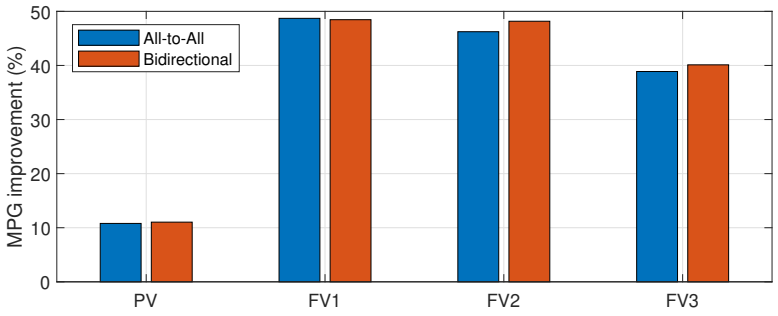

Figure 4.17: The results of MPG improvements of the study of communication topology.

4.4.3 The Influence of Kuramoto Gain

The purpose of this study of Kuramoto gain is to show what will happen if an improper Kuramoto gain is used. The results also promote the use of the suggested approach for design of the Kuramoto gain.

Again, the same setup of four vehicles travelling around 40 mph is adopted, but here the two cases studied are both with A2A communication and $\tau_i = 0.5$ s for all vehicles. In the first case of this study of Kuramoto gain, $K = 0.1047$ from the guideline is used. Therefore, it is exactly the same case as the first case in Section 4.4.2, of which the simulation results are show in in Figure 4.15. For the second case here, the Kuramoto gain is intentionally increased to 10 times larger than the one obtained from the suggested approach, i.e. $K = 1.047$ in the second case. The simulation results of the second case are shown in Figure 4.18. It can be seen that compared to the first case in Figure 4.15, which is with K from proper design, the acceleration during transient for the second case is more drastic. This more drastic transient behavior leads to the drop of MPG improvements, as summarized in Figure 4.19.

From (4.11), we can see that the virtual oscillators will simply evolve their phase angles with the same frequency after synchronization, since the sinusoidal terms will vanish when they achieve the same phase angles. In other words, the Kuramoto gain

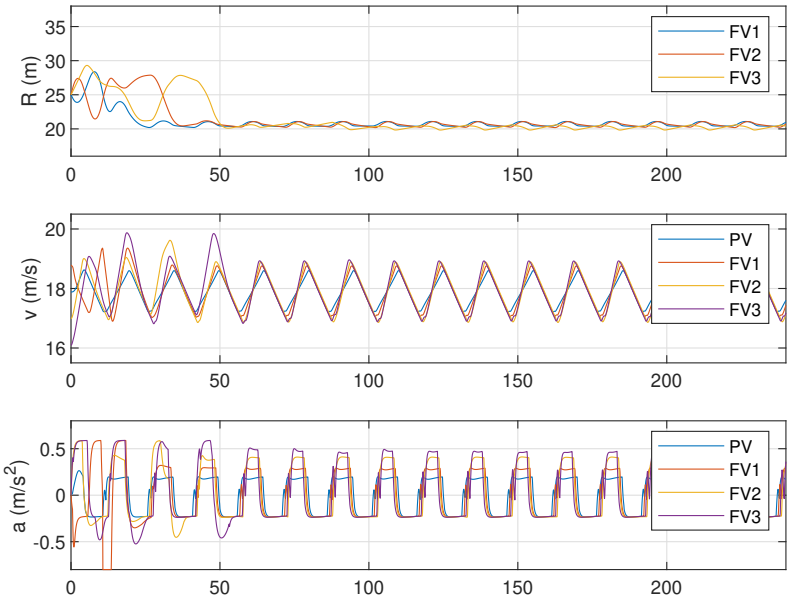

Figure 4.18: The trajectories of the case with with 10 times the Kuramoto gain from theory.

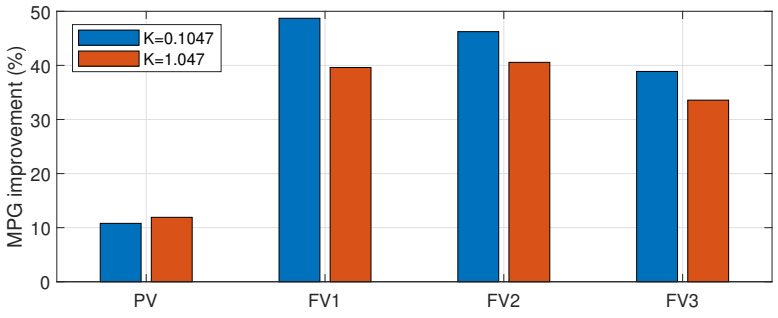

Figure 4.19: The results of MPG improvements of the study of Kuramoto gain.

mainly affects the transient behavior before synchronization. Too large a Kuramoto gain will thus lead to more drastic transient as shown in this simulation study. On the other hand, if the Kuramoto gain is too small, the synchronization process will take longer time than desired. Again, the proposed guidelines provide an approach to choosing suitable Kuramoto gain, if the communication is undirected.

4.5 Further Discussions on the Analysis Results

One of the major goals of this chapter is to detail how to design the parameters of the PnG synchronization method proposed in Chapter III. The major results were previously summarized and presented by giving the step-by-step guidelines of the parameter design for the proposed PnG synchronization method in Section 4.3.5. Here, some key points are further elaborated with a gradually enlarged scope.

From the sensitivity analysis of a single PnG vehicle, it is discovered that the MPG values are not sensitive to the amounts of speed oscillations. This finding will simplify the study on platoon performance, since we can remove fuel saving from the scope and only focus on synchronization and platoon compactness. Therefore, in determining the PnG period, only the capabilities of the tracking controllers, characterized by the settling time, are considered, but not about the fuel economy. The tracking controllers are important for the success of synchronization,

In the case study of different communication topology, the results show that by using the presented approach to determine the Kuramoto gain, similar performance in terms of convergence and fuel savings can be achieved. However, for less connected communication topology (e.g. BD), the Kuramoto gain needs be larger if we wish to achieve the same convergence performance as that of more connected topology like A2A. This"high gain" control may raise some concerns in practical applications. In this research, the communication delay is not considered. A large Kuramoto gain may lead to less robustness if communication delay or other uncertainties exist.

It is also pointed out that mixing PnG vehicles with too different actuator dynamics in a platoon would result in large range oscillations for those vehicles with faster actuator dynamics. It is similar to the concept that the load that can be carried through by a series circuit is limited by the weakest component. Therefore, separating vehicles with different actuator dynamics to form different platoons would maintain the platoon compactness, while not letting individuals sacrifice.

4.6 Conclusions and Future Work

In this chapter, the research of PnG synchronization is continued by conducting the analysis of the proposed synchronization method. The analysis starts from the sensitivity analysis of Speed-PnG of a single vehicle. It is shown that the amount of speed oscillation does not influence the fuel savings of Speed-PnG as long as the speed oscillation is small. From the sensitivity analysis, we also find out that even though the fuel saving potentials by PnG are sensitive to road grade, statistically PnG may be able to achieve higher MPG compared with PnG on totally flat roads. It is based on the assumption that on average the roads people encounter are flat. Numerical simulations based on real road profiles with round trips validate this finding.

Further, the conclusion that speed oscillation does not affect the fuel saving potentials leads us to focus only on the role of PnG period for successful synchronization and not for fuel savings. Then based on the principle of not having interfered actuator dynamics, controller dynamics, and virtual oscillator dynamics, the step-by-step guidelines for the design of the controller gains, the Kuramoto gain, and PnG period are presented. In particular, the theorem in [96] on the convergence rate of Kuramoto oscillators considering the undirected communication topology is utilized to design proper Kuramoto gain. A series of simulation studies are also demonstrated to validate the key findings and arguments from the analysis.

In this research, we focus on how to successfully synchronize the PnG platoons.

From simulations, we can see that after synchronization, the oscillations of inter-vehicle ranges can be significantly reduced and thus argue that PnG synchronization is able to maintain the compactness of platoons. However, proper range policies that are flexible enough and able to take care of different requirements/preferences of ride comfort and fuel savings, are still needed. The development of such range policies, which ensure safety while keeping the platoon compact, is the work worth pursuing in the future. Also, the influence of communication delay and the measures to counter this influence is worth more research.

CHAPTER V

Experimental Study

5.1 Introduction

This chapter presents the experimental study using an automated Lincoln MKZ hybrid vehicle. The experiment is conducted on open roads, including locals and highways. In literature, the examples of PnG experiments using real vehicles include Toyota Prius (hybrid) on a chassis dynamometer [18], Renault Clio 3 Eco 2 (ICE) [50] on a test track, and Nissan X-trail (ICE) [22] on a test course. In these three papers, only [22] is carried out with an automated vehicle, but with relatively low speed (around 40 kph). With the automated Lincoln MKZ hybrid, we can more easily implement PnG at different speeds. From the experiment, we wish to obtain more comprehensive knowledge of PnG operations.

The rest of this chapter is as follows. In Section 5.2, the test vehicle is introduced. Section 5.3 details the experimental procedure and the data processing. The experiment result is presented in Section 5.4. Finally, Section 5.5 gives the conclusions and future work.

Parameter	Description	Value	Unit
M_v	vehicle weight	1950	kg
C_d	air drag coefficient	0.275	-
A_v	vehicle frontal area	2.08	m^2
ρ_a	air density	1.225	kg/m^3
f_r	rolling resistance	0.01	-
r_w	effective tire radius	0.347	m
g	acceleration of gravity	9.81	m/s^2
C_{bat}	battery capacity	1.4	kWh

Table 5.1: The vehicle parameters of 2015 Lincoln MKZ hybrid.

5.2 The Test Vehicle

The test vehicle is an automated 2015 Lincoln MKZ hybrid, which is a power-split hybrid with a 2.0L Atkinson engine and CVT transmission. The drive-by-wire control capability of this platform is developed by the provider of autonomous technology projects, AutonomouStuff, in collaboration with Dataspeed Inc. The control of the test vehicle is in the framework of robotic operating system (ROS). In the ROS framework, signals are published and subscribed with the concept of nodes. In experiment, a laptop connected to the vehicle computer via an ethernet cable serves as the control node. The control node receives signals about the current vehicle status and then determines the control commands to be published.

The instantaneous fuel consumption information is not provided through the framework of ROS. Instead, a controller area network (CANbus) interface is used to access the fuel rate signal, as well as other important signals, via the on-board diagnostics (OBD) port. This test vehicle is also equipped with the real-time kinetics (RTK) GPS, which can provide accurate positioning information. The vehicle parameters used in this study are summarized in Table 5.1.

5.3 Methodology

This section explains how the PnG experiment is conducted. Since the detailed model and engine map of the test vehicle are not available, we assign different target pulsing accelerations to change the engine operating points as a way to explore the unknown engine map. The fuel economy of PnG cases is then compared with that of the constant-speed (CS) cases to see whether we can benefit from PnG operations in terms of fuel saving. The details of the experimental process are as follows.

5.3.1 Experiment Setup

Five different speeds, ranging from 30 mph to 70 mph, are tested. Each speed is with a CS case as the baseline and with the PnG cases oscillating around this speed with different levels of pulsing acceleration. For speeds of 30, 40, and 50 mph, the tests are conducted on Sutton road, a countryside road north of Ann Arbor, Michigan, while the cases of 60 and 70 mph are on the Michigan highway M-14 between Exit 10 and Exit 15. The length and elevation obtained from Google Earth of these two test routes are shown in Figure 5.1 and Figure 5.2 respectively. The highway route is flat with slope between only $\pm 0.8\%$ in both directions, while the route for low speeds is a little hilly, with maximum slope 5.7% and -3.7%. The slope of test routes may influence the fuel consumption and is therefore compensated as explained later in this section.

In addition to the fuel rate information, other signals such as torque and speed of engine, motor, and generator, and battery SOC, voltage, current, and temperature, are accessed from CANbus via the OBD port. As to the vehicle location, speed, and traveled distance, we rely on the RTK recordings. The RTK base station is at the Mcity test facility of the University of Michigan. Even though RTK is a high-precision positioning technology, it is not able to provide very accurate elevation information as other GPS devices due to the limitations of satellites. Therefore, in computing

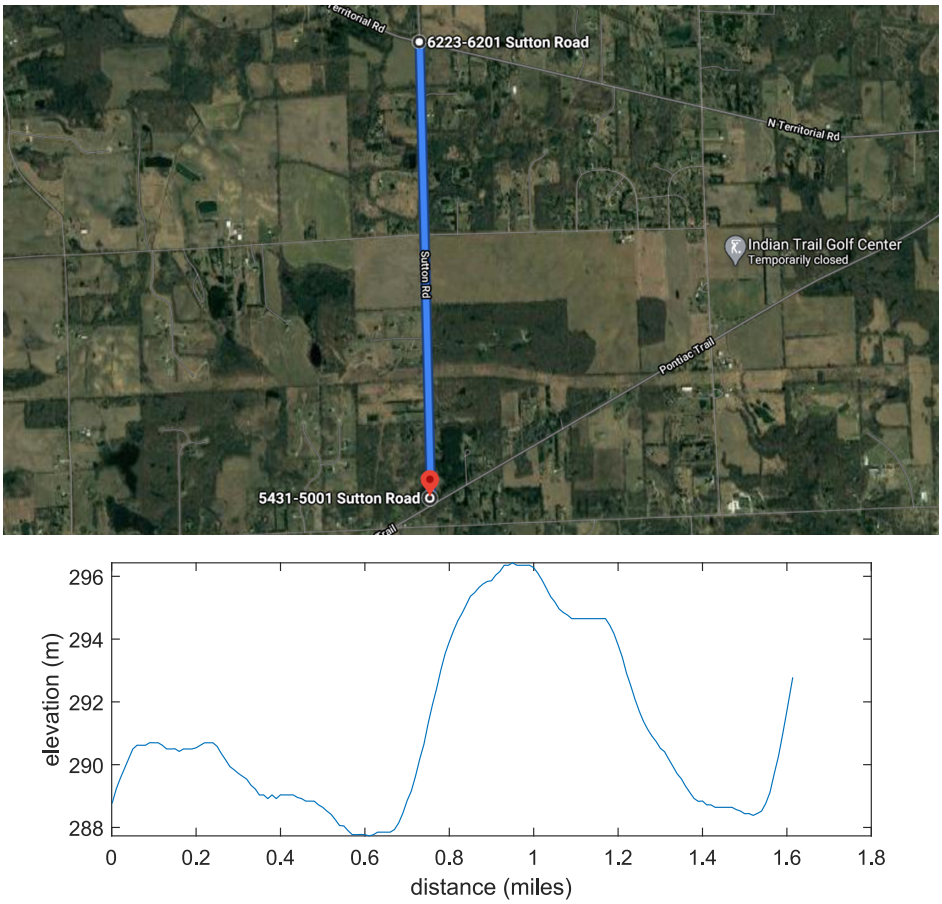

Figure 5.1: The test route for low speed cases: Sutton road. The distance is measured from the upper point of the road segment (north: up).

the corrected MPG for compensating the influence of road slope, we resort to the Google Earth elevation and assume that it is more reliable than the RTK elevation. In particular, the latitude and longitude signals from RTK, which are not affected by the satellite limitations as for elevation, are utilized to interpolate for the elevation information given by the Google Earth data.

For each trial of the cases, including CS and PnG ones, a round trip is conducted. In other words, a trial of low speeds includes driving southbound once and northbound once on the Sutton road; a trial of high speeds included driving from Exit 10 to Exit 15 once and from Exit 15 to Exit 10 once on the highway M-14. In addition, because of relative short route and long duty cycles of pure motor driving, four trials are

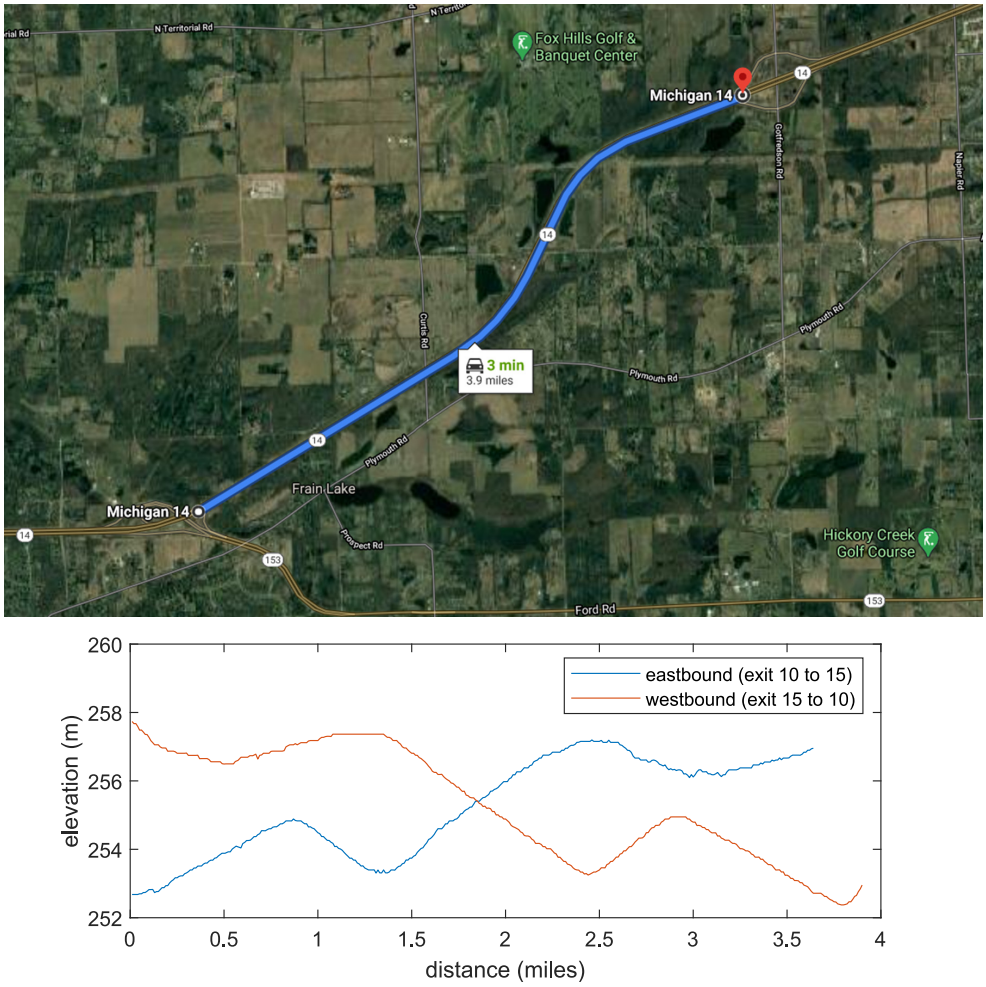

Figure 5.2: The test route for high speed cases: Michigan highway M-14 between exit 10 and exit 15 (north: up).

conducted for CS cases from 30 to 50 mph, whereas all the PnG cases and CS cases of 60 and 70 mph contain only one trial. The target pulsing accelerations of PnG cases for low speeds, 30 to 50 mph, are assigned as 0.2, 0.5, and 0.8 m/s^2. For 60 mph, 0.2 and 0.5 m/s^2 are used, and 0.1 and 0.2 m/s^2 are implemented for 70 mph. However, due to missing data segments from CANbus recording, the result of 30 mph with 0.5 m/s^2 will not be presented.

5.3.2 Control Implementation

For the CS cases the built-in cruise control function of the test vehicle is used. As to the PnG cases, the control commands to vehicle are sent via the ROS framework. To better react to the traffic and test environment, only the longitudinal dynamics is controlled automatically while the steering wheel is operated by a driver. Originally, it is intended to switch to neutral gear while in the gliding phase, which is anticipated to achieve higher PnG potential. However, the test vehicle is not able to fulfill this command, likely due to the inner safety strategy. The details of how PnG is implemented are as follows.

5.3.2.1 Pulse-and-Glide Switching

Since there is no preceding vehicles to follow, the switching between pulsing and gliding phases is decided solely by the vehicle speed. The switching speeds are derived based on the rule-based switching approach in [39]. This approach involves a target phase portrait as shown in Figure 5.3 that is constructed from the defined pulsing curve

$$\begin{aligned} \Delta v &= -\bar{a}_{\text{pls}} \cdot t \\ \Delta x &= \Delta x_{\max} - \tfrac{1}{2}\bar{a}_{\text{pls}} \cdot t^2,\ t \in (-\infty, +\infty) \end{aligned} \tag{5.1}$$

and gliding curve

$$\begin{aligned} \Delta v &= -\bar{a}_{\text{gld}} \cdot t \\ \Delta x &= \Delta x_{\min} - \tfrac{1}{2}\bar{a}_{\text{gld}} \cdot t^2,\ t \in (-\infty, +\infty), \end{aligned} \tag{5.2}$$

where Δv and Δx are respectively the speed error with respect to the average speed (30 to 70 mph in the experiment) and the distance error with respect to the distance traveled with the average speed, and $\bar{a}_{\text{pls}}$ and $\bar{a}_{\text{gld}}$ are the pulsing and gliding accelerations. The pulsing acceleration $\bar{a}_{\text{pls}}$ is assigned as the value of target pulsing acceleration in each case, while the gliding acceleration $\bar{a}_{\text{gld}}$ is as the free-gliding acceleration derived from the vehicle parameters in Table 5.1. Ideally, the vehicle will travel following the target phase portrait and we can then solve for the intersection points of the pulsing and gliding curves after assigning the allowed distance error, $\Delta x_{\max}$ and $\Delta x_{\min}$. The solved intersection points give the switching speeds. When the vehicle speed reaches upper switching speed, it switches from pulsing to gliding. On the contrary, it switches from gliding to pulsing once the lower switching speed has been reached. In the experiment, the allowed distance error, $\Delta x_{\max}$ and $\Delta x_{\min}$ are set as 3 m and -3 m respectively.

5.3.2.2 Pulsing Control

In the pulsing phase, the vehicle is controlled to follow the target acceleration; in the gliding phase, it is let glide freely. When to switch to the other phase is determined with the approach introduced above. Because the engine and motor operations of the test vehicle cannot be directly controlled due to the limitation of the test platform, we send the throttle command as the control input instead. As to how this throttle command will be fulfilled, it is determined by the strategy of the test vehicle itself. This subsection describes the control implemented in the pulsing phase.

First, a throttle map is constructed using the test vehicle in the Mcity test facility

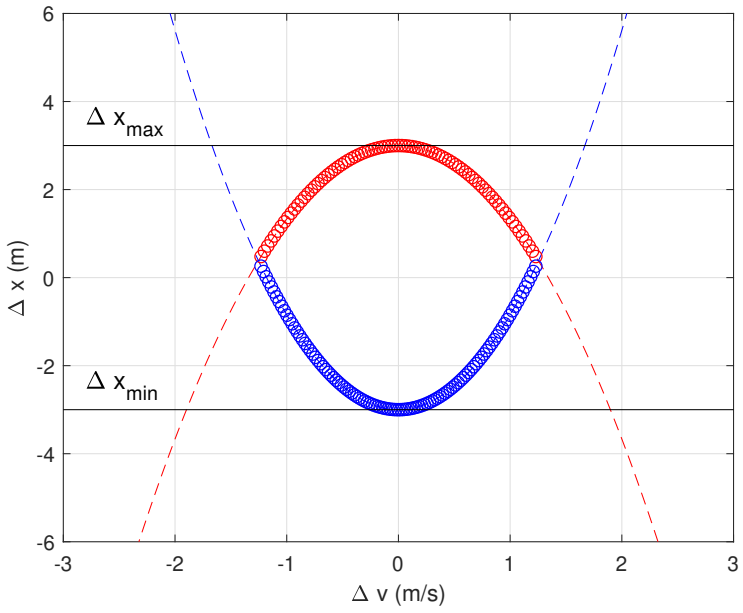

Figure 5.3: The example of the phase portrait for deciding the PnG switching timing. The dashed lines are the pulsing and gliding curves defined in (5.1) and (5.2), and the circles highlight the phase portrait with red corresponding to the pulsing phase and blue to the gliding phase. The black lines indicate the allowed distance errors.

of the University of Michigan. Multiple runs starting from zero speed with different throttle commands are conducted. Each run is with a fixed throttle command. The acceleration and speed trajectories are then recorded to construct the throttle map. By looking up this throttle map, we can determine how much the throttle level should be commanded at a given speed to achieve the target acceleration. In addition, to cope with the influence of road slope, the accelerations of the throttle map are also compensated. The slope of the road segment used for the runs to construct the throttle map is roughly 2.5%. In the experiment, the current road slope is computed from the RTK signals. A low-pass filter is also applied on-line to remove the high-frequency noises of the computed road slope. Then, the target acceleration with the addition of the acceleration resulting from road slope is used to obtain the throttle command via the throttle map.

Furthermore, a feedback mechanism is necessary to deal with the uncertainties and measurement errors in the experiment, e.g., the RTK elevation error mentioned in Section 5.3.1. In this experimental study, the proportional-integral-derivative (PID) control is used. Even though in the experiment we directly have a target acceleration to be tracked, due to the high noise of instantaneous acceleration signal, the PID control is implemented with the feedback of vehicle speed rather than acceleration. More specifically, the target acceleration is integrated to obtain the target speed, and the error between current speed and target speed is fed into the PID controller to adjust the throttle command that is decided from the throttle map.

In summary, a feedback-feedforward control composed of the PID control and the outcome of the throttle map gives the final throttle command to the test vehicle. This throttle command will try to fulfill the target acceleration in the pulsing phase. This way, we can test whether fuel saving can be achieved by changing the powertrain operating points with different pulsing accelerations.

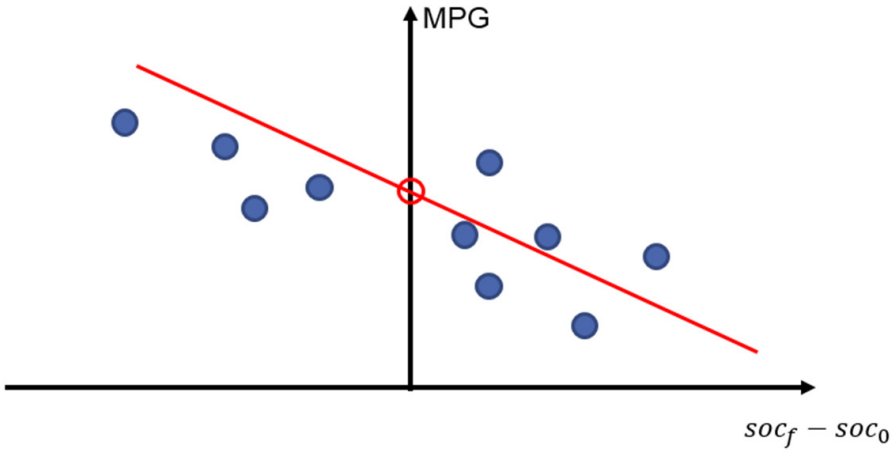

Figure 5.4: The schematic diagram of the linear regression approach for correcting MPG due to SOC variations. The red circle corresponds to the corrected MPG with zero SOC variation. SOC_f and SOC_0 are final and initial SOC.

5.3.3 Data Processing

From the CANbus, we can access the fuel rate information. It is then combined with the traveled distance computed from the RTK signals to obtain the MPG values. However, the MPG values need to be corrected to consider the battery SOC changes in all cases to have a fair comparison.

The linear regression method in [99] is adopted to correct the MPG values. The concept of this approach can be understood via Figure 5.4. For each test scenario, the MPG values and the differences between the final and initial SOCs of each trial are recorded. Then a straight line that best fits the data points of test trials is constructed. The corrected MPG value corresponding to zero SOC variation, which represents the fuel economy of this test scenario, can be obtained through this fitted straight line.

To have reliable results from the linear regression method for correcting the MPG values, more data points are required. For this reason, a moving window approach is applied to the CS cases. Similar concept is applied to the PnG cases, but based on the

PnG cycles. Figure 5.5 shows the idea of the moving window approach. Each time, we fix a window length and move the window along the time axis with a 5 s step. Then, we can obtain several MPG values corresponding to each window of this window length. Those MPG values are corrected using the linear regression method explained above. The window length is gradually increased such that the corrected MPG values under different window length can be drawn. However, with the segmentation of the data of the trials, if the road slope variation in each segment is large, then it becomes a factor influencing the MPG results. Therefore, we extend the linear regression method to include one more dimension, the elevation change, for the low speed cases. As we can see from Figure 5.1, there are large road slope variations on the Sutton road. Therefore, the linear regression method for low speed cases corrects both the SOC and elevation variations, as schematically shown in Figure 5.6. The corrected MPG thus represents the fuel economy with zero changes of SOC and elevation. As to the PnG cases, the data segmentation is based on the PnG cycles to better capture the performance of PnG operations. The corrected MPG is computed by considering one PnG cycle, two PnG cycles, and so on and so forth. In this approach, shorter window length or less number of PnG cycles renders less averaging effect on the data segments. The averaging effect is anticipated to be able to remove the disturbances and/or measurement errors. On the contrary, longer window length or covering more PnG cycles leads to less reliable results due to less data points in the linear regression. For each case, at last the corrected MPG corresponding to the tightest 95% confidence interval is chosen as the fuel economy of this case.

As explained in Section 5.3.1, the elevation information is obtained from interpolating the Google Earth data using the RTK's longitude and latitude instead of resorting to the RTK's elevation directly.

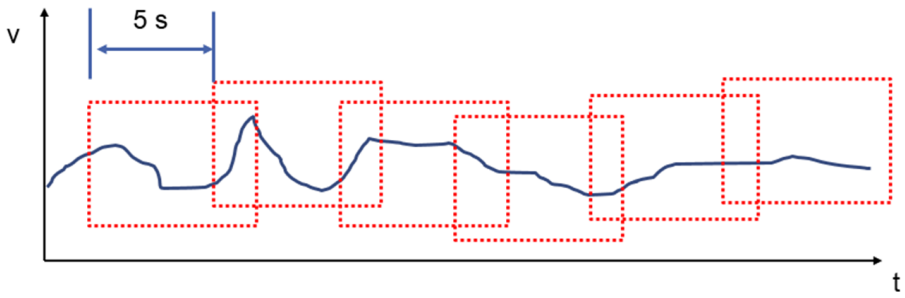

Figure 5.5: The schematic diagram of the moving window approach for correcting MPG.

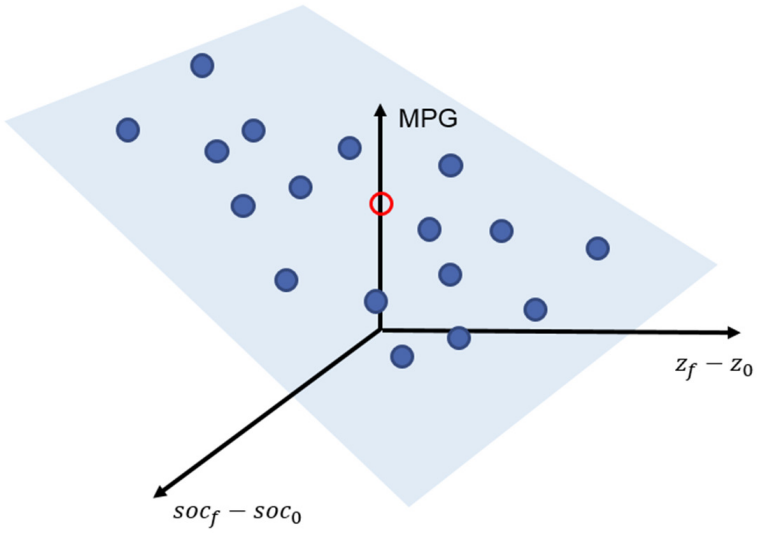

Figure 5.6: The schematic diagram of the linear regression approach for correcting MPG for both SOC variation and elevation variation for low speed cases. The red circle corresponds to the corrected MPG with zero SOC variation and zero elevation change. SOC_f and SOC_0 are final and initial SOC, and z_f and z_0 are final and initial elevation.

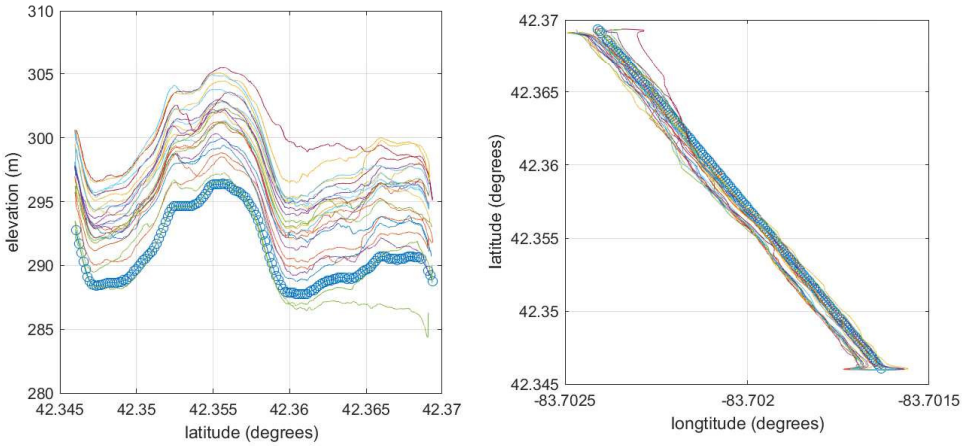

Figure 5.7: The latitude, longitude, and elevation from RTK in low speed cases compared with the Google Earth data. The blue lines with circles are the Google Earth data.

5.4 Results and Discussions

5.4.1 The RTK Performance

Unlike the highway M-14, the Sutton road is less flat, of which the road slope can reach as high as 5.7%. Therefore, the MPG correction for elevation variation is required for low speed cases. The RTK readings for low speed cases are plotted along with the Google Earth data in Figure 5.7. We can see that the elevation from RTK deviates from the Google Earth elevation as much as roughly 10 m. Some parts of the RTK elevation are not simply the vertical shifts of the Google Earth elevation. Therefore, in the MPG correction process the elevation variations happening in the data segments may be different, even if in reality the test vehicle was driving through exactly the same road segments. On the other hand, we can also see that there are some deviations of the RTK latitude and longitude from the Google Earth data. However, since the Sutton road is almost in north-south direction, we assume that the errors in RTK latitude are negligible. The RTK latitude is still used to interpolate the Google Earth data for the elevation, as explained previously.

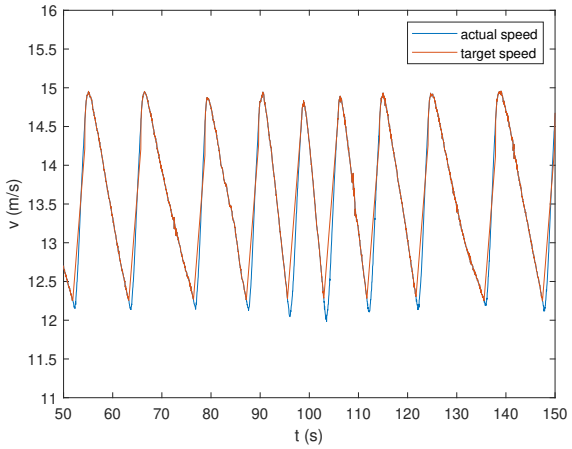

Figure 5.8: Part of the speed trajectory of the PnG case at 30 mph with 0.8 m/s^2 target pulsing acceleration. The actual root-mean-square acceleration during pulsing is 1.1 m/s^2.

5.4.2 The Performance of Throttle Control

As described in Section 5.3.2.2, the PID control with feedforward is applied to set the throttle command to achieve the target pulsing acceleration. This PID control is based on the speed tracking error rather than the acceleration tracking error due to high noise of the instantaneous acceleration signal. However, the delay of the powertrain response tends to result in higher acceleration. Shown in Figure 5.8 is part of the speed trajectory of the PnG case at 30 mph with 0.8 m/s^2 as an example. We can see that in the pulsing phases, the vehicle speed starts to increase roughly 1 s slower than the target speed. The PID controller then will demand higher throttle level to compensate for the resulting speed error, then leading to higher acceleration. The actual root-mean-square acceleration of this example is 1.1 m/s^2, higher than the target acceleration 0.8 m/s^2.

Even though the throttle control may lead to higher accelerations than the target values, the purpose is to create different pulsing accelerations to explore the unknown engine map. Precise control of the acceleration is not necessary in this experimental study.

target pulsing acceleration	30 mph	40 mph	50 mph	60 mph	70 mph
0.2 m/s^2 (0.1 m/s^2 for 70 mph)	2.8%	-0.2%	-0.7%	-16.0%	-16.9%
0.5 m/s^2 (0.2 m/s^2 for 70 mph)	-	13.1%	1.4%	-28.1%	-15.4%
0.8 m/s^2	-7.2%	-12.0%	-31.8%	-	-

Table 5.2: Improvements of corrected MPG in the PnG experiment. The result of 0.5 m/s^2 at 30 mph is not presented due to data missing resulted from CANbus recording issues.

5.4.3 The Fuel Saving Results of PnG Operation

The engine operating points and the corrected MPG results with actual root-mean-square pulsing acceleration are shown in Figure 5.9 to Figure 5.13 for cases of 30 mph to 70 mph, respectively. The result of the case with 0.5 m/s^2 is not presented due to the incomplete data recording from CANbus. It can be observed that the engine operating points gradually migrate away from those of the CS cases as the pulsing acceleration increases. The improvements of corrected MPG are summarized in Table 5.2. We can see that the improvement of fuel economy from PnG is achieved in low speed cases, reaching 13.1% at 40 mph. However, at 60 mph and 70 mph, PnG operation leads to lower fuel economy compared with the constant-speed driving.

The CS cases controlled by the built-in cruising control function of the test vehicle behave like SOC-PnG at low speeds. We can see from Figure 5.14 as an example that while the vehicle is driven by engine, the battery is also charged at the same time. This leads to the increase of battery SOC. When the engine is turned off, the vehicle is driven by the motor to maintain the constant speed, which results in the decrease of SOC. On the other hand, from Figure 5.15 we can see that the engine is switched on and off with much higher frequency compared with the CS case in Figure 5.14 due to the PnG operation. During pulsing, the powertrain uses both engine and motor to provide the driving force. During gliding, regenerative braking happens. However, the regenerative braking here is not desired due to the energy conversion loss. The kinetic energy from pulsing is originally intended to let the vehicle glide freely in

the gliding phase. However, the regenerative braking shortens the gliding durations, which leads to more frequent engine turning on compared with the situation where the powertrain can be disengaged and there is no regenerative braking in the gliding phase. The involvement of the electric path of powertrain, including motor driving in the pulsing phase and regenerative braking in the gliding phase, results in the degradation of PnG performance of fuel saving. This is because the vehicle body is a more efficient energy buffer than the battery.

Figure 5.16 and Figure 5.17 plot respectively the trajectories of the CS case and PnG case of 60 mph as examples for high speeds. It can be observed that the behavior of powertrain in PnG is similar to that of the low speed PnG cases, but the SOC-PnG behavior is not shown in the CS case at high speeds. Instead, the engine is turned on to drive the vehicle in the whole process.

Theoretically, the fuel saving potential for both the SOC-PnG and the Speed-PnG, and the combination of the two like the PnG operations in this experiment, decreases with the increase of vehicle speed. As the speed increases, the required driving power also increases. When the driving power gradually reaches the point where the concave region of the fuel-rate curve ends (Figure 1.3), the fuel saving potential becomes less. This is likely the reason why the SOC-PnG behavior disappears for CS cases at 60 and 70 mph in the experiment. As shown by the PnG cases at low speeds, the fuel saving potential may be lost if the pulsing acceleration is too high. On the contrary, too low a pulsing acceleration may not be able to effectively let the engine be operated at more efficient points.

Overall, the fuel savings obtained in our experiment are not as significant as those reported in literature, e.g. 43% in [22]. The reasons can be summarized as follows.

- Unknown engine map. The sweet spot of the engine for this test vehicle is unavailable, so we sort of conducted trial-and-errors by assigning different pulsing accelerations. The sweet spot was thus difficult to visit during the experiment.

- Indirect control of the powertrain. The test vehicle only accepted the throttle command as the control input, rather than the engine and motor torques. In other words, as we gave the throttle command translated from the target pulsing acceleration, how the powertrain fulfilled this throttle is its own decision, which made visiting the engine sweet spot even more difficult.

- Interference of the regenerative braking. The test vehicle automatically started regenerative braking as we switched to gliding phases. This behavior shortened the gliding phases and wasted the kinetic energy stored during the pulsing phases. Therefore, the overall PnG fuel saving potentials were much degraded. Also, the test vehicle did not allow to shift to the neutral gear when the vehicle was moving, so we could not prevent the regenerative braking by switching to the neutral gear.

In a nutshell, if with engine map and the direct control of powertrain and transmission, we anticipate to see significant fuel saving results in the experiment.

5.5 Conclusions and Future work

In this chapter, the experimental study of PnG using an automated Lincoln MKZ hybrid is presented. Even though the engine cannot be directly controlled and the engine map is not available, by giving the throttle command based on different target pulsing accelerations, improved fuel economy by PnG operation is observed in some cases. At low speeds, the MPG improvement reaches 13.1%. Even without PnG, the test vehicle is already efficient as a result of the hybrid control strategy, e.g., the SOC-PnG behavior in CS cases at low speeds. On the other hand, being unable to switch to neutral gear during gliding degrades the PnG potential, as the regenerative braking will be automatically activated in gliding phases.

In this experiment, the powertrain of the test vehicle is a black box. How the

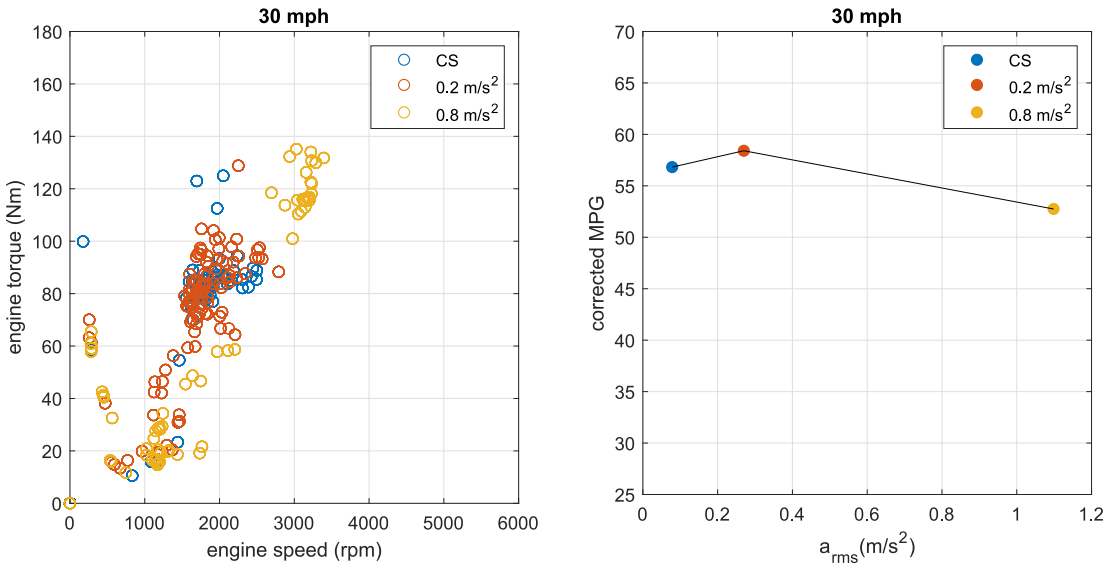

Figure 5.9: The engine operating points and corrected MPG of the experiment results of cases with 30 mph. The result of 0.5 m/s^2 at 30 mph is not presented due to data missing resulted from CANbus recording issues.

vehicle fulfills the throttle command is decided by the unknown powertrain control strategy. Therefore, in the future, if production vehicles are intended to have PnG functions, the powertrain control must be developed along with the consideration of PnG operations. Also, ride comfort is still an important aspect that is highly linked to the success of PnG commercialization.

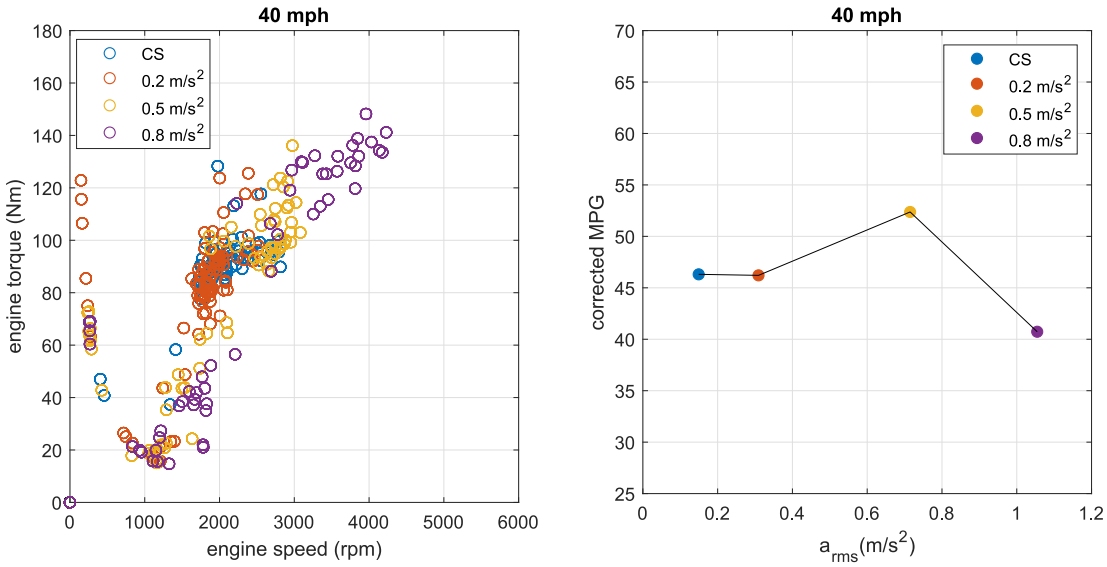

Figure 5.10: The engine operating points and corrected MPG of the experiment results of cases with 40 mph.

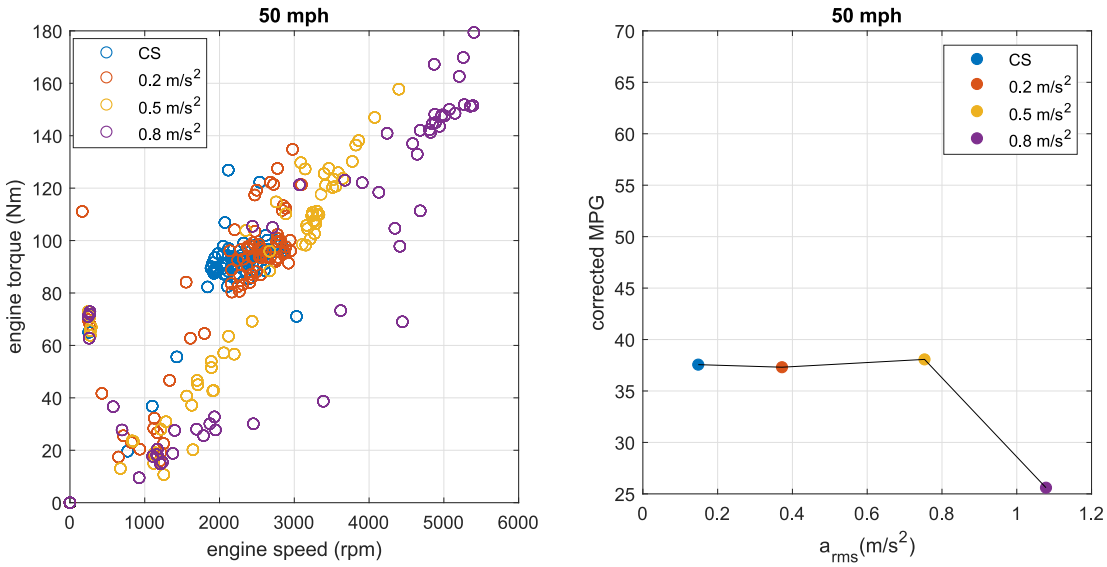

Figure 5.11: The engine operating points and corrected MPG of the experiment results of cases with 50 mph.

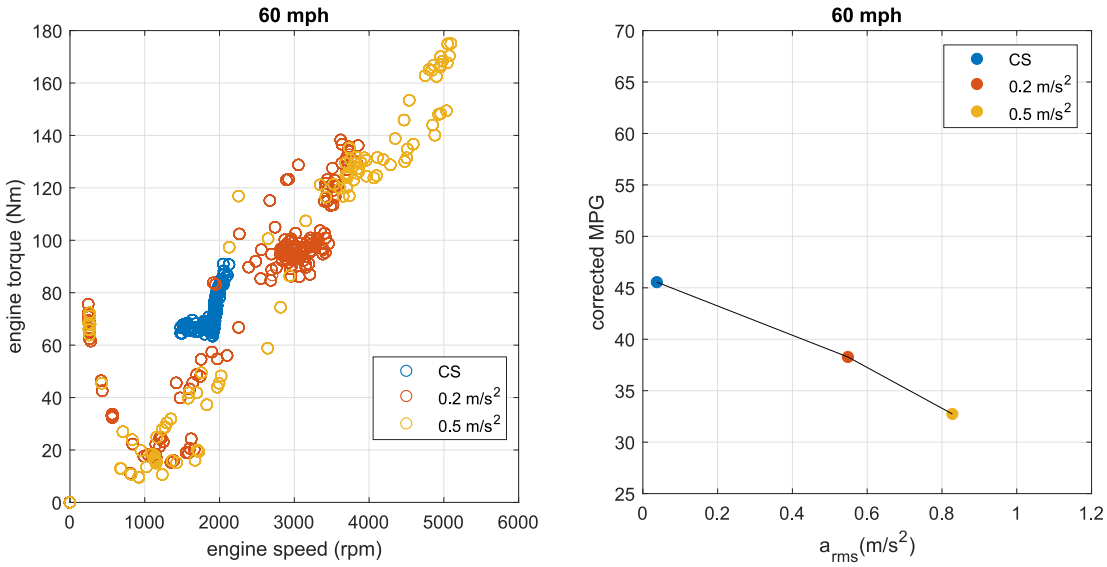

Figure 5.12: The engine operating points and corrected MPG of the experiment results of cases with 60 mph.

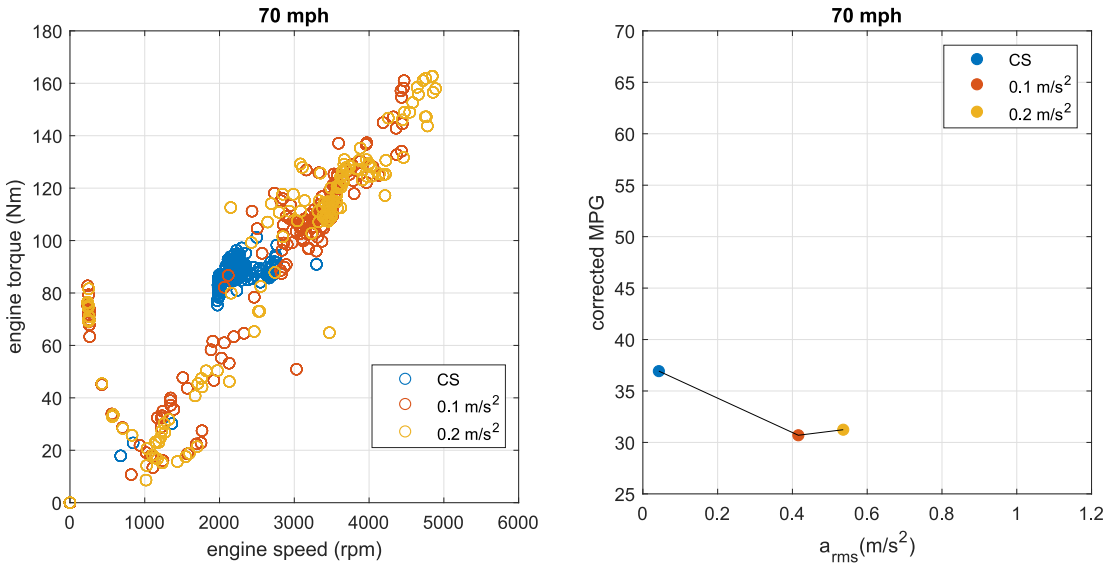

Figure 5.13: The engine operating points and corrected MPG of the experiment results of cases with 70 mph.

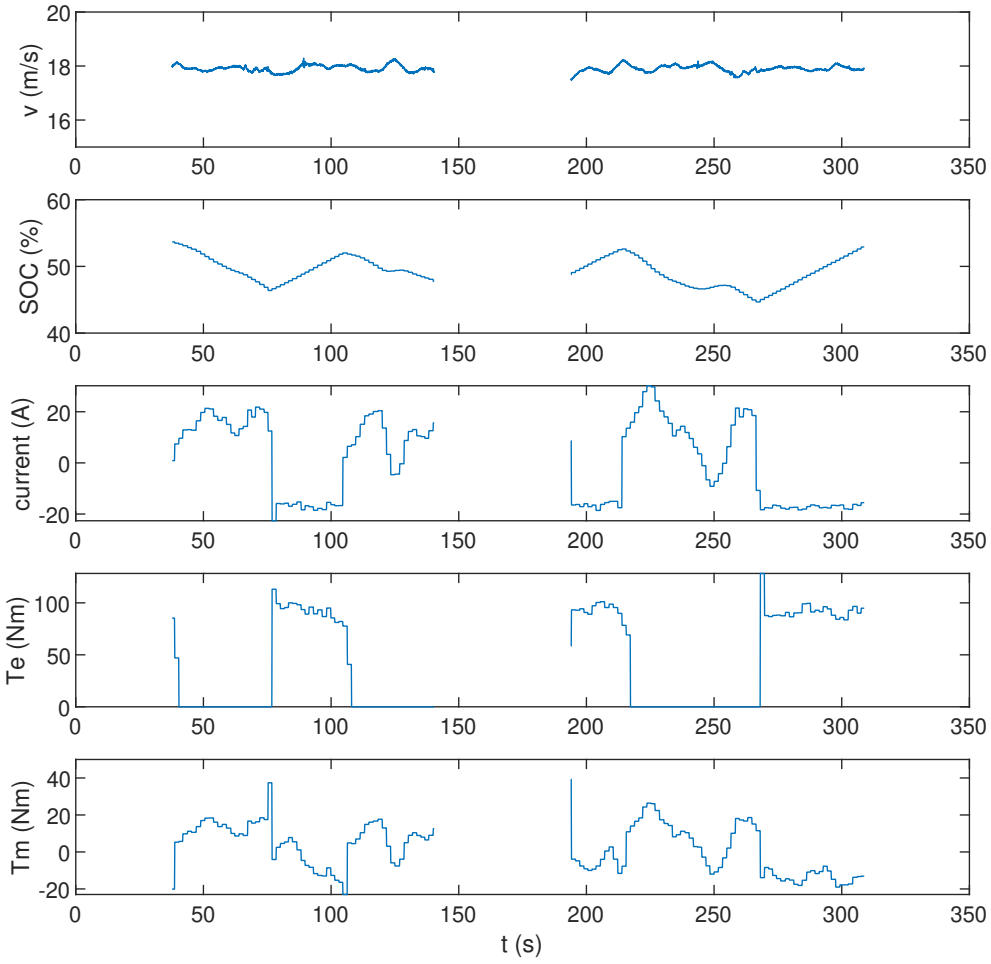

Figure 5.14: The experiment trajectories of one trial of the CS case at 40 mph. The data segments during turning in the round trip are removed.

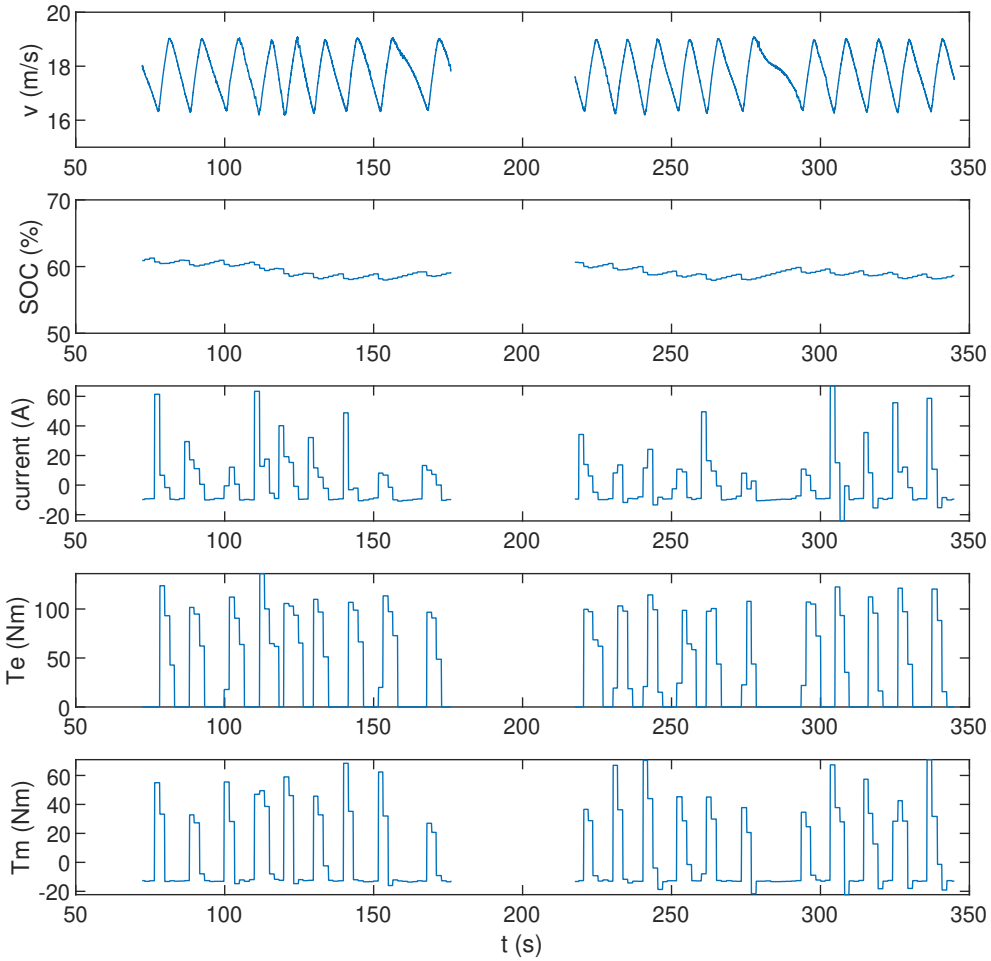

Figure 5.15: The experiment trajectories of the PnG case at 40 mph with 0.5 m/s^2 target pulsing acceleration. The data segments during turning in the round trip are removed.

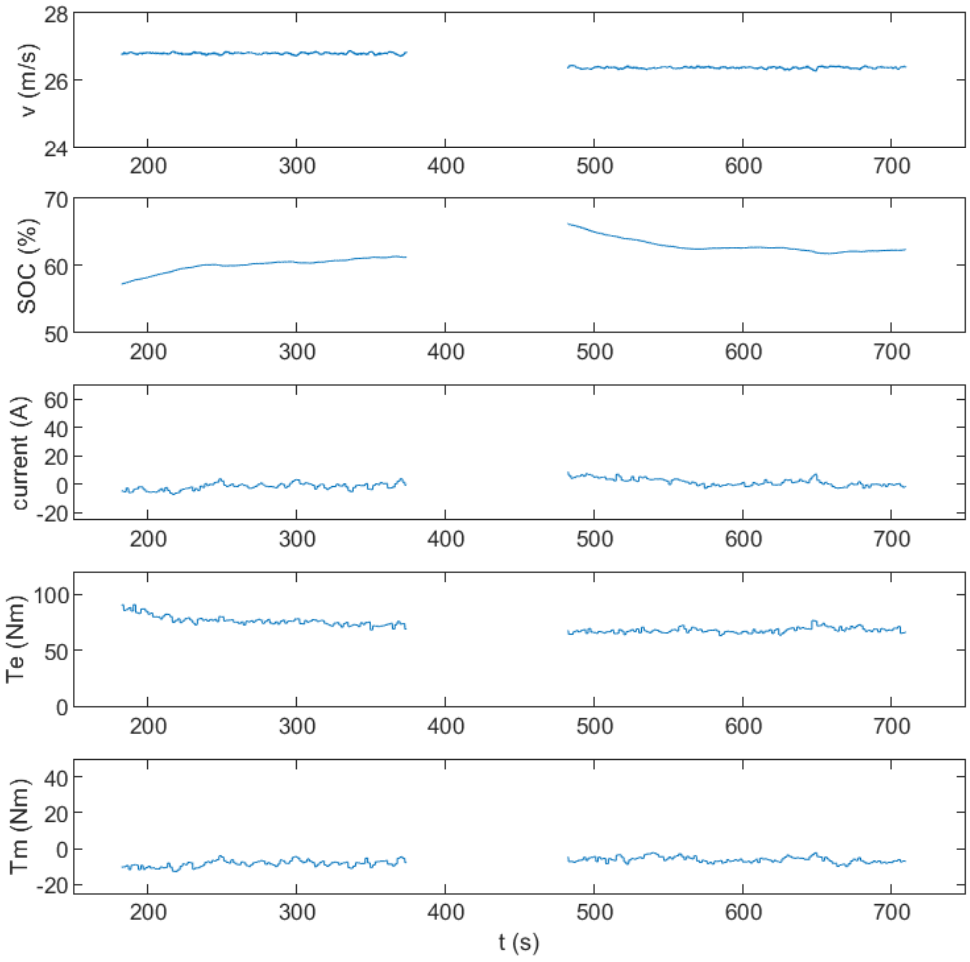

Figure 5.16: The experiment trajectories of the CS case at 60 mph. The data segments during turning in the round trip are removed.

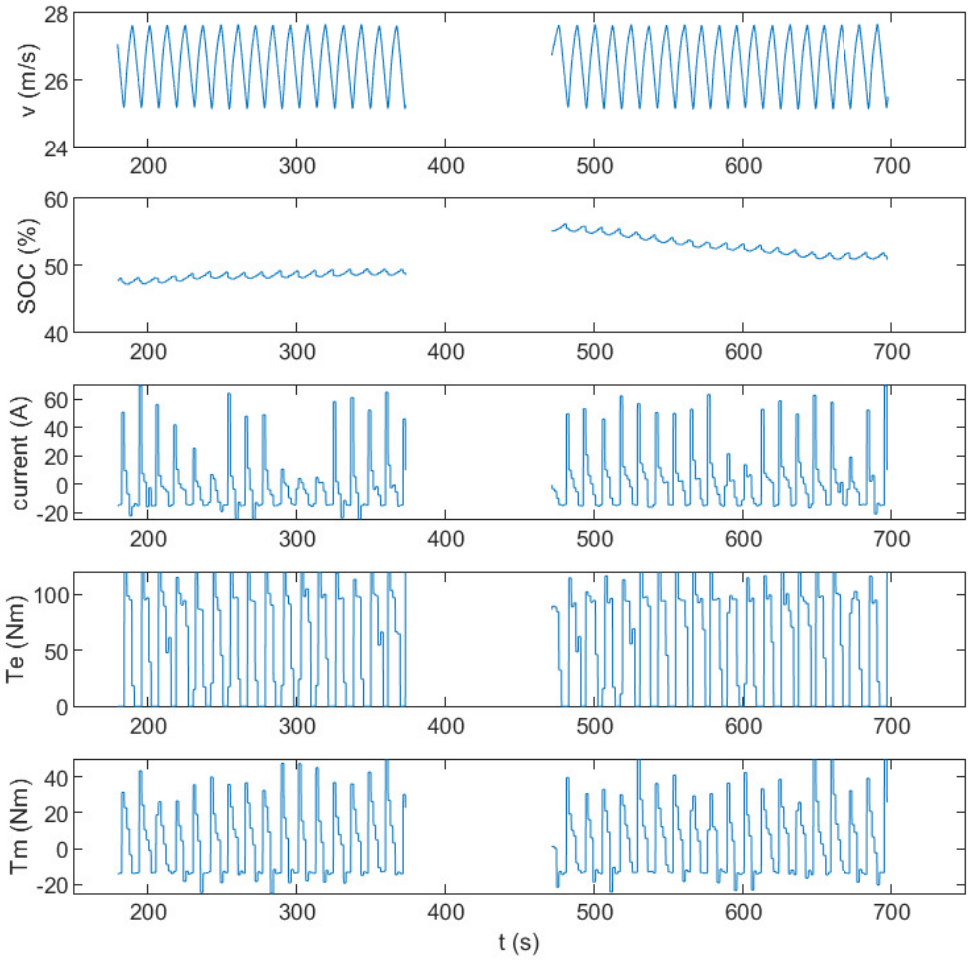

Figure 5.17: The experiment trajectories of the PnG case at 60 mph with 0.2 m/s^2 target pulsing acceleration. The data segments during turning in the round trip are removed.

CHAPTER VI

Conclusions and Future Work

6.1 Conclusions

The overarching goal of this research is to realize CACC through PnG as a way to pursue more possibilities for fuel saving. In Chapter II, a control method based on MPC is proposed for the purpose of effectively leveraging ride comfort requirement for fuel saving. Chapter III presents a PnG synchronization method based on the Kuramoto oscillator model for heterogeneous platoons and the analysis of this method is in Chapter IV. The results of real experiments using an automated Lincoln MKZ hybrid are presented in Chapter V. The contributions of this research can be summarized as follows.

- A control method based on the minimum-time control is developed for PnG implementation on HEVs in car-following. This method is on-line implementable and helps address the trade off between fuel saving and ride comfort, while achieving SOC sustenance.

- Real driving data from Safety Pilot dataset [75] is analyzed to set the ride comfort requirement for PnG. The PnG fuel saving potential is also studied using the naturalistic driving data from Safety Pilot dataset.

- A decentralized control approach for PnG synchronization in heterogeneous platoons based on the Kuramoto oscillation model is presented. This approach only relies on local communication and is able to maintain the fuel saving potentials of different vehicles while keeping the platoons compact.

- The guidelines for designing control and platooning parameters for the proposed method for PnG synchronization are presented. These step-by-step design instructions ensure the successful implementation of the proposed control method.

- The PnG experiment is conducted using an automated Lincoln MKZ hybrid vehicle and 13% MPG improvement is observed at low speed.

6.2 Future Work

In this research, we seek the fuel saving potential of combining PnG and CACC, starting from the car-following problem and then to the platooning of PnG vehicles. With the encouraging results demonstrated in this dissertation, there are some potential research directions that can be explored further to facilitate the implementation of PnG in real applications.

Study of ride comfort requirements under PnG operations. Ride comfort is one of the major concerns that people have for PnG. In this research, a control framework for PnG with ride comfort considered is developed. Due to the lack of research on ride comfort under very low frequency oscillation, the Safety Pilot dataset is used to obtain a requirement of ride comfort. However, from our experience of real PnG experiment, this requirement may be too conservative such that part of the fuel saving potential is not exploited. Therefore, a thorough study on the reactions of human bodies under PnG operations is necessary, which can promote the commercialization of PnG.

A high-level decision making strategy for (de)activating PnG or not.

From the simulation study using the Safety Pilot data as the PV speed in car-following, we see that there are cases where PnG will result in more fuel consumption. Therefore, it is necessary to have a high-level decision making strategy to tell whether the current driving environment is suitable for PnG or not.

High-level controls that can wisely optimize the performance of PnG operations in different situations. In this dissertation, it is assumed that the allowed range oscillation and time headway of range policy are given. These parameters can be wisely chosen with the considerations of the characteristics of ego vehicle, the driver's preferences, and how the PV is driven. Moreover, the approaches for deciding these parameters should have the capabilities to handle the changing environment efficiently.

Design of range policies for vehicle platooning. In this research, it is shown that the inter-vehicle range oscillations can be reduced using the proposed PnG synchronization method. However, the design of range policies that can further keep the platoons compact while ensuring safety is needed.

A strategy for vehicle grouping. In the simulation study, it is pointed out with slowly-responsive vehicles in a platoon, other PnG vehicles may need to have large position oscillations in order to synchronize with those slow vehicles. Therefore, grouping vehicles with similar characteristics to form platoons might still a good idea in terms of the whole platoon performance, even though the proposed method is for heterogeneous platoons.

Study of the influence of communication delay on PnG synchronization In this research, the communication delay is not considered. Further study of it on the PnG platooning method proposed is needed, as it might degrade the robustness of the PnG platoons.

The study of component durability under PnG operations. The PnG operations alternately turn on and off the engine to achieve fuel savings. Whether

this type of operations poses any substantial effects on the related hardware and how to improve it is also an important topic.

Low-level actuator controller design. In this dissertation, we focus on the ride comfort requirement of acceleration at a higher level. In fact, how the PnG is implemented by the powertrain may also play an important role for ride comfort, especially at the moments of PnG switchings. This low-level actuator control may also directly influence the durability of related hardware. For HEVs, a possible solution that could be explored is to utilize the electric machines to improve the NVH issues, as in [100] the vibration during engine start is reduced by the motor control.

BIBLIOGRAPHY

BIBLIOGRAPHY

[1] U.S. Energy Information Administration. *Energy Consumption by Sector*, 2020. https://www.eia.gov/totalenergy/data/monthly/pdf/sec2_3.pdf.

[2] U.S. Energy Information Administration. *Short-Term Energy Outlook*, 2020. https://www.eia.gov/outlooks/steo/pdf/steo_full.pdf.

[3] U.S. Energy Information Administration. Annual Energy Outlook 2020 with projections to 2050. 2020.

[4] National Highway Traffic Safety Administration. *Corporate Average Fuel Economy.* https://www.nhtsa.gov/laws-regulations/corporate-average-fuel-economy.

[5] Martinez-Botas Ricardo, Pesiridis Apostolos, and MingYang Yang. Overview of boosting options for future downsized engines. *Science China Technological Sciences*, 54(2):318–331, 2011.

[6] Lynette W Cheah. *Cars on a diet: the material and energy impacts of passenger vehicle weight reduction in the US.* PhD thesis, Massachusetts Institute of Technology, 2010.

[7] R Buchheim, K-R Deutenbach, and H-J Lückoff. Necessity and premises for reducing the aerodynamic drag of future passenger cars. *SAE Transactions*, pages 758–771, 1981.

[8] Jerome Barrand and Jason Bokar. Reducing tire rolling resistance to save fuel and lower emissions. *SAE International Journal of Passenger Cars-Mechanical Systems*, 1(2008-01-0154):9–17, 2008.

[9] Timothy Johnson and Ameya Joshi. Review of vehicle engine efficiency and emissions. *SAE International Journal of Engines*, 11(6):1307–1330, 2018.

[10] Feng Zhou, Shailesh N Joshi, Raphael Rhote-Vaney, and Ercan M Dede. A review and future application of rankine cycle to passenger vehicles for waste heat recovery. *Renewable and Sustainable Energy Reviews*, 75:1008–1021, 2017.

[11] Daniel Türler, Deborah Hopkins, and Howdy Goudey. Reducing vehicle auxiliary loads using advanced thermal insulation and window technologies. Technical report, SAE Technical Paper, 2003.

[12] Oliver P Taylor, Richard Pearson, and Richard Stone. Reduction of co 2 emissions through lubricant thermal management during the warm up of passenger car engines. Technical report, SAE Technical Paper, 2016.

[13] Guang Wu, Xing Zhang, and Zuomin Dong. Powertrain architectures of electrified vehicles: Review, classification and comparison. *Journal of the Franklin Institute*, 352(2):425–448, 2015.

[14] Otmar Bitsche and Guenter Gutmann. Systems for hybrid cars. *Journal of power sources*, 127(1-2):8–15, 2004.

[15] Andreas A Malikopoulos. Supervisory power management control algorithms for hybrid electric vehicles: A survey. *IEEE Transactions on intelligent transportation systems*, 15(5):1869–1885, 2014.

[16] Joeri Van Mierlo, Gaston Maggetto, Erik Van de Burgwal, and Raymond Gense. Driving style and traffic measures-influence on vehicle emissions and fuel consumption. *Proceedings of the Institution of Mechanical Engineers, Part D: Journal of Automobile Engineering*, 218(1):43–50, 2004.

[17] Elmer Grant Gilbert. Vehicle cruise: Improved fuel economy by periodic control. 1976.

[18] Jeongwoo Lee. *Vehicle inertia impact on fuel consumption of conventional and hybrid electric vehicles using acceleration and coast driving strategy*. PhD thesis, Virginia Tech, 2009.

[19] B Jawad, E Marck, D Tingley, Tony Salvati, J McCoy, A Ondes, E Poota, and Vida Floma. Best practices for an sae supermileage® vehicle. Technical report, SAE Technical Paper, 2001.

[20] Ziheng Pan. *Design and Control Optimization of Hybrid Electric Vehicles: from Two-Wheel-Drive to All-Wheel-Drive Vehicles*. PhD thesis, 2019.

[21] Kevin McDonough, Ilya Kolmanovsky, Dimitar Filev, Diana Yanakiev, Steve Szwabowski, and John Michelini. Stochastic dynamic programming control policies for fuel efficient in-traffic driving. In *2012 American Control Conference (ACC)*, pages 3986–3991. IEEE, 2012.

[22] Yuto Imanishi, Naoyuki Tashiro, Yoichi Iihoshi, and Takashi Okada. Development of predictive powertrain state switching control for eco-saving acc. Technical report, SAE Technical Paper, 2017.

[23] Shaobing Xu, Shengbo Eben Li, Huei Peng, Bo Cheng, Xiaowu Zhang, and Ziheng Pan. Fuel-saving cruising strategies for parallel hevs. *IEEE Transactions on vehicular technology*, 65(6):4676–4686, 2015.

[24] Su-Yang Shieh, Tulga Ersal, and Huei Peng. Pulse-and-glide operation for parallel hybrid electric vehicles with step-gear transmission in automated car-following scenario with ride comfort consideration. In *2019 American Control Conference (ACC)*, pages 959–964. IEEE, 2019.

[25] Lewis M Clements and Kara M Kockelman. Economic effects of automated vehicles. *Transportation Research Record*, 2606(1):106–114, 2017.

[26] Tulga Ersal, Ilya Kolmanovsky, Neda Masoud, Necmiye Ozay, Jeffrey Scruggs, Ram Vasudevan, and Gabor Orosz. Connected and automated road vehicles: state of the art and future challenges. *Vehicle System Dynamics*, 58(5):672–704, 2020.

[27] Gábor Orosz. Connected cruise control: modelling, delay effects, and nonlinear behaviour. *Vehicle System Dynamics*, 54(8):1147–1176, 2016.

[28] Fatima Hanani, Aziz Soulhi, and Rabiae Saidi. Towards a framework for smart city wireless communication: Conclusions drawn from smart transport case study. 2006.

[29] Jackeline Rios-Torres and Andreas A Malikopoulos. Automated and cooperative vehicle merging at highway on-ramps. *IEEE Transactions on Intelligent Transportation Systems*, 18(4):780–789, 2016.

[30] Liuhui Zhao, Andreas Malikopoulos, and Jackeline Rios-Torres. Optimal control of connected and automated vehicles at roundabouts: An investigation in a mixed-traffic environment. *IFAC-PapersOnLine*, 51(9):73–78, 2018.

[31] Jiaqi Ma, Xiaopeng Li, Steven Shladover, Hesham A Rakha, Xiao-Yun Lu, Ramanujan Jagannathan, and Daniel J Dailey. Freeway speed harmonization. *IEEE Transactions on Intelligent Vehicles*, 1(1):78–89, 2016.

[32] Xianan Huang and Huei Peng. Speed trajectory planning at signalized intersections using sequential convex optimization. In *2017 American Control Conference (ACC)*, pages 2992–2997. IEEE, 2017.

[33] Vicente Milanés, Steven E Shladover, John Spring, Christopher Nowakowski, Hiroshi Kawazoe, and Masahide Nakamura. Cooperative adaptive cruise control in real traffic situations. *IEEE Transactions on intelligent transportation systems*, 15(1):296–305, 2013.

[34] John B Kenney. Dedicated short-range communications (dsrc) standards in the united states. *Proceedings of the IEEE*, 99(7):1162–1182, 2011.

[35] Gerrit JL Naus, Rene PA Vugts, Jeroen Ploeg, Marinus JG van De Molengraft, and Maarten Steinbuch. String-stable cacc design and experimental validation: A frequency-domain approach. *IEEE Transactions on vehicular technology*, 59(9):4268–4279, 2010.

[36] Michael Zabat, Nick Stabile, Stefano Farascaroli, and Frederick Browand. The aerodynamic performance of platoons: A final report. 1995.

[37] Kristin J Malakorn and Byungkyu Park. Assessment of mobility, energy, and environment impacts of intellidrive-based cooperative adaptive cruise control and intelligent traffic signal control. In *Proceedings of the 2010 IEEE International Symposium on Sustainable Systems and Technology*, pages 1–6. IEEE, 2010.

[38] S Eben Li and Huei Peng. Strategies to minimize the fuel consumption of passenger cars during car-following scenarios. *Proceedings of the Institution of Mechanical Engineers, Part D: Journal of Automobile Engineering*, 226(3):419–429, 2012.

[39] Shengbo Eben Li, Huei Peng, Keqiang Li, and Jianqiang Wang. Minimum fuel control strategy in automated car-following scenarios. *IEEE Transactions on Vehicular Technology*, 61(3):998–1007, 2012.

[40] Shengbo Eben Li, Xiaosong Hu, Keqiang Li, and Changsun Ahn. Mechanism of vehicular periodic operation for optimal fuel economy in free-driving scenarios. *IET Intelligent Transport Systems*, 9(3):306–313, 2014.

[41] Sergio Bittanti, Giorgio Fronza, and Guido Guardabassi. Periodic control: A frequency domain approach. *IEEE Transactions on Automatic Control*, 18(1):33–38, 1973.

[42] Cyriel Diels and Jelte E Bos. Self-driving carsickness. *Applied ergonomics*, 53:374–382, 2016.

[43] Carey Whitehair and Hosam Denlinger, Michelleand Fathy. Pulse-and-glide driving with drivability constraints: A pontryagin approach. 2018.

[44] Christian Sohn, Jakob Andert, and Dejan Jolovic. An analysis of the tradeoff between fuel consumption and ride comfort for the pulse and glide driving strategy. *IEEE Transactions on Vehicular Technology*, 2020.

[45] Christian Sohn, Jakob Andert, and Rodrigue N Nanfah Manfouo. A driveability study on automated longitudinal vehicle control. *IEEE Transactions on Intelligent Transportation Systems*, 2019.

[46] Shengbo Eben Li, Kun Deng, Yang Zheng, and Huei Peng. Effect of pulse-and-glide strategy on traffic flow for a platoon of mixed automated and manually driven vehicles. *Computer-Aided Civil and Infrastructure Engineering*, 30(11):892–905, 2015.

[47] Martin Treiber, Ansgar Hennecke, and Dirk Helbing. Congested traffic states in empirical observations and microscopic simulations. *Physical review E*, 62(2):1805, 2000.

[48] Shengbo Eben Li, Renjie Li, Jianqiang Wang, Xiaosong Hu, Bo Cheng, and Keqiang Li. Stabilizing periodic control of automated vehicle platoon with minimized fuel consumption. *IEEE Transactions on Transportation Electrification*, 3(1):259–271, 2016.

[49] Shengbo Eben Li, Xiaoxue Zhang, Renjie Li, Zhitao Wang, Hailiang Chen, and Zhe Xin. Optimal periodic control of connected multiple vehicles with heterogeneous dynamics and guaranteed bounded stability. *IEEE Intelligent Transportation Systems Magazine*, 2018.

[50] C Freitas Salgueiredo, Olivier Orfila, Guillaume Saint Pierre, Philippe Doublet, Sébastien Glaser, Stéphane Doncieux, and Véronique Billat. Experimental testing and simulations of speed variations impact on fuel consumption of conventional gasoline passenger cars. *Transportation Research Part D: Transport and Environment*, 57:336–349, 2017.

[51] Ali Syed, Gang George Yin, Abhilash Pandya, Hongwei Zhang, et al. Control of vehicle platoons for highway safety and efficient utility: Consensus with communications and vehicle dynamics. *Journal of systems science and complexity*, 27(4):605–631, 2014.

[52] Mario Di Bernardo, Alessandro Salvi, and Stefania Santini. Distributed consensus strategy for platooning of vehicles in the presence of time-varying heterogeneous communication delays. *IEEE Transactions on Intelligent Transportation Systems*, 16(1):102–112, 2014.

[53] Charles Desjardins and Brahim Chaib-Draa. Cooperative adaptive cruise control: A reinforcement learning approach. *IEEE Transactions on intelligent transportation systems*, 12(4):1248–1260, 2011.

[54] Jeroen Ploeg, Nathan van de Wouw, and Henk Nijmeijer. Fault tolerance of cooperative vehicle platoons subject to communication delay. *IFAC-PapersOnLine*, 48(12):352–357, 2015.

[55] Carlos Massera Filho, Marco H Terra, and Denis F Wolf. Safe optimization of highway traffic with robust model predictive control-based cooperative adaptive cruise control. *IEEE Transactions on Intelligent Transportation Systems*, 18(11):3193–3203, 2017.

[56] Michał Sybis, Vladimir Vukadinovic, Marcin Rodziewicz, Paweł Sroka, Adrian Langowski, Karolina Lenarska, and Krzysztof Wesołowski. Communication aspects of a modified cooperative adaptive cruise control algorithm. *IEEE Transactions on Intelligent Transportation Systems*, 20(12):4513–4523, 2019.

[57] Weinan Gao, Jingqin Gao, Kaan Ozbay, and Zhong-Ping Jiang. Reinforcement-learning-based cooperative adaptive cruise control of buses in the lincoln tunnel corridor with time-varying topology. *IEEE Transactions on Intelligent Transportation Systems*, 20(10):3796–3805, 2019.

[58] Chaoxian Wu, Yuan Lin, and Azim Eskandarian. Cooperative adaptive cruise control with adaptive kalman filter subject to temporary communication loss. *IEEE Access*, 7:93558–93568, 2019.

[59] Francesco Acciani, Paolo Frasca, Geert Heijenk, and Anton Stoorvogel. Stochastic string stability of vehicle platoons via cooperative adaptive cruise control with lossy communication. *arXiv preprint arXiv:1905.04779*, 2019.

[60] Shixi Wen, Ge Guo, Bo Chen, and Xiue Gao. Cooperative adaptive cruise control of vehicles using a resource-efficient communication mechanism. *IEEE Transactions on Intelligent Vehicles*, 4(1):127–140, 2018.

[61] Shixi Wen, Ge Guo, Bo Chen, and Xiue Gao. Event-triggered cooperative control of vehicle platoons in vehicular ad hoc networks. *Information Sciences*, 459:341–353, 2018.

[62] Chaojie Wang, Siyuan Gong, Anye Zhou, Tao Li, and Srinivas Peeta. Cooperative adaptive cruise control for connected autonomous vehicles by factoring communication-related constraints. *Transportation Research Part C: Emerging Technologies*, 113:124–145, 2020.

[63] Dominik Lang, Thomas Stanger, Roman Schmied, and Luigi del Re. Predictive cooperative adaptive cruise control: Fuel consumption benefits and implementability. In *Optimization and optimal control in automotive systems*, pages 163–178. Springer, 2014.

[64] Dominik Moser, Roman Schmied, Harald Waschl, and Luigi del Re. Flexible spacing adaptive cruise control using stochastic model predictive control. *IEEE Transactions on Control Systems Technology*, 26(1):114–127, 2017.

[65] Hao Liu, Xiao-Yun Lu, and Steven E Shladover. Traffic signal control by leveraging cooperative adaptive cruise control (cacc) vehicle platooning capabilities. *Transportation research part C: emerging technologies*, 104:390–407, 2019.

[66] Mohammed Hamad Almannaa, Hao Chen, Hesham A Rakha, Amara Loulizi, and Ihab El-Shawarby. Field implementation and testing of an automated eco-cooperative adaptive cruise control system in the vicinity of signalized intersections. *Transportation research part D: transport and environment*, 67:244–262, 2019.

[67] Ziran Wang, Guoyuan Wu, and Matthew Barth. Distributed consensus-based cooperative highway on-ramp merging using v2x communications. Technical report, SAE Technical Paper, 2018.

[68] Siyuan Gong. Autompc: Efficient multi-party computation for secure and privacy-preserving cooperative control of connected autonomous vehicles. In *SafeAI@ AAAI*, 2019.

[69] Matthew Jagielski, Nicholas Jones, Chung-Wei Lin, Cristina Nita-Rotaru, and Shinichi Shiraishi. Threat detection for collaborative adaptive cruise control in connected cars. In *Proceedings of the 11th ACM Conference on Security & Privacy in Wireless and Mobile Networks*, pages 184–189, 2018.

[70] Alberto Petrillo, Antonio Pescapé, and Stefania Santini. A collaborative approach for improving the security of vehicular scenarios: The case of platooning. *Computer Communications*, 122:59–75, 2018.

[71] Roberto Merco, Zoleikha Abdollahi Biron, and Pierluigi Pisu. Replay attack detection in a platoon of connected vehicles with cooperative adaptive cruise control. In *2018 Annual American Control Conference (ACC)*, pages 5582–5587. IEEE, 2018.

[72] Yoshiki Kuramoto. Self-entrainment of a population of coupled non-linear oscillators. In *International symposium on mathematical problems in theoretical physics*, pages 420–422. Springer, 1975.

[73] Juan A Acebrón, Luis L Bonilla, Conrad J Pérez Vicente, Félix Ritort, and Renato Spigler. The kuramoto model: A simple paradigm for synchronization phenomena. *Reviews of modern physics*, 77(1):137, 2005.

[74] Alex Arenas, Albert Díaz-Guilera, Jurgen Kurths, Yamir Moreno, and Changsong Zhou. Synchronization in complex networks. *Physics reports*, 469(3):93–153, 2008.

[75] Debby Bezzina and James Sayer. Safety pilot model deployment: Test conductor team report. *Report No. DOT HS*, 812(171):18, 2014.

[76] Garth P McCormick. Computability of global solutions to factorable nonconvex programs: Part i—convex underestimating problems. *Mathematical programming*, 10(1):147–175, 1976.

[77] Laurent Bako, Dulin Chen, and Stéphane Lecoeuche. A numerical solution to the minimum-time control problem for linear discrete-time systems. *arXiv preprint arXiv:1109.3772*, 2011.

[78] Fariba Fahroo and I Michael Ross. Advances in pseudospectral methods for optimal control. In *AIAA guidance, navigation and control conference and exhibit*, page 7309, 2008.

[79] Michael A Patterson and Anil V Rao. Gpops-ii: A matlab software for solving multiple-phase optimal control problems using hp-adaptive gaussian quadrature collocation methods and sparse nonlinear programming. *ACM Transactions on Mathematical Software (TOMS)*, 41(1):1, 2014.

[80] Feng Han, Yi Tan, and Jayan Eledath. Preceding vehicle trajectory prediction by multi-cue integration. In *MVA*, pages 575–578, 2007.

[81] Rohit Pandita and Derek Caveney. Preceding vehicle state prediction. In *2013 IEEE Intelligent Vehicles Symposium (IV)*, pages 1000–1006. IEEE, 2013.

[82] Michael J Griffin and John Erdreich. Handbook of human vibration, 1991.

[83] ISO. Evaluation of human exposure to whole-body vibration - part 3: Evaluation of exposure to whole-body z-axis vertical vibration in the frequency range 0.1 to 0.63 hz. ISO 2631/3-1985(E), 1985.

[84] David M Hamby. A review of techniques for parameter sensitivity analysis of environmental models. *Environmental monitoring and assessment*, 32(2):135–154, 1994.

[85] Marta V Faria, Gonçalo O Duarte, Roberto A Varella, Tiago L Farias, and Patrícia C Baptista. How do road grade, road type and driving aggressiveness impact vehicle fuel consumption? assessing potential fuel savings in lisbon, portugal. *Transportation Research Part D: Transport and Environment*, 72:148–161, 2019.

[86] Shahab Sheikholeslam and Charles A Desoer. Longitudinal control of a platoon of vehicles with no communication of lead vehicle information: A system level study. *IEEE Transactions on vehicular technology*, 42(4):546–554, 1993.

[87] Peter Seiler, Aniruddha Pant, and Karl Hedrick. Disturbance propagation in vehicle strings. *IEEE Transactions on automatic control*, 49(10):1835–1842, 2004.

[88] Ioannis Lestas and Glenn Vinnicombe. Scalability in heterogeneous vehicle platoons. In *2007 American Control Conference*, pages 4678–4683. IEEE, 2007.

[89] Prabir Barooah and Joao P Hespanha. Error amplification and disturbance propagation in vehicle strings with decentralized linear control. In *Proceedings of the 44th IEEE conference on Decision and Control*, pages 4964–4969. IEEE, 2005.

[90] DVAHG Swaroop and J Karl Hedrick. Constant spacing strategies for platooning in automated highway systems. 1999.

[91] Jeroen Ploeg, Dipan P Shukla, Nathan van de Wouw, and Henk Nijmeijer. Controller synthesis for string stability of vehicle platoons. *IEEE Transactions on Intelligent Transportation Systems*, 15(2):854–865, 2013.

[92] Xiangheng Liu, Andrea Goldsmith, Sunider Sonia Mahal, and J Karl Hedrick. Effects of communication delay on string stability in vehicle platoons. In *ITSC 2001. 2001 IEEE Intelligent Transportation Systems. Proceedings (Cat. No. 01TH8585)*, pages 625–630. IEEE, 2001.

[93] Srdjan S Stankovic, Milorad J Stanojevic, and Dragoslav D Siljak. Decentralized overlapping control of a platoon of vehicles. *IEEE Transactions on Control Systems Technology*, 8(5):816–832, 2000.

[94] S Darbha and PR Pagilla. Limitations of employing undirected information flow graphs for the maintenance of rigid formations for heterogeneous vehicles. *International journal of engineering science*, 48(11):1164–1178, 2010.

[95] Yujia Wu, Shengbo Eben Li, Yang Zheng, and J Karl Hedrick. Distributed sliding mode control for multi-vehicle systems with positive definite topologies. In *2016 IEEE 55th Conference on Decision and Control (CDC)*, pages 5213–5219. IEEE, 2016.

[96] Ali Jadbabaie, Nader Motee, and Mauricio Barahona. On the stability of the kuramoto model of coupled nonlinear oscillators. In *Proceedings of the 2004 American Control Conference*, volume 5, pages 4296–4301. IEEE, 2004.

[97] Chris Godsil and Gordon F Royle. *Algebraic graph theory*, volume 207. Springer Science & Business Media, 2001.

[98] Miroslav Fiedler. Laplacian of graphs and algebraic connectivity. *Banach Center Publications*, 25(1):57–70, 1989.

[99] Richard TM Smokers, S Ploumen, M Conte, L Buning, and K Meier-Engel. Test methods for evaluating energy consumption and emissions of vehicles with electric, hybrid and fuel cell power trains. 2000.

[100] Naoto Kawabata, Masashi Komada, and Takayoshi Yoshioka. Noise and vibration reduction technology in the development of hybrid luxury sedan with series/parallel hybrid system. Technical report, SAE Technical Paper, 2007.